2016

Kinetics of Turnover of Actin and Regulators in Motile Cells

Laura Marie McMillen
Lehigh University

Kinetics of Turnover of Actin and Regulators in Motile Cells

by
Laura McMillen

A Dissertation
Presented to the Graduate and Research Committee
of Lehigh University
in Candidacy for the Degree of
Doctor of Philosophy
in
Physics

Lehigh University
May 23^{rd}, 2016

Approved and recommended for acceptance as a dissertation in partial fulfillment of the requirements for the degree of Doctor of Philosophy.

Laura M. McMillen

Kinetics of Turnover of Actin and Regulators in Motile Cells.

Date

Dimitrios Vavylonis, Dissertation Chair

Accepted Date

Committee Members:

Jim Gunton

A. Peet Hickman

Anand Jagota

Daniel Ou-Yang

Acknowledgments

I am very grateful to my advisor Dimitrios Vavylonis for his patience and helpfulness in guiding me through the research process. I've learned a lot through our discussions and his willingness to answer any question I ask regardless of its relevance. I'm also thankful to the members of our research group both alumni and present members, their willingness to put their own work on hold in order to help others learn was gracious and kind.

I also gained so much support from all of my friends who were always ready to lend an ear and give helpful advice. My grandparents and in-laws have been a constant loving presence throughout grad school and always been so supportive and encouraging. My parents have been one of the biggest influences throughout this process. I'm not sure I can find the words to express my gratitude for all they have done for me. They are always willing to help in any way they can regardless of what that entails, but mostly I appreciate the unending love that they clearly have to give. Finally, without my husband, Josh, I never would have made it through this program. His constant love, support, and respect for me are unparalleled and so appreciated.

Table Of Contents

List of Figures

List of Tables

Abstract

In this thesis I study the diffusion and reaction of the Arp2/3 complex, capping protein, and actin protein in the cytoplasm of eukaryotic cells with computational modeling in order to study the turnover of protein within the lamellipodium. The Arp2/3 complex and capping protein are important regulators of the actin network in the lamellipodium. The Arp2/3 complex nucleates branches of new actin filaments off the sides of existing filaments, while capping protein is a protein that attaches to the end of existing actin filaments and stops them from polymerizing further at that end. My research consists of three separate projects. First, I study the kinetics of the Arp2/3 complex and capping protein through a reaction diffusion model that has been motivated from previous modeling work by Smith et al. [1] which uses SiMS (Single Molecule Speckle microscopy) data from Naoki Watanabe (Kyoto University). In this work I utilize this model to run simulations of FRAP (Fluorescence Recovery After Photobleaching) which are then compared with experimental data from Lai et al. [2] and Kapustina et al. [3] Second, I developed a reaction diffusion model for actin that models turnover of actin in the lamellipodium which also utilizes SiMS data in order to compare to experimental photoactivation data from Eric Vitriol and James Zheng (Emory University). This model includes effects of knocking down Thymosin $\beta 4$ on actin kinetics within the lamellipodium. Third, I developed a 3D whole cell model with particle diffusion. This model accounts for the effect of geometry of the cell on the kinetics of actin where our previous model and simulation mentioned above did not. It also accounts for kinetics and turnover of actin within the cell center while our previous models mentioned above only accounted for actin within

the lamellipodium.

In the first part, we study the distribution of capping protein (CP) and Arp2/3 protein complex that regulate actin polymerization in the lamellipodium through capping and nucleation of free barbed ends. We modeled the kinetics of capping protein and Arp2/3 complex in the lamellipodium using data from prior SiMS microscopy experiments. In these experiments, slowly-diffusing proteins appear as extended clouds while proteins bound to the actin filament network appear as speckles that undergo retrograde flow. Speckle appearance and disappearance events correspond to assembly and dissociation from the actin filament network and speckle lifetimes correspond to the dissociation rate. We use the measured rates of capping protein and Arp2/3 complex in a Monte Carlo simulation that includes particles in association with a filament network and diffuse in the cytoplasm. We consider two separate pools of diffuse proteins, representing fast and slowly-diffusing species. Accounting for the observed slowly-diffusing cytoplasmic pool of capping protein with diffusion coefficients on the order of 0.5 μm^2/s, which could represent severed actin filament fragments or membrane-bound capping protein, leads to gradients in the diffuse pool. We show that the results of models with such slow diffusion coefficients are consistent with prior FRAP experiments. By comparing single molecule data to prior FRAP experiments of the Arp2/3 complex, we provide estimates for the ratio of bound to diffuse complexes and calculate conditions where Arp2/3 recycling by diffusion may become limiting. We discuss the implications of slowly diffusing populations and suggest experiments to distinguish among mechanisms that influence long range transport.

Second, we have developed a diffusion-reaction model useful generally for actin in the lamellipodium with three distinct diffusive species of actin: recycled, cytoplasmic, and membrane-bound actin. The actin bound to the actin network can dissociate into recycled actin, R, which could be the slowly diffusing oligomers mentioned above. The recycled actin can reversibly rebind to the network or become faster diffusing cytoplasmic actin, G_C, with a lifetime τ_R. Fast diffusing cytoplasmic actin, G_C, can

reversibly bind to the network or become bound to the membrane with a spatially dependent rate, $k(x)$, where x is the distance from the leading edge of the cell. Then the membrane bound protein, G_M, can either bind to the network, or it can turn back into fast diffusing cytoplasmic protein, G_C, with a lifetime, τ_M. The rates for the diffuse pools of actin to become bound actin are calculated using SiMS data. This model is described by a set of partial differential equations. These partial differential equations are solved by allowing them to relax using the Monte Carlo method in a 2D particle simulation. FRAP and photoactivation can be modeled with this simulation by deleting particles in a region of interest (or outside the ROI) and advancing the simulation in time. Our 2D particle simulation is then propagated through time using the Monte Carlo method. In this section we conclude that diffusion is fast enough for delivery of diffuse actin to the leading edge of the cell and suggest that Thymosin $\beta 4$ aids in the fast diffusion of diffuse actin through the lamellipodium to the leading edge of the cell.

Third, we created a 3D model of the whole cell that includes only reaction and diffusion of actin. In doing this, we show that diffusion is sufficient for movement of actin to various parts of the cell without the need for an active transport mechanism which has been a matter of debate. The diffusion, however, is close to limiting. In the lamellipodium of our simulated cell we use a previously established model (from the previous two sections) which includes two diffuse pools of actin, one which is slowly diffusing and the other which diffuses more quickly, as well as a pool representing actin bound to the filamentous network. One difference is that we adjust this model to fit a circular geometry for the lamellipodium around the whole cell. We also consider actin in the cell center which is either diffuse or in filamentous form and can react to become the other state. The filamentous actin in the cell center is assumed to be either cortical actin or stress fibers. In this model the rates in which actin reacts to become another pool are taken from measurements done by SiMS and FRAP. With this whole cell model we are then able to simulate photoactivation and FRAP in various parts of the cell to compare with experiment and show that

diffusion and reaction can account for the effects seen in these studies with the ratio of polymerized actin to diffuse actin in the cell middle being an important factor. We discuss the implications for the proposal of the existence of diffuse actin specifically targeted to cell sub-compartments.

Chapter 1

Introduction to Actin Dynamics in the Lamellipodium

1.1 Lamellipodium of crawling cells

Cells move by various methods: blebbing, flagella, and crawling. In this dissertation we model proteins within the lamellipodium on cells that move by crawling with a lamellipodium. A lamellipodium is a thin (100-200 nm thick) sheet like protrusion on a cell (Figure 1.1 A). The lamellipodium is responsible for aiding in movement of cells that crawl. Within the lamellipodium there are many proteins. The protein that is responsible for much of the structure within the lamellipodium is actin. Actin is a globular protein that can polymerize and form a filament that is a double-stranded right-handed helix. There are many other proteins within the lamellipodium whose function is to regulate various aspects of actin polymerization and depolymerization.

Within the lamellipodium, actin forms a densely branched network, an example of this is shown in Figure 1.1. This image is taken using electron microscopy and the cell type is a fish keratocyte [4]. From this image, it can be seen that close to the leading edge the actin network is densely branched while far from the leading edge the filaments are long and not densely branched which suggests that some remodeling

occurs in between those spaces since retrograde flow is occurring which is a flow rearward of the entire network away from the leading edge [4].

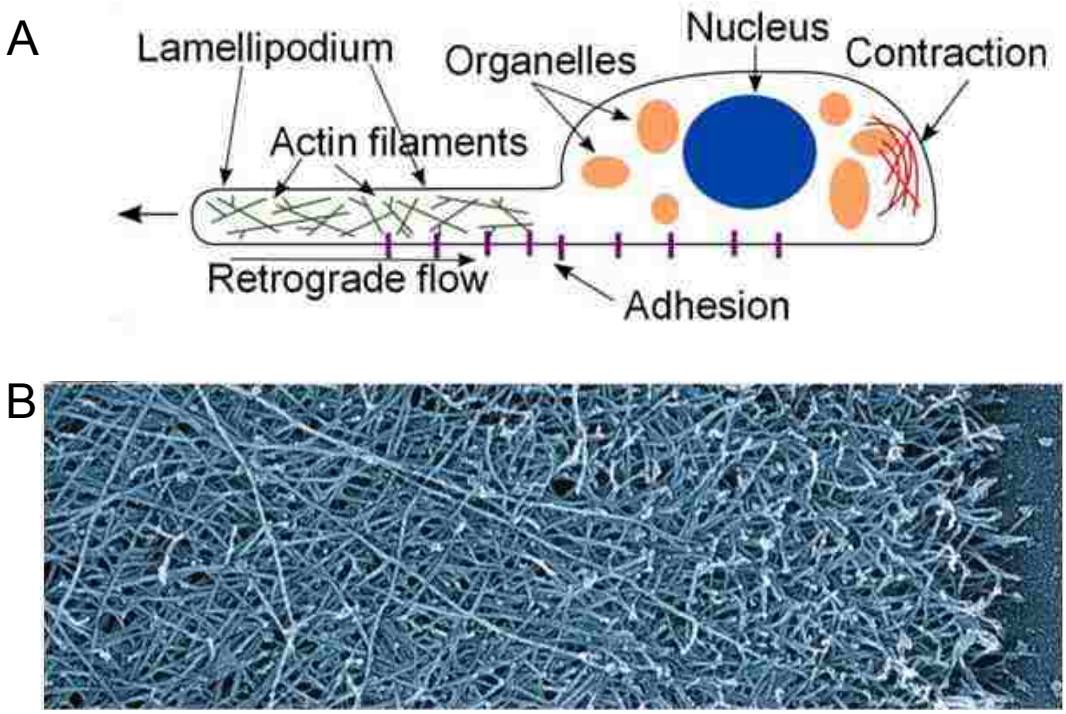

Figure 1.1: A) Cartoon of a crawling cell. B) Example of electron microscopy images of the actin network within the lamellipodium [4]

Actin is a polar filament and has a barbed and pointed end. The barbed end has a higher affinity than the pointed end for adding new monomers to its end while the pointed end has a higher affinity for depolymerizing than the barbed end does [4]. Filamentous actin is also referred to as F-actin. Monomeric actin is also called G-actin which stands for globular actin.

In the dendritic nucleation model described in [4] and shown in Figure 1.2 many actin regulators are present and each has a different function. In this model, F-actin undergoes retrograde flow away from the leading edge. As the ATP actin hydrolyzes and becomes ATP actin it will begin to disassemble away from the leading edge

either spontaneously or with the assistance of cofilin, which is a protein that aids in speeding actin filament severing, and it may disassemble into small pieces of filament called oligomers or it may disassemble directly into monomers [5]. It is unclear if the oligomers completely depolymerize or if they then rebind to the network [1].

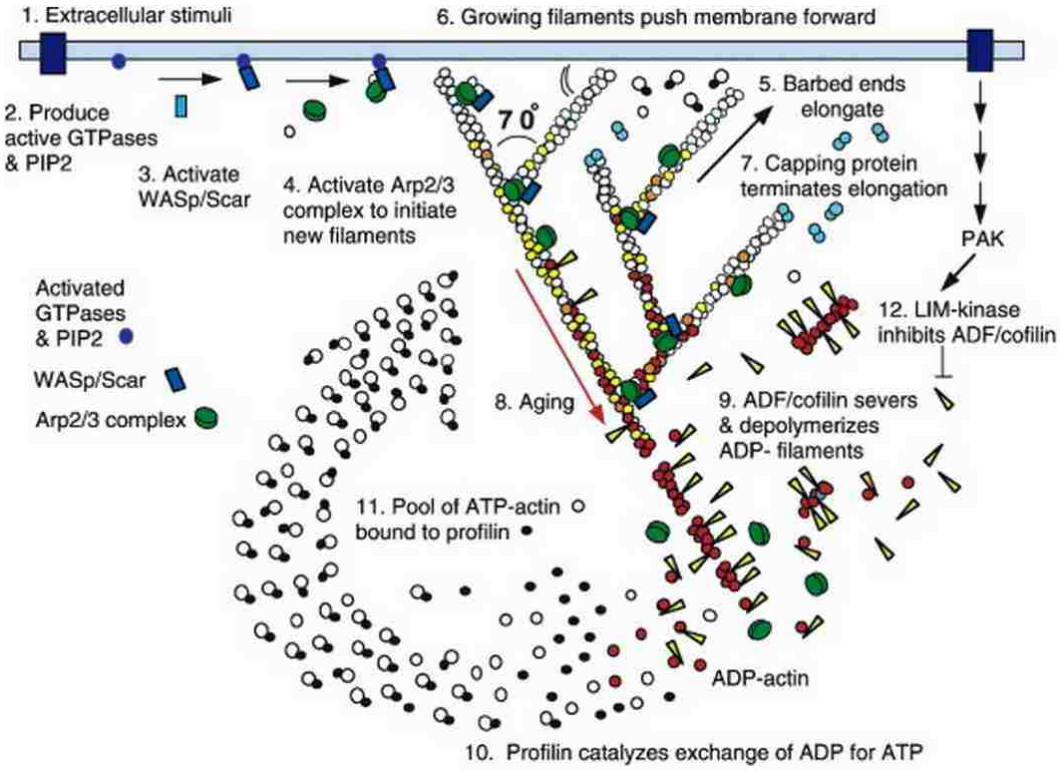

Figure 1.2: Dendritic Nucleation model from [4]

Some important regulating proteins within the lamellipodium are the Arp2/3 complex and capping protein. The Arp2/3 complex is an actin filament nucleator: it binds to the side of a pre-existing actin filament and then a new actin filament begins to grow off the old filament at an angle of 70 degrees between the two filaments [4]. Before the Arp2/3 complex can bind to an actin filament and nucleate a new filament must be activated first by an activating protein complex such as WASp or other various activators. WASP localizes near the membrane at the leading edge

and so the Arp2/3 complex must diffuse to the membrane so that it can bind to WASP. Recent experiments suggest that the Arp2/3 complex and WASp then diffuse together laterally along the membrane until they find a filament to bind to the filamentto in which case the activated Arp2/3 complex will bind and WASP will fall off [6].

Capping protein binds to the barbed end of the actin filament and prevents more actin monomers from being added to the filament. For in vitro studies, capping protein tends to stay bound to the actin network with a lifetime on the order of minutes [7], whereas in vivo studies find that capping protein has a lifetime of association of about 2 s [8].

In this thesis, we are trying to study how specific proteins individually associate and dissociate with the actin network in the lamellipodium. Our modeling focuses only on one protein at a time and does not directly take into account the effect of other proteins on the protein of interest. While modeling a certain protein we are interested in the effect of kinetics and turnover of that protein and the effect of slow diffusion (compared to an actin monomer) being included in the protein model. We want to know how oligomers (small fragments of filament that are slowly diffusing) affect the dynamics of the actin network. We also want to answer whether diffusion is fast enough to allow protein to get to the leading edge of the cell or if active transport is needed to aid in this. We are also interested in understanding the effect of geometry on diffusion of protein within the cell as well as how actin within the center of the cell affects actin dynamics within the lamellipodium; however, gradients can exist within the concentration profiles of each protein which suggests that diffusion would have some limits.

In this chapter I will introduce experimental methods that measure protein dynamics within live cells in order to understand how these techniques work especially in the context of comparing our simulations to experimental results produced by these methods. Some methods that will be discussed are: fluorescence recovery after photobleaching, single molecule speckle microscopy, photoactivation, fluorescence

decay after photoactivation, and fluorescence loss after photobleaching. Then I will introduce a previous model by Smith et al. [1] that I will later build upon to create some more accurate models for the Arp2/3 complex and capping protein as well as a model for actin that allows for the ability of the protein to bind to the membrane. I will also utilize this model in a whole cell model where I use the model from Smith et al. [1] for the reaction and diffusion of actin protein within the cell's lamellipodium. We will show that diffusion is fast enough for delivery of protein to the leading edge through our reaction diffusion models that compare well with experimental data.

1.2 Experimental methods for measuring protein dynamics in live cells

Observing protein movement within a live cell can be difficult because techniques that allow the best resolution within the cell also often require killing the cell, this defeats the purpose of observing protein dynamics. Below are a few techniques that involve live cell imaging.

1.2.1 Fluorescence Recovery after Photobleaching (FRAP)

Fluorescence recovery after photobleaching (FRAP) is a technique in which the cell is made to express a fluorescently tagged target protein [9]. A laser is shown in the region of interest (ROI) and the laser makes the fluorophores in that region stop fluorescing. For the duration of the experiment the fluorescent tag on the protein remains off. There are still fluorescently labeled proteins outside the region of interest at the time of bleaching which are then free to diffuse and then react in the ROI. An example of experimental FRAP is shown in Figure 1.3 A. In the 2nd panel down the fluorescence of EGFP-actin near the leading edge of the lamellipodium has been turned off in the ROI, but then as time progresses more fluorescence can be seen coming into the ROI. This is the recovery in intensity which is monitored and can

be seen in graphs in Figures 1.3 B and C, which monitors both the front (0-0.5 μm from the leading edge) and back (2.5-3.0 μm from the leading edge.)

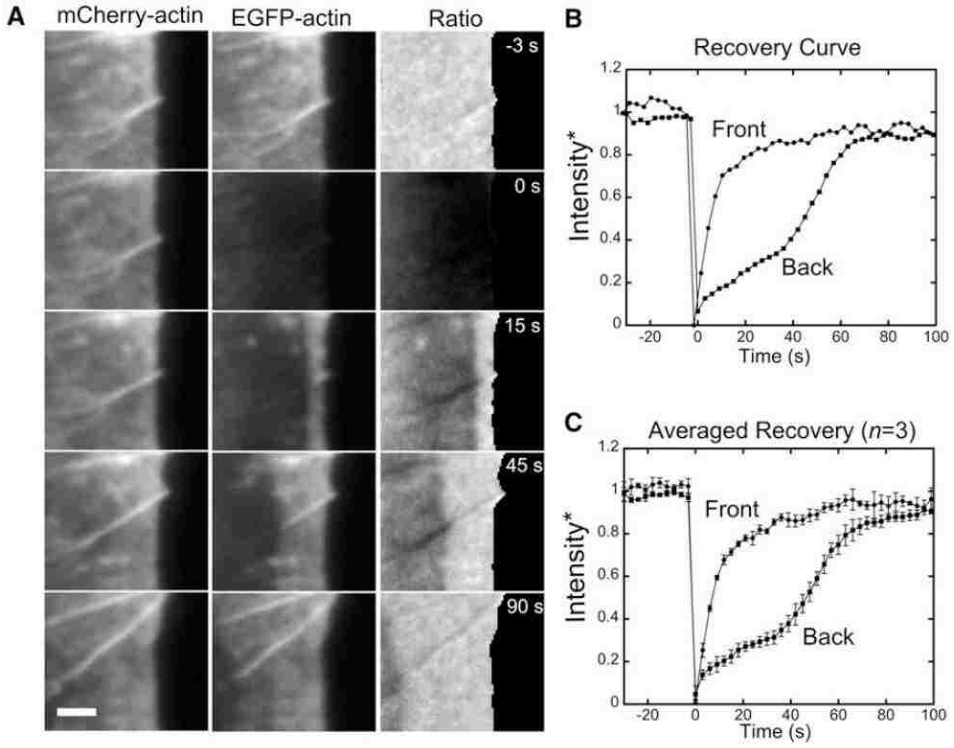

Figure 1.3: Example of FRAP of EGFP-actin in XTC cells at leading edge in Smith et al. [1] (A) Experimental FRAP performed on XTC cells, Left column: mCherry-actin tagged, center column: EGFP-actin tagged, right column: ratio of EGFP-actin to mCherry-actin channel [1] (B) Normalized recovery curves of a single FRAP experiment with the front curve measured from 0-0.5 μm and the back measured from 2.5- 3.0 μm from the leading edge.[1] (C) FRAP recovery curves for 3 experiments instead of one, measured in the same way as in (B) [1]

From these curves it is possible to measure the recovery times to learn about time scale of the turnover of the actin network. It is also possible to measure the retrograde flow rate from the recovery curves. One problem with FRAP is that the laser intensity used in order to turn off the fluorophores is often very high. A very

intense laser has the potential to cause damage to the cell which is why it is very important to monitor the cell throughout the experiment to make sure damage is not occuring. The left column of Figure 1.3 A is an example of a control experiment to watch the underlying actin structures to ensure they are not damaged within the cell by the laser [1].

1.2.2 Single Molecule Speckle Microscopy (SiMS)

Single molecule speckle microscopy (SiMS) is a live cell imaging technique for observing single molecules moving within a cell. The cell is made to express a very low concentration of a GFP-tagged protein as opposed to a high concentration of EGFP-actin, an example of which is seen in Figure 1.4 A [10]. Then a portion of the lamellipodium is imaged such that it is possible to see single fluorophores. The imaging takes place with an exposure time of the camera which is typically 0.5-1.0 s. This exposure time makes is possible to see fluorophores which are bound to the network very brightly as speckles and diffusing fluorophores are seen as broadly distributed clouds [1].

A speckle is defined as a single fluorophore which is bound to protein that has incorporated into the actin network [10]. Examples of these speckles can be seen in Figure 1.4 B. Since the speckles appear when they bind to the network, where the binding event occurs can be measured as a function of distance from the leading edge. These events can be recorded and then binned into a histogram of appearances shown in Figure 1.4 C which is called an appearance profile. How long the speckle remains attached to the actin network is also measured. The speckle is tracked throughout time, and the time the speckle remains bound is called the speckle lifetime. The speckle lifetimes are binned and put into a histogram of speckle lifetimes shown in Figure 1.4 D.

Similarly to FRAP it is possible to measure the retrograde flow of the network along with time scales of the turnover with SiMS microscopy. However SiMS microscopy can also give information about protein dynamics at a small scale including

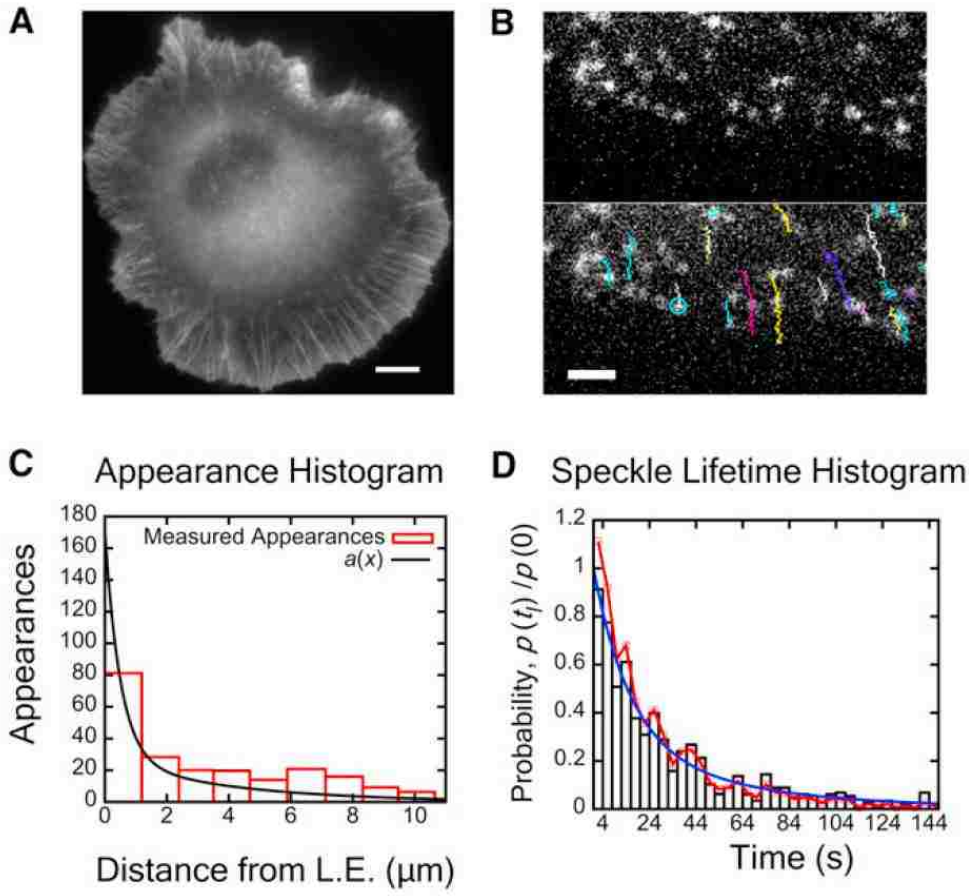

Figure 1.4: Example of XTC SiMS data (A) Example of XTC cell expressing EGFP-actin at a concentration high enough to see structures such as F-actin bundles within lamellipodium Scale bar 8 μm [1] (B) Example of SiMS image of small portion of the lamellipodium. Scale bar 2.65 μm [1] (C) Histogram of speckle appearances (binding events) as a function of distance from the leading edge Scale bar 8 μm [1] (D) Histogram of speckle lifetimes which is how long the speckle remains bound to the actin network. Scale bar 8 μm [1]

information about binding and unbinding events.

1.2.3 Photoactivation (PA)

Photoactivation is a technique in which a live cell is made to express a protein that has an attached photoactivatable fluorescent tag. A laser is then shown on the region of interest [11]. This makes the tags within the ROI begin to fluoresce. One can then watch how the fluorescence decays within the ROI and how the fluorescence then moves outside of the ROI [11]. An example of this technique is seen in Figure 1.5 where the entire center of the cell is photoactivated. Then the fluorescence quickly moves to the leading edge of the cell [12]. The fluorescence intensity increase at the leading edge and the fluorescence intensity decrease in the center of the cell can be quantified over time in Figure 1.5 B.

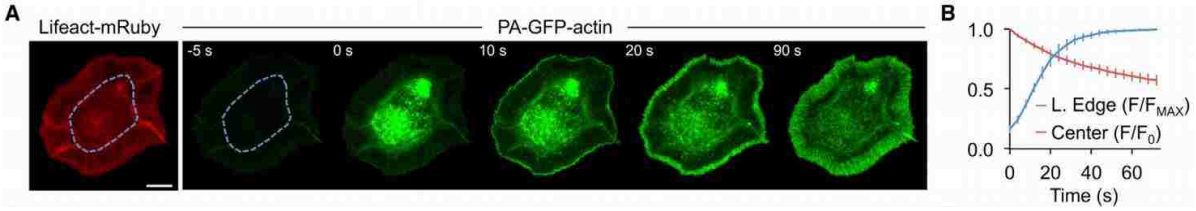

Figure 1.5: Example of Photoactivation in a CAD cell from Vitriol et al. (A) Example of Photoactivation of cell center in [12] (B) Normalized fluorescence intensities over time in the cell center and at the leading edge from [12]

1.2.4 Fluorescence Decay after Photoactivation (FDAP)

Fluorescence decay after photoactivation is a technique in which a region is photoactivated and then the decay in fluorescence within that region is observed to study how diffusion and reaction of the fluorescently tagged protein is occurring within that region. Another method of FDAP is s-FDAP which stands for sequential-FDAP and is used to measure changes in a protein's localization and movement within a cell as well as the concentration of the photoactivated protein [13]. A diagram of the process of FDAP is shown in Figure 1.6 A. First the entire sample is photobleached to allow for less noise, then a small portion of the sample is photoactivated and allowed to

decay in fluorescence intensity. The fluorescence decay is monitored and once a new plateau of fluorescence is reached a mobile and immobile fraction can be measured against the original fluorescence level as seen in the figure [13]. Figure 1.6 B shows what a graph of the intensity of the fluorescence would look like over time for FDAP [13].

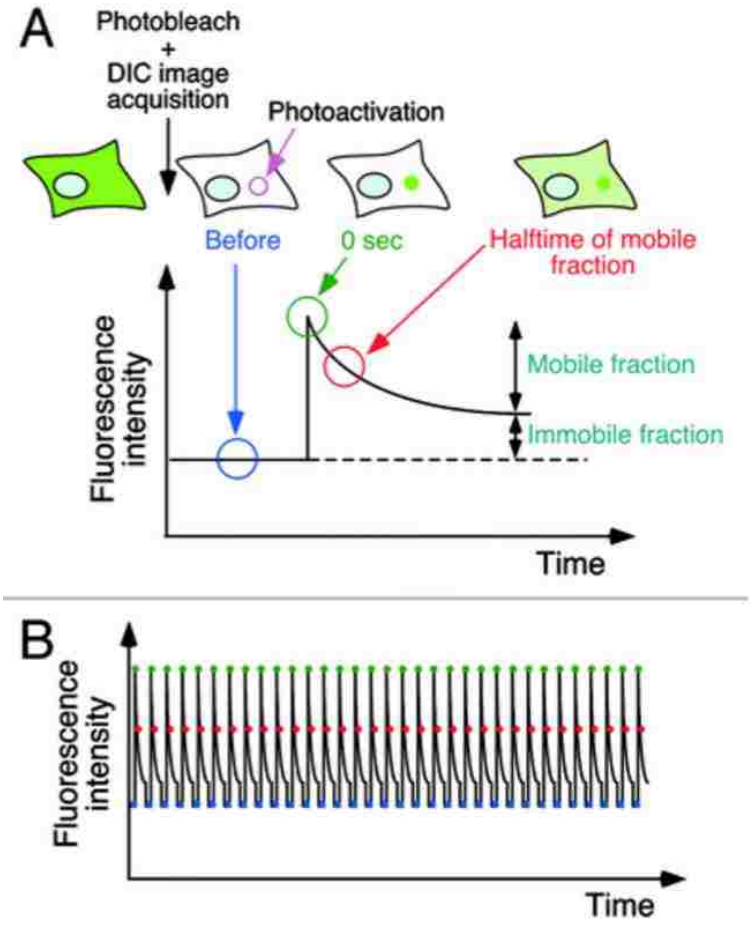

Figure 1.6: Example of FDAP from Kiuchi et al. A) Diagram showing the process of FDAP. B) Graph showing s-FDAP intensity over time. Figure from [13]

1.2.5 Fluorescence Loss after Photobleaching (FLAP)

The technique fluorescence loss after photobleaching (FLAP) is very similar to the technique fluorescence recovery after photobleaching (FRAP). Both techniques involve a cell expressing a certain fluorescent protein and then turning off that fluorescence within a certain region. The difference is that with FRAP, the region that is bleached is the region of interest and the recovery of fluorescence within that region is monitored. However, with FLAP, how the loss of fluorescence spreads throughout the cell is more of interest than the region that is bleached [14].

1.3 Previous Models of Actin Turnover in the Lamellipodium

Previous work on modeling EGFP-actin FRAP data while utilizing actin SiMS data was done in [1]. This was done in order to address a controversy in the field which is that SiMS and FRAP data seem to disagree. Most of the FRAP recovery occurs very near to the leading edge which would mean that almost all the binding events to F-actin also occur very near to the leading edge (Figure 1.3). However, SiMS microscopy data shows that binding to the actin network is actually distributed throughout the lamellipodium as seen in Figure 1.4 C.

In the paper by Smith et al. [1], two models are presented: a model considering monomers as the only diffuse actin species and the model with both monomers and oligomers contributing to appearance events [1]. The model considering monomers as the only diffuse actin species in Figure 1.7 A allows for only two pools of actin: F-actin and G-actin, while the model with both monomers and oligomers contributing to appearance events which is in Figure 1.7 B allows for three pools of actin: F-actin, G-actin and O-actin. F-actin is filamentous actin, G-actin is globular actin (or monomeric actin) and O-actin is oligomeric actin.

The appearance rate (Figure 1.4 C) is used in the calculation of the rates to

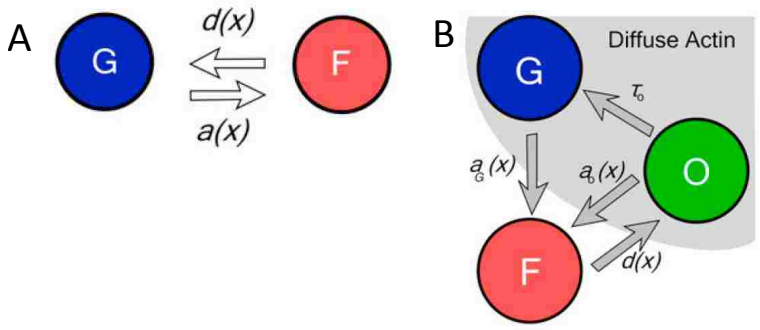

Figure 1.7: Two models in Smith et al. (A) Diagram representing model with monomers as only diffuse actin species (B) Diagram representing model with both monomers and oligomers contributing to appearance events [1]

become F-actin is defined as

$$a(x) = G_\infty K \left[A_1 e^{-x/\lambda_1} + A_2 e^{-x/\lambda_2} \right], \tag{1.1}$$

where x is the distance from the leading edge and the constants A_1, A_2, λ_1, and λ_2 in 1.1 are found by fitting the appearance profile found using the SiMS appearance profile and fitting it with a double exponential [1]. It is imposed for this definition that $A_1 + A_2 = 1$. In the model with both monomers and oligomers contributing to appearance events the term in this appearance rate with λ_1 corresponds to the appearances due to G-actin, while the term with λ_2 corresponds to the appearances due to O-actin. The parameter G_∞ is the concentration of G-actin far from the leading edge, and the parameter K adjusts the ratios of F- to G-actin.

Lifetimes measured in the SiMS microscopy technique (Figure 1.4 D) can also be fitted with a double exponential:

$$\frac{p(t)}{p_0} = C_1 e^{-t/\tau_1} + C_2 e^{-t/\tau_2}, \tag{1.2}$$

where τ_1 and τ_2 are lifetimes of F-actin and C_1 and C_2 are coefficients that allow for a good fit to the measured histogram of lifetimes from SiMS.

The appearance profile (Equation 1.1) and the lifetime distribution (Equation 1.2) are then used to find the profile of F-actin concentration. In order to find the bound profile, a Green's function is needed:

$$Y(x, x') = \Theta(x - x')\frac{1}{v_r}\int_{\frac{x-x'}{v_r}}^{\infty} p(t)dt. \tag{1.3}$$

This Green's function tells how much F-actin that starts at x' moves to x by retrograde flow (v_r) without dissociating [1]. The F-actin steady state profile as a function of distance from the leading edge can then be written:

$$F(x) = \int_0^{\infty} Y(x, x')a(x')dx'. \tag{1.4}$$

The function, $F(x)$, can then be used to write diffusion reaction equations for the model considering monomers as the only diffuse actin species (Figure 1.7 A). The retrograde flow of F-actin is balanced by appearances and disappearances, as is the diffusion of G-actin [1]

$$v_r\frac{\partial F(x)}{\partial x} = D\frac{\partial^2 G(x)}{\partial x^2} = a(x) - d(x). \tag{1.5}$$

In this equation, $G(x)$ is the G-actin concentration profile as a function of distance from the leading edge. Equation 1.5 can then be solved for $G(x)$,

$$G(x) = G_{\infty} - \frac{v_r}{D}\int_x^{\infty} F(x')dx'. \tag{1.6}$$

Both $G(x)$ and $F(x)$ are shown in Figure 1.8 A-B for the model considering monomers as the only diffuse actin species with K values of 0.5 s^{-1} or 0.75 s^{-1} respectively and a retrograde flow rate of $v_r = 0.05$ μm/s and a diffusion coefficient of D = 4 $\mu m/s^2$ [1].

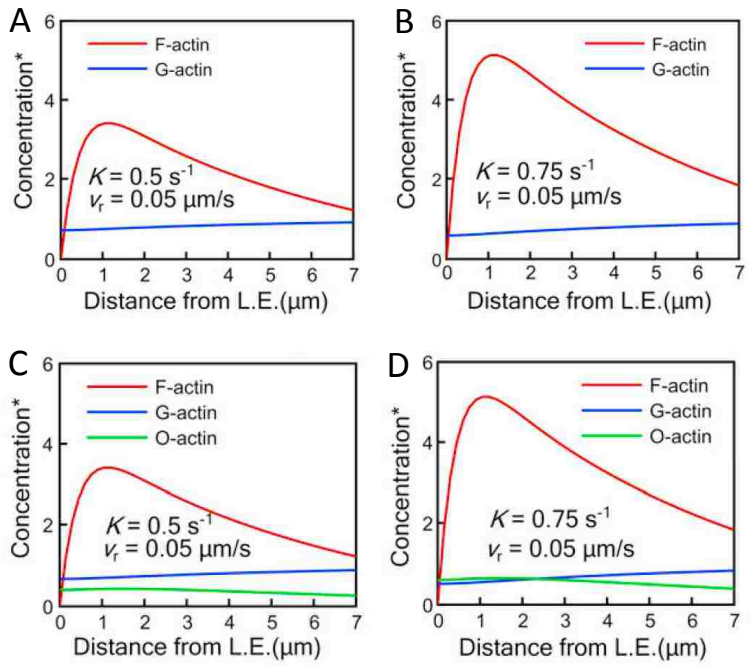

Figure 1.8: Steady State profiles for model with single diffuse species and model with two diffuse species (A-B) Steady state profiles for the model with only monomers as diffuse species with different K values (C-D) Steady state profiles for the model with monomers and oligomers as diffuse species with different K values [1]

Then with these models, the authors in [1] implemented a stochastic 2D particle simulation to simulate FRAP. The rates in which the diffuse protein becomes F-actin are,

$$r_{G\to F}(x) = \frac{a_G(x)}{G(x)}. \tag{1.7}$$

The rates for the model considering monomers as the only diffuse actin species are shown in Figure 1.9 A. FRAP is simulated by deleting all particles within the region of interest. The system then advances forward in time where at each time step, the program then decides how to advance each particle based on the rules that follow. If the particle is in the G-actin pool, then the particle can bind with the

rate given in equation 1.7 or if it does not bind the particle in the G-actin pool will diffuse. If the particle is in the F-actin pool, then the lifetime of that particle is compared to the time in which that particle has been in the F-actin pool. When the lifetime is up the particle in the F-actin pool goes into the G-actin pool and begins to diffuse.

An example of the FRAP simulation for the model considering monomers as the only diffuse actin species is shown in Figure 1.9 B and the recovery for FRAP is shown in Figure 1.9 C where the front recovery and back recovery are monitored. The front is defined as 0-0.5 μm from the leading edge while the back is defined as 2.5-3.0 μm from the leading edge. This is compared to experimental FRAP data which is included in Figure 1.9 C for comparison. The parameter K is varied to find a fit to the experimental data and a value of K of 0.75 s^{-1} has the best fit to experimental data [1]. The front of the lamellipodium recovers quickly, while comparatively the back of the lamellipodium recovers more slowly. However, the back recovery does have a small amount of initial recovery that is very slow until the retrograde flow brings the F-actin that assembled near the leading edge to the back of the lamellipodium which causes recovery to happen much more quickly.

In the model with both monomers and oligomers contributing to appearance events shown in Figure 1.7 B the steady state reaction diffusion equations are as follows

$$v_r \frac{\partial F(x)}{\partial x} = a_o(x) + a_G(x) - d(x) \tag{1.8}$$

$$D_G \frac{\partial^2 G(x)}{\partial x^2} = a_G(x) - \frac{1}{\tau_o} O(x) \tag{1.9}$$

$$D_o \frac{\partial^2 O(x)}{\partial x^2} = a_o(x) - d(x) + \frac{1}{\tau_o} O(x) \tag{1.10}$$

F-actin is the same as given in Equation 1.4 [1]. Equations 1.8-1.10 can be solved analytically for $O(x)$ and $G(x)$:

$$O(x) = \tau_o \cosh\left(\frac{x}{\sqrt{D_o \tau_o}}\right) \int_o^\infty f(x') \exp\left(\frac{-x'}{\sqrt{D_o \tau_o}}\right) dx' - \tau_o \int_0^x f(x') \sinh\left(\frac{x - x'}{\sqrt{D_o \tau_o}}\right) dx', \tag{1.11}$$

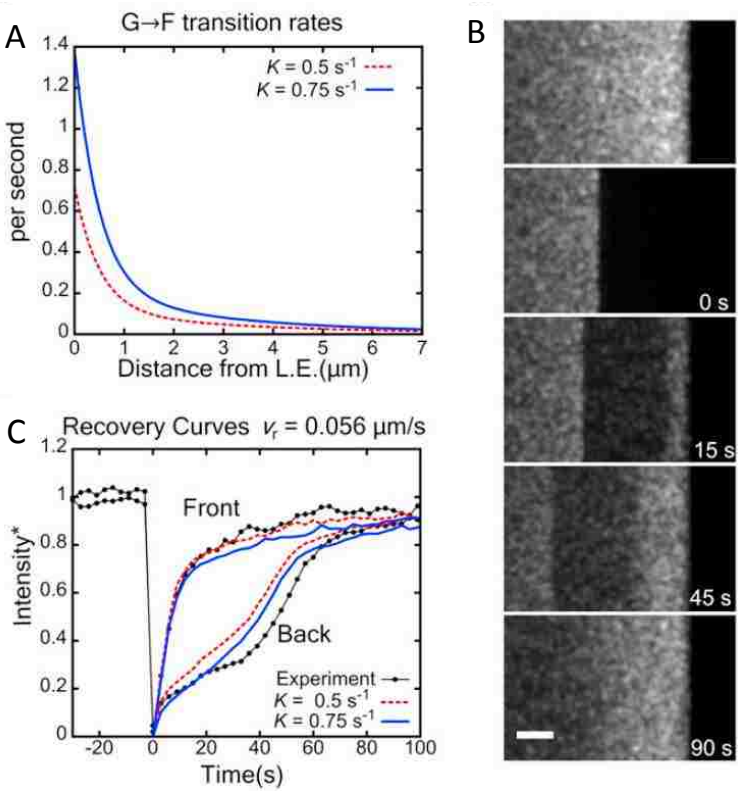

Figure 1.9: Recovery from model with monomers as only diffuse species (A) Reaction rates from both G-actin to F-actin (B) Example of FRAP simulation images for the model with monomer as only diffuse species simulation Scale bar: 2 μ m (C) Recovery for the model with monomer as only diffuse species simulation front and back of lamellipodium where front is 0-0.5 μm from the leading edge and back is 2.5-3.0 μm [1]

$$G(x) = G_\infty - \frac{D_o}{D_G} O(x) - \frac{v_r}{D_G} \int_x^\infty F(x')dx', \tag{1.12}$$

where $f(x) = a_G(x) - v_r \partial F(x)/\partial x$ [1]. The graphs of the steady state equations for the model with both monomers and oligomers contributing to appearance events are shown in Figure 1.8 C-D. From these equations one can calculate the binding

rate of the the oligomers to F-actin,

$$r_{O\to F}(x) = \frac{a_o(x)}{O(x)}. \tag{1.13}$$

This rate along with the rate for G-actin to F-actin are shown in Figure 1.10 A. FRAP simulations were done for the model with both monomers and oligomers contributing to appearance events similar to those done for the model considering monomers as the only diffuse actin species [1]. The steps for each particle at each time step are also similar to the previously described model except that one new species of particle is added. Instead of the F-actin becoming G-actin when the lifetime is up, the F-actin will now become O-actin when the lifetime is up. Then the O-actin can either bind to the network with a binding rate in Equation 1.13 or it can diffuse slowly with $D = 0.5\ \mu m^2/s$ until its lifetime is up in which case it will become G-actin.

An example of the FRAP simulation run with the model with both monomers and oligomers contributing to appearance events is shown in Figure 1.10 B. The recovery curves are plotted in Figure 1.10 C. Compared to the model considering monomers as the only diffuse actin species, the model with both monomers and oligomers contributing to appearance events gives a better fit to the experimental data. This is likely because the lag in recovery at the back of the lamellipodium is caused by oligomers rebinding locally to the F-actin network [1].

Another model by Lewalle et al. [15] models FRAP and photoactivation using a probabilistic model that has a set length scale of each factor such as incorporation and dissociation of the actin network as well as barbed and pointed ends and assumes that they are proportional. In the end all barbed, pointed, capped ends and junctions decay with the same length scale away from the leading edge. Their model includes distributed turnover, but no oligomers and assumes that the diffusion of G-actin is fast. In this model, the authors simulated FRAP and find a good fit from their theoretical model with their experimental FRAP [15].

Some previous models have been proposed to describe lamellipodial actin dynamics similarly to Smith et al [1]; however, they account only for polymerization

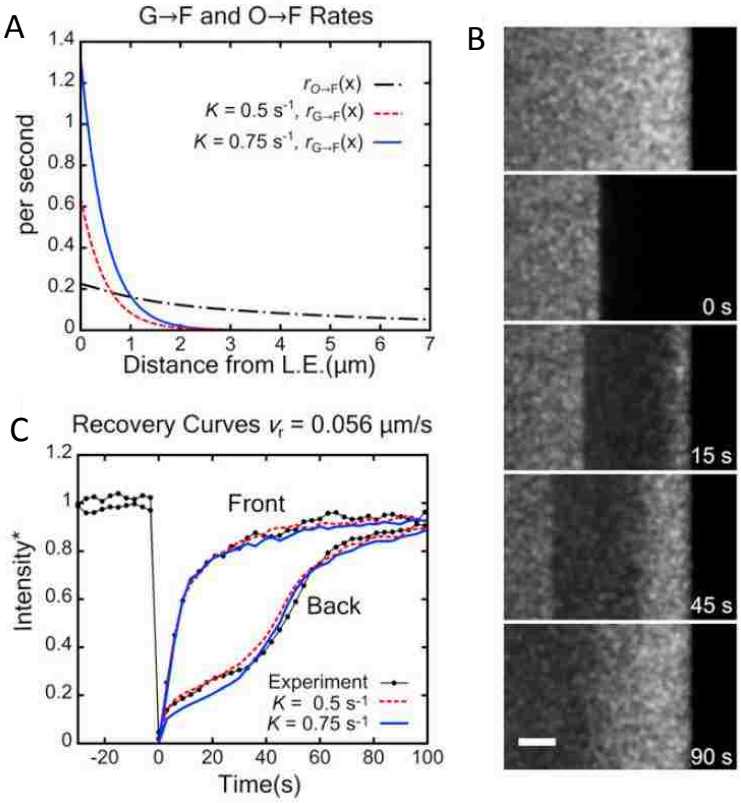

Figure 1.10: Recovery for model with monomers and oligomers as diffuse species (A) Reaction rates from both O and G-actin to F-actin (B) Example of FRAP simulation images for the model with monomers and oligomers as diffuse species simulation Scale bar: 2 μm (C) Recovery for the model with monomers and oligomers as diffuse species simulation front and back of lamellipodium where front is 0-0.5 μm from the leading edge and back is 2.5-3.0 μm [1]

of actin at the leading edge of the cell [16, 17, 18, 19]. Others have utilized known reactions at the leading edge and include assembly and disassembly throughout the lamellipodium [20, 21, 22, 23]. However, [20, 21, 22, 23] do not model FRAP or utilize SiMS data in their models and simulations. Another study was done to model FLAP [24]; however, this model did not include distributed turnover of actin throughout the leading edge [1].

1.4 Outline for thesis

In this thesis I will address the turnover of actin and regulators in three sections. First, I will discuss the diffusive dynamics of capping protein and the Arp2/3 complex in the lamellipodium by utilizing a reaction and diffusion model and implementing that with a 2D Monte Carlo particle simulation. It is also debated whether SiMS microscopy data and FRAP data are compatible because they seemingly give opposing results; we will show that these two techniques are compatible for these two proteins but highlight different aspects of the dynamics of these proteins. It is estimated that approximately 50% of diffuse capping protein in the lamellipodium is slowly diffusing [25]. We want to study implications of why the capping protein is slowly diffusing and suggest mechanisms that may be occurring. The possibilities are that either it is slowly diffusing while bound to an actin oligomer or it is bound to the membrane and diffusing slowly on the membrane of the cell. We compare model results that include each of these separately and suggest experiments to distinguish the two possibilities. The Arp2/3 complex is also known to diffuse slowly [6]. The authors in [6] observe the Arp2/3 complex diffuses slowly on the membrane in a lateral fashion before incorporating into the actin network and undergoing retrograde flow with the network. We make a model based on this observation and compare our model with FRAP experiments.

Second, I will study actin dynamics within the lamellipodium while comparing to photoactivation experiments in Cath.a differentiated cells. In this study we are interested in explaining the enhancement of G-actin measured at the leading edge of these cells as well as finding if diffusion is sufficiently fast for allowing fluorescently tagged actin to arrive at the leading edge of these cells without active transport. We also study the effect of Thymosin $\beta 4$ knockdown on actin turnover dynamics and kinetics. In order to do this we use a model that accounts for three separate diffuse pools of actin, each with different kinetics, as well as one bound pool of actin. This model is implemented into a 2D Monte Carlo particle simulation that allows for simulation of both FRAP and photoactivation.

Third, our 2D simulation used in the previous 2 sections is limited in that it does not account for geometry of the cell or actin within the center of the cell, which is where a large portion of the actin resides within a cell. Similar models described above are used within the lamellipodium portion of the 3D simulated cell but are simply extended to 3D and written in polar coordinates. Medial actin is also added both in diffuse form as well as bound form. The bound actin within the cell center is assumed to be either in stress fibers, non-stress fibers, or cortical actin which are the main types of F-actin in the cell middle. These 3D simulations are used to compare to photoactivation experiments performed in [12]. We also want to address a debate within the field if diffusion is fast enough for delivery of actin monomers to the leading edge of the cell or if active transport is needed [24, 26] and find if a portion of actin within the lamellipodium stays within the lamellipodium and does not diffuse into the cell center.

The models included in this thesis are not complete models that include every regulator that could possibly affect each protein. Instead each model is a part that intends to answer smaller questions with the end goal that at some point enough knowledge could be gathered to make a model that includes all regulators within a cell to understand all protein kinetics and how each protein affects the others.

Chapter 2

Diffusive Dynamics of Capping Protein and Arp2/3 Complex in the Lamellipodium

2.1 Introduction

As discussed in Chapter 1, the lamellipodial protrusions at the leading edge of motile cells have been studied extensively, both due to their importance in cell motility and as model systems of cytoskeletal dynamics [27, 28, 29, 30, 31]. In the lamellipodium, actin filaments form a dynamic network that polymerizes primarily close to the leading edge of the cell, with the filament barbed ends pointing toward the cell membrane. In the dendritic nucleation model, many of these filaments are created as branches off pre-existing filaments [4]. Filament capping by capping protein (CP) regulates the concentration of free ends. As filaments polymerize, the whole actin network undergoes retrograde flow towards the cell center. The difference between the rates of polymerization and retrograde flow results in net lamellipodial protrusion or retraction. The actin subunits in the filament that move towards the back of the network break off from the filament network due to cofilin-induced severing into

oligomers. The disassembled pieces further depolymerize into monomers and are recycled close to the leading edge by diffusion. Since all lamellipodial components have to be recycled, the transport of disassembled proteins through the cytoplasm back towards the leading edge is an important component of the kinetics in lamellipodia. Some studies suggested that diffusion is fast enough to deliver actin subunits to the leading edge [13, 12] while others have proposed a role for active transport mechanisms [24, 26]. As discussed in chapter 1, theoretical work has shown how diffusion may become limiting, depending on both the value of the diffusion coefficient in the cytoplasm as well as the spatial distribution of sources and sinks of actin subunits in the cytoplasm [20, 1]. One of the difficulties in directly measuring the existence of gradients of diffuse actin experimentally is that the diffuse population is a small fraction of the actin in filaments. Further, the dynamics in photoactivation or photobleaching experiments reflect a combination of reaction and diffusion that can be hard to disentangle [1, 32] . Recent studies have shown how mathematical models based on data obtained by single molecule speckle (SiMS) microscopy can be combined with fluorescence recovery after photobleaching (FRAP) or photoactivation (PA) studies to model the dynamics of the diffuse actin pool [12, 1] . In SiMS, cells contain fluorescently labeled proteins at a concentration sufficiently low to resolve single molecules [10]. If a fluorescent protein is diffusing freely in the lamellipodium, it will appear as a diffuse background or localized cloud, depending on its diffusion coefficient and the exposure time of the camera. When the tagged protein binds to the actin network it appears as a speckle undergoing retrograde flow while it remains bound to the network. Speckle disappearance reflects dissociation of the tagged protein to the diffuse pool. By contrast, cells in FRAP or PA experiments typically contain a large fraction of labeled protein that leads to spatially extended intensity fields, the redistribution of which around an area of interest reflects the dynamics of reaction, retrograde flow, and diffusion [1]. The model of Smith et al. [1] used SiMS data as input to suggest that accounting for a population of slowly diffusing actin oligomers, the result of actin filament severing, allows for a better fit of the

model to the FRAP data due to local release and rebinding to the actin filament network. Comparison of an extension of the Smith at el. model to photoactivation PA experiments further supported the existence of a recycling pool at the back of the lamellipodium together with a fast-diffusing pool that delivers subunits close to the leading edge at nearly the diffusion-controlled rate [12]. Capping protein and the Arp2/3 complex are two of the most important regulators of actin dynamics in cells and in in vitro reconstitution experiments [33]. This chapter extends the approach of Smith et al. to the study of the diffusive dynamics of capping protein and Arp2/3 complex for which both SiMS and FRAP data have been performed in lamellipodia (albeit by different groups on different cell systems). Similar to the case of diffuse actin, it is possible that both exhibit significant concentration gradients in their diffuse pool. For example, slowly-diffusing capping proteins have indeed been observed by SiMS [25], which may reflect capping protein bound to slowly-diffusing actin oligomers or to the membrane. The Arp2/3 complex has also been observed to form a slowly-diffusing complex with its activators prior to attachment to the actin network [6] . However the implications of this observation on its turnover kinetics has not been modeled. In the following sections we first introduce the general framework of our mathematical model with one bound species and two diffuse populations. We then proceed to apply it to capping protein and Arp2/3 complex dynamics to derive concentration profiles across the lamellipodium at steady state. The focus throughout is on lamellipodia of stationary cells at steady state with steady retrograde flow and no net protrusion and retraction. We discuss the implications of the calculated concentration gradients in the control of cell motility.

2.2 Methods

2.2.1 Calculating Steady State Profiles

Since proteins in the lamellipodium are frequently associating to larger complexes or binding to the membrane, we consider the simplest model to account for this

behavior that has two distinct cytoplasmic populations. A fast diffusing cytoplasmic population, C_{fast}, and a slow diffusing cytoplasmic population, C_{slow}, are shown in the cartoon of the model in Figure 2.1, which is an extension of the model used in Smith et al. [1]. Bound cytoplasmic protein, B, can depolymerize into either C_{fast} with probability s_1 or C_{slow} with probability s_2, where $s_2 = 1 - s_1$. The diffuse protein C_{fast} can become bound protein with spatially dependent rate $r_{C_{fast}}(x)$, and C_{slow} can become bound with spatially dependent rate $r_{C_{slow}}(x)$, where x is the distance from the leading edge. The diffuse component C_{fast} can become C_{slow} with a lifetime of τ_{Cfast}, and the component C_{slow} can become C_{fast} with a lifetime of $\tau_{C_{slow}}$.

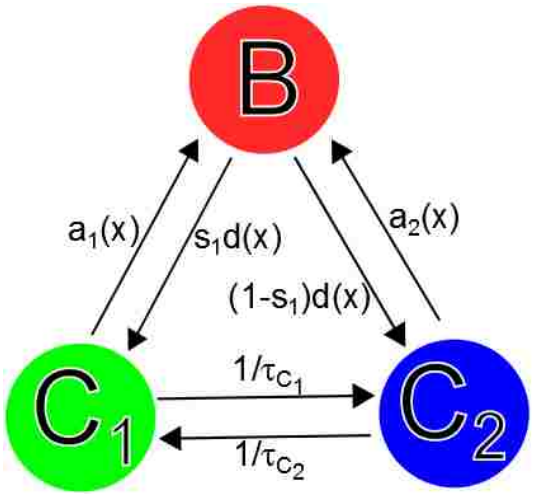

Figure 2.1: Diffusion reaction model for actin binding proteins and protein complexes in lamellipodia. The three species are bound (B), fast diffusing in the cytoplasm (C_{fast}), and slow diffusing in the cytoplasm (C_{slow}). The lifetimes of C_{fast} and C_{slow} respectively are $\tau_{C_{fast}}$ and $\tau_{C_{slow}}$. The appearance rates $a_{C_{fast}}(x)$ and $a_{C_{slow}}(x)$ that depend on the distance to the leading edge x are defined in Equations 2.2 and 2.3 and the detachment rate $d(x)$ is defined in Equation 2.8. The parameter s_1 is the probability for the bound protein to dissociate into C_{fast} and $s_2 = 1 - s_1$.

In SiMS microscopy (Figure 2.2A), each speckle that appears is a fluorescently tagged protein that becomes bound from the cytoplasmic pool. Where the speckle

appears with respect to distance from the leading edge is recorded and the appearances are then binned in a histogram. This appearance profile, an example of which is shown in Figure 2.2B, is the sum of two separate appearance profiles, $\mathrm{a}_{\mathrm{C_{fast}}}(x)$ and $\mathrm{a}_{\mathrm{C_{slow}}}(x)$, due to the fast and slow cytoplasmic pools as follows:

$$a(x) = a_{\mathrm{C_{fast}}}(x) + a_{\mathrm{C_{slow}}}(x). \tag{2.1}$$

The units of $a(x)$ are μM/s. While in some cases it is possible to use SiMS to monitor the diffusive state of the protein prior to becoming bound, how the profile is split into two components can be an assumption of the model. Generally, the speckle appearance profile can be fitted by a double exponential with two length-scales λ_{short} and λ_{long}. We define $\mathrm{C_{fast,\infty}}$ and $\mathrm{C_{slow,\infty}}$ to be the concentrations of $\mathrm{C_{fast}}$ and $\mathrm{C_{slow}}$ respectively at distances far from the leading edge of the cell. Using $\mathrm{C_\infty} = \mathrm{C_{fast,\infty}} + \mathrm{C_{slow,\infty}}$ to normalize concentrations, the constant K defines the magnitude of the association reactions:

$$a_{\mathrm{C_{fast}}}(x) = KC_\infty \left(A_1^{\mathrm{C_{fast}}} e^{-x/\lambda_{\mathrm{short}}} + A_2^{\mathrm{C_{fast}}} e^{-x/\lambda_{\mathrm{long}}} \right) \tag{2.2}$$

$$a_{\mathrm{C_{slow}}}(x) = KC_\infty \left(A_1^{\mathrm{C_{slow}}} e^{-x/\lambda_{\mathrm{short}}} + A_2^{\mathrm{C_{slow}}} e^{-x/\lambda_{\mathrm{long}}} \right), \tag{2.3}$$

where the dimensionless coefficients in Equations 2.2 and 2.3 satisfy $\mathrm{A}_1^{\mathrm{C_{fast}}} + \mathrm{A}_2^{\mathrm{C_{fast}}} + \mathrm{A}_1^{\mathrm{C_{slow}}} + \mathrm{A}_2^{\mathrm{C_{slow}}} = 1$.

SiMS microscopy also measures the lifetime distribution for protein speckles, $p(t)$ that typically shows weak dependence upon distance from the leading edge, within a range of a few μm [10, 25, 8]. In the examples we consider in this chapter, it is fitted with a single exponential:

$$p(t) = 1/\tau \left(e^{-t/\tau} \right). \tag{2.4}$$

An example of a lifetime distribution is shown in Figure 2.2C for capping protein speckles. The bound protein profile, $B(x)$, can be calculated analytically using the

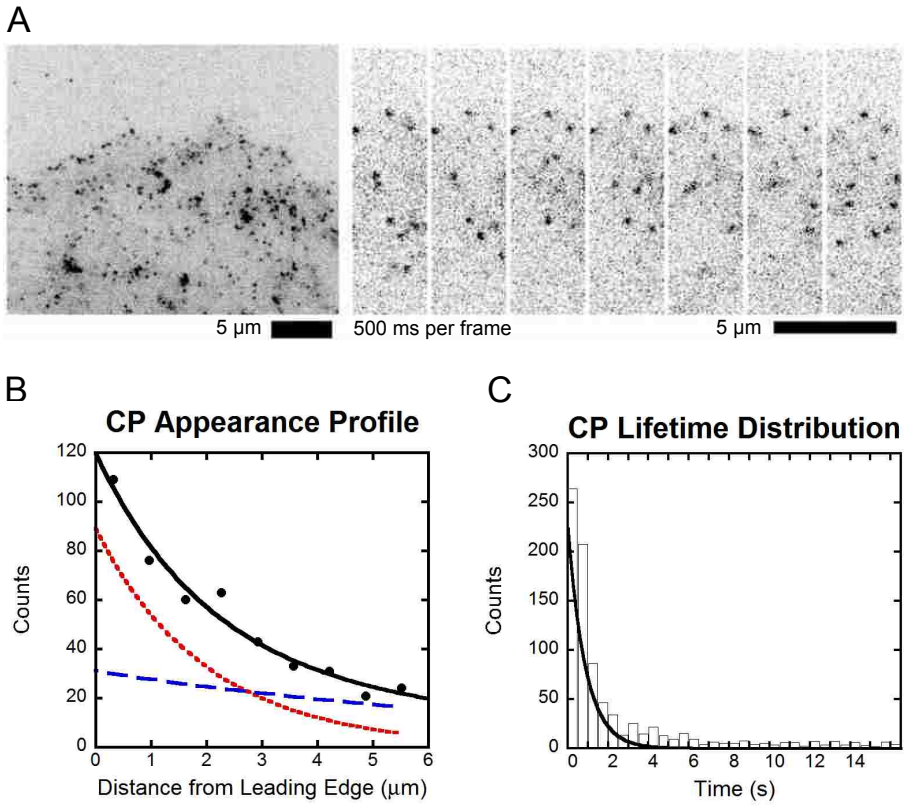

Figure 2.2: Capping protein single molecule speckle microscopy data. (A) Example image of SiMS microscopy in an XTC cell expressing EGFP-CPβ1 (left) and time lapse images (right) [8]. (B) Appearance profile for capping protein fit with a double exponential. Dashed (blue) and dotted (red) curves are each the separate single exponential distributions (A_1=0.74 A_2=0.26 λ_{short}=2.0 μm λ_{long}= 8.65 μm in Equations 2.15 -2.17). Data from [8]. (C) Lifetime distribution of capping protein speckles fit with a single exponential with decay time τ=2.0 s. Data reproduced from [8].

function $Y(x, x')$, which gives the amount of bound protein at that came from x' due to retrograde flow, taking into account the lifetime distribution:

$$Y(x, x') = \Theta(x - x')\frac{1}{v_r}\int_{\frac{x-x'}{v_r}}^{\infty} p(t)dt. \tag{2.5}$$

The parameter v_r is the retrograde flow in the lamellipodium, and Θ is the step

function. Using $Y(x, x')$ one can find the profile of bound protein $B_1(x)$ and $B_2(x)$ due to each of the diffuse species, $\mathrm{C_{fast}}$ and $\mathrm{C_{slow}}$, respectively, such that $B(x) = B_1(x) + B_2(x)$, where:

$$B_1(x) = \int_0^\infty Y(x, x') a_{\mathrm{C_{fast}}}(x') dx' \tag{2.6}$$

$$B_2(x) = \int_0^\infty Y(x, x') a_{\mathrm{C_{slow}}}(x') dx'. \tag{2.7}$$

The steady state reaction diffusion equations that describe the system in Figure 2.1 are as follows:

$$v_r \frac{\partial B(x)}{\partial x} = a(x) - d(x) \tag{2.8}$$

$$D_{\mathrm{C_{fast}}} \frac{\partial^2 C_{\mathrm{fast}}}{\partial x^2} = a_{\mathrm{C_{fast}}}(x) - s_1 d(x) + \frac{1}{\tau_{\mathrm{C_{fast}}}} C_{\mathrm{fast}}(x) - \frac{1}{\tau_{\mathrm{C_{slow}}}} C_{\mathrm{slow}}(x) \tag{2.9}$$

$$D_{\mathrm{C_{slow}}} \frac{\partial^2 C_{\mathrm{slow}}}{\partial x^2} = a_{\mathrm{C_{slow}}}(x) - (1 - s_1) d(x) + \frac{1}{\tau_{\mathrm{C_{slow}}}} C_{\mathrm{slow}}(x) - \frac{1}{\tau_{\mathrm{C_{fast}}}} C_{\mathrm{fast}}(x). \tag{2.10}$$

Parameters $D_{C_{\mathrm{fast}}}$ and $D_{C_{\mathrm{slow}}}$ are the diffusion coefficients for C_{fast} and C_{slow} respectively and $d(x)$ is the detachment rate of bound proteins to the cytoplasm, which is found by solving Equation 2.8, given $a(x)$ and $B(x)$ from Equations 2.1, 2.6, and 2.7. Equation 2.8 is a transport equation that shows how retrograde flow of B is balanced by the association and detachment. Equation 2.9 balances diffusion of C_{fast} with association and detachment of the fast species and conversion between fast and slow diffusing states. The parameter s_1 is the probability for the bound protein to dissociate into C_{fast}. Equation 2.10 is the same as Equation 2.9 except for the slowly diffusing species C_{slow}. The concentrations far from the leading edge obey: $C_{\mathrm{slow},\infty}/C_{\mathrm{fast},\infty} = \tau_{C_{\mathrm{slow}}}/\tau_{C_{\mathrm{fast}}}$. Equations 2.1-2.10 can be solved numerically to find $C_{\mathrm{fast}}(x)/C_{\mathrm{fast},\infty}$ and $C_{\mathrm{slow}}(x)/C_{\mathrm{slow},\infty}$ given v_r, $\tau_{C_{\mathrm{fast}}}$, $\tau_{C_{\mathrm{slow}}}$, $D_{C_{\mathrm{fast}}}$, $D_{C_{\mathrm{slow}}}$, s_1 , and the parameters that define $a_{C_{\mathrm{fast}}}(x)$, $a_{C_{\mathrm{slow}}}(x)$, and $p(t)$. The method used involves adding time dependence to Equations 2.9 and 2.10 and allowing them to relax for a sufficiently long time:

$$\frac{\partial C_{\mathrm{fast}}}{\partial t} = D_{\mathrm{C_{fast}}} \frac{\partial^2 C_{\mathrm{fast}}}{\partial x^2} - a_{\mathrm{C_{fast}}}(x) + s_1 d(x) - \frac{1}{\tau_{\mathrm{C_{fast}}}} C_{\mathrm{fast}}(x) + \frac{1}{\tau_{\mathrm{C_{slow}}}} C_{\mathrm{slow}}(x) \tag{2.11}$$

$$\frac{\partial C_{\text{fast}}}{\partial t} = D_{\text{C}_{\text{slow}}} \frac{\partial^2 C_{\text{slow}}}{\partial x^2} - a_{\text{C}_{\text{slow}}}(x) + (1 - s_1)d(x) - \frac{1}{\tau_{\text{C}_{\text{slow}}}} C_{\text{slow}}(x) + \frac{1}{\tau_{\text{C}_{\text{fast}}}} C_{\text{fast}}(x). \tag{2.12}$$

We impose a no-flux boundary condition at the leading edge: diffusion to the leading edge is balanced by the retrograde flow taking the bound protein away from the leading edge.

2.2.2 Calculation of Rate Constants Based on Steady State Profile and Monte Carlo Simulation

The local rates with which the cytoplasmic protein binds to the network from the fast and slow diffusing states can be found using the appearance profiles and the cytoplasmic protein profiles calculated in the preceding subsection:

$$r_{C_{\text{fast}}} = \frac{a_{C_{\text{fast}}}(x)}{C_{\text{fast}}(x)} \tag{2.13}$$

$$r_{C_{\text{slow}}} = \frac{a_{C_{\text{slow}}}(x)}{C_{\text{slow}}(x)}. \tag{2.14}$$

These are the reaction rates for C_{fast} to convert into B_1 and for C_{slow} into B_2. We used the model in Figure 2.1 to create a 2D Monte Carlo simulation of independent particles in the lamellipodium by extending the method of Smith et al. [1]. The simulation was initialized using the steady state concentrations evaluated by Equations 2.11 and 2.12. At each simulation step that corresponds to time dt (chosen to be sufficiently small), the following processes occur:

1. Each diffusing particle is displaced by a distance chosen from the 2D free diffusion propagator with the corresponding diffusion coefficient.

2. Particles in the bound state undergo movement by distance $v_r dt$ that corresponds to retrograde flow.

3. The rates in Equations 2.13 and 2.14 are used to choose whether or not a diffusing particle converts to the bound state.

4. The lifetime of each particle that converts to the bound state is chosen from the SiMS distribution $p(t)$.

5. Bound particles convert to the diffusing state when their lifetime has been reached. Parameter s_1 is used to determine the fraction of these particles that become fast or slowly diffusing.

6. The fast and slow diffusing species convert between each other with probabilities chosen from exponential distributions with average lifetimes $\tau_{C_{\text{fast}}}$ and $\tau_{C_{\text{slow}}}$, respectively.

The side boundary conditions in our simulation are reflective. Any bound protein that exists at the back of the simulation box is converted into a diffusing protein and subsequently recycled. To model FRAP experiments, particles in a defined region are deleted. Particles outside of the region are then able to move into the bleached region. Recovery curves can be thus measured and compared to experimental data. To model photoactivation PA experiments, particles outside of the photoactivated region are deleted and the particles are then able to diffuse and react in the manner described above.

2.3 Results

2.3.1 Application to Capping Protein Dynamics

We first apply the general model of Section 2 to capping protein, the lamellipodial dynamics of which have been studied in prior studies with both FRAP and SiMS, though in different cell systems. Kapustina et al. [3] analyzed FRAP data of fibroblast cells expressing EGFP-CapZ in a circular region of diameter 5 μm centered at 5 μm from the leading edge of the cell [34]. They fitted the recovery to a model that used Virtual Cell (which is a computational tool used for modeling and simulations of cell biology) with various components to find values for the diffusion coefficient of capping protein in the cytoplasm, D=5-10 $\mu\text{m}^2/\text{s}$, and for its lifetime when bound to the actin network, $\tau = 10$ s. These values are different to those measured with SiMS

microscopy of XTC cells [25, 8] (Figure 2.2A) where capping protein was found to associate over an extended area of the lamellipodium (Figure 2.2B) but with a large slowly diffusing cytoplasmic pool with $D \approx 0.5$ μm^2/s and to have a shorter bound lifetime, $\tau \approx 2$ s (Figure 2.2C) [25, 8]. While both studies show a short lifetime of bound capping protein compared to the lifetime of polymerized actin that is 24-30 s in lamellipodia [10, 25], they indicate quantitatively different transport modes in the lamellipodia. Our goal in this Section is finding out if the measured SiMS microscopy parameters from Miyoshi et al. can be used to fit the FRAP data from Kapustina et al. and to study the implications for the concentration profile of capping protein across the lamellipodia.

Since the full model of Fig. 1 has many parameters in the subsequent section we consider two previously-proposed possibilities for the reasons behind slow capping protein diffusion: one being that capping protein is bound to severed actin oligomers, the other being that capping protein binds to the membrane. We use the SiMS data of Figure 2.2 to calculate rate constants for our Monte Carlo simulation. We then simulate bleaching of a 5 μm by 5 μm square region centered 5 μm from the leading edge to compare to the data of Kapustina et al. using a circular bleach region (this difference in shape has only a small effect on the recovery curve). In the simulations for capping protein below we used a typical value for retrograde flow, v_r= 0.03 μm/s [35].

Model including Oligomers

We first consider the model with oligomers shown in Figure 2.3A, B, a specific case of the general model (Figure 2.1). The motivation for this model is the suggested existence of short actin filaments (actin oligomers) in the lamellipodium, a result of cofilin-mediated severing [1]. If severed actin filaments are capped by capping protein, this could explain why 50% of capping protein has been observed in a slowly diffusing state with diffusion coefficient ≈ 0.5 μm^2/s [25]. In this model C_{fast} represents capping protein heterodimers diffusing in the cytoplasm and C_{slow} represents capping

protein heterodimers attached to the barbed end of an actin oligomer diffusing in the cytoplasm. The bound protein can only dissociate into capped oligomers, C_{slow}, that can either rebind to the network or become uncapped and convert to C_{fast}.

We assume that both fast and slow diffusing species can bind to the network, representing capping of free barbed ends and re-binding of oligomers to the lamellipodial network, respectively. Since SiMS only measures the total appearance profile $a(x)$ (Figure 2.2B), an additional assumption in our model is how $a(x)$ is split into $a_{C_{\text{fast}}}(x)$ and $a_{C_{\text{slow}}}(x)$. The authors of [1] suggested that oligomer rebinding contributes to a large fraction of actin speckle appearance at the back of the lamellipodium. We expect the behavior of capping protein to follow the behavior of actin oligomer rebinding. Since the total appearance profile can be fit to a double exponential (Figure 2.2B), we assume that the appearance rates are broken up such that $a_{C_{\text{fast}}}(x)$ corresponds to the short length scale and $a_{C_{\text{slow}}}(x)$ to the long length scale:

$$a_{C_{\text{fast}}}(x) = KC_{\infty}A_1 e^{-x/\lambda_{\text{short}}} \tag{2.15}$$

$$a_{C_{\text{slow}}}(x) = KC_{\infty}A_2 e^{-x/\lambda_{\text{long}}}, \tag{2.16}$$

with $A_1 = 0.74$, $A_2 = 0.26$, $\lambda_{\text{short}} = 2.0$ μm and $\lambda_{\text{long}} = 8.65$ μm (see dotted and dashed line in Figure 2.2B). The profile $a_{C_{\text{fast}}}(x)$ accounts for the appearances due to C_{fast} close to the leading edge, whereas the profile $a_{C_{\text{slow}}}(x)$ accounts for the appearances due to C_{slow} (Figure 2.2 B) that are more distributed throughout the lamellipodium. Several parameters in the model can be calculated from prior experiments or their range can be estimated. The lifetime distribution of capping protein bound to the network, $p(t)$ (Figure 2.2 C) can be fit with a single exponential where τ = 2.0 s [8]. The lifetime of the capping protein bound to the actin oligomer ($\tau_{C_{\text{slow}}}$) is likely in the range of the lifetime of an actin oligomer, 5-30 seconds [1]. The diffusion coefficients of the slow component is $D_{C_{\text{slow}}} = 0.5$ μm^2/s [25] and $D_{C_{\text{fast}}}$ =2-5 μm^2/s is expected, comparable to the diffusion coefficient of actin monomers [12, 32]. Another important parameter, K, in the simulation controls the ratio of the concentration of bound protein to cytoplasmic protein. We estimated this from experimental data

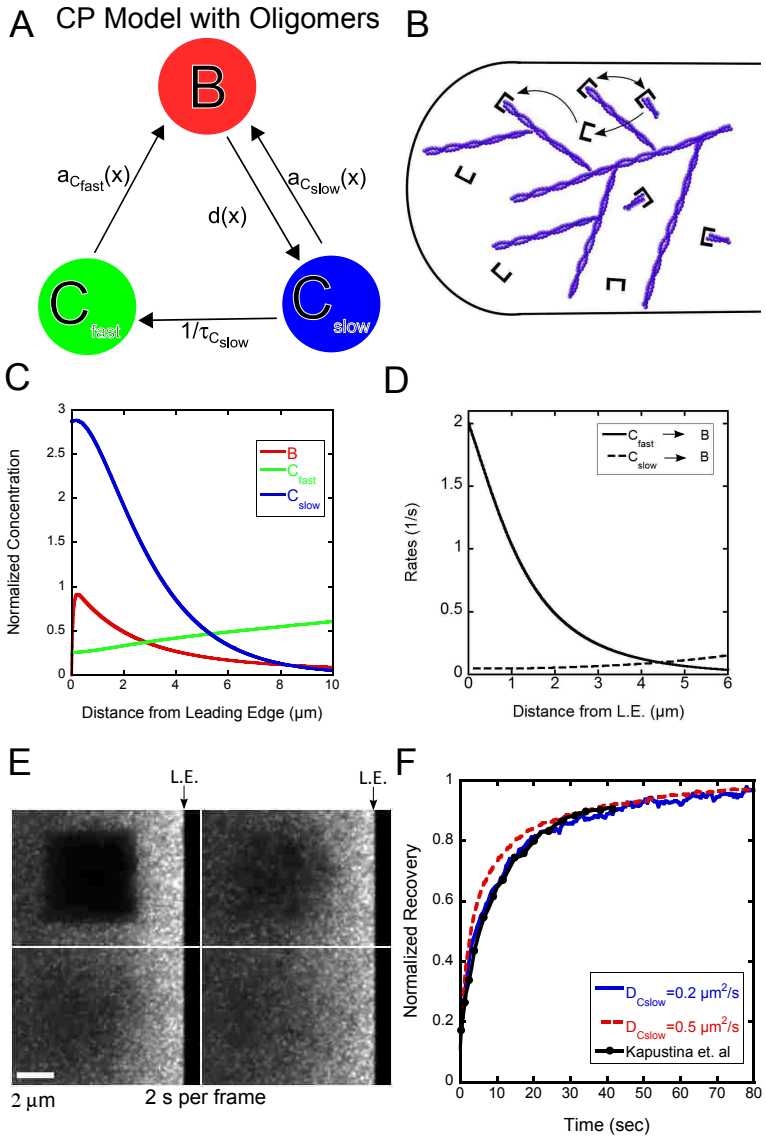

Figure 2.3: Results of model with oligomers for capping protein. (A, B) Schematic and cartoon of model with oligomers for capping protein. (C) Steady state concentration profiles for capping protein. (D) Binding rates as function of distance. (E) Snapshot images of simulated FRAP. (F). FRAP curves compared to experimental data from Kapustina et al. [3]. The ending time of the experimental measurement (40 s) is normalized to the value of the simulation at 40 s. The simulated recovery is normalized to one at long times. Simulations in panels C-F use $K = 0.5\ \mathrm{s}^{-1}$, $D_{C_{\mathrm{fast}}} = 2.0\ \mu\mathrm{m}^2/\mathrm{s}$, $D_{C_{\mathrm{slow}}} = 0.2\ \mu\mathrm{m}^2/\mathrm{s}$, $v_r = 0.03\ \mu\mathrm{m/s}$, $\tau = 2.0$ s, and $\tau_{C_{\mathrm{slow}}} = 13.0$ s, except for the labeled curve in F that has $D_{C_{\mathrm{slow}}} = 0.2\ \mu\mathrm{m}^2/\mathrm{s}$.

from the Watanabe lab from [25] and using SpeckleTrackerJ to count the number of speckles that correspond to bound protein and the number of diffusing proteins that appear as broadened speckle "clouds" [25]. The measured ratio of cytoplasmic protein to bound protein was estimated to be 2.3 to 1. Scanning the model parameters within the range described in the preceding paragraph allows us to run the simulation to obtain fits to FRAP data. The simulated FRAP was applied to a steady state initialized with the concentrations found after relaxing Equations 2.11 and 2.12 in time. Figure 2.3C shows the steady state concentration profiles using $K = 0.5$ s^{-1}, $D_{C_{\text{fast}}} = 2.0$ μm^2/s, $D_{C_{\text{slow}}} = 0.2$ μm^2/s , v_r= 0.03 μm/s, $\tau = 2.0$ s and $\tau_{C_{\text{slow}}} = 13.0$ s. With this value of K, the resulting profile has a big fraction of slowly-diffusing capping proteins, consistent with our measured ratio of bound to diffuse species. The reaction rates for the simulation, as function of distance from the leading edge, found using the concentration profile in Equations 2.11 and 2.12, are shown in Figure 2.3D. The rate for C_{slow} to bind to the network is very small compared to the rate for C_{fast} to bind to the network (even though appearances due to C_{slow} account for a large fraction of appearance at the back of the lamellipodium, see Fig. 2B). In order to obtain good fits to the experimental FRAP data for capping protein, the lifetime $\tau_{C_{\text{slow}}}$ needs to be maximized, and the diffusion coefficient $D_{C_{\text{fast}}}$ needs to be minimized, within the range of values described above and the range that gives non-negative concentration profiles in the model equations. An example of simulated FRAP is shown in Figure 2.3E while Figure 2.3F shows the recovery of the intensity in the bleached region along with the recovery in Kapustina et al. The recovery curve for $D_{C_{\text{slow}}} = 0.5$ μm^2/s that uses the same parameters as Figure 2.3C is an overall good fit to the experimental curve, however the initial recovery is more rapid compared to experiment. The fit can be improved using $D_{C_{\text{slow}}} = 0.2$ μm^2/s (and other parameters unchanged) that gives a slightly slower initial recovery and fits the experimental data more accurately. The above results show that parameters measured with SiMS can be used to model the FRAP data in [3], using a smaller diffusion coefficient $D_{C_{\text{slow}}}$ and faster dissociation time τ compared to the parameters

used in the fit in [3] . The diffusion of long-lived oligomers out of the bleached region contributes to making the recovery slower initially and a value $\tau_{C_{\text{slow}}} \approx 13$ s is needed for a good fit. This is in agreement with that fact that slowly-diffusing speckles can be tracked for a few seconds and thus the lifetime of the slowly-diffusing capping protein is likely in the range of 5-30 s [25] (note: $\tau_{C_{\text{slow}}}$ cannot become much longer than a threshold above which the calculated C_{fast} becomes negative). Even though the dissociation time $\tau = 2$ s is small compared to the measured FRAP half-time, the bound species is a small fraction of the total amount.

Model with Membrane Binding

Another way of accounting for slowly diffusing capping protein is considering that capping protein binds and diffuses along the membrane [25]. Membrane binding can occur through a fast-diffusing state in the cytoplasm or by membrane-induced uncapping of capped barbed ends. The model shown in Figure 2.4A, B is another possible mechanism of why capping protein dissociates so frequently from the actin network and diffuses slowly. CARMIL is a membrane bound protein complex that also binds capping protein and may account for the very short lifetime of capping protein bound to the actin filament [36][37][38]. In this model only fast diffusing cytoplasmic protein is able to become bound (representing capping of barbed ends) so that the appearance rate is:

$$a(x) = a_{C_{\text{fast}}}(x) = KC_\infty \left(A_1 e^{-x/\lambda_{\text{short}}} + A_2 e^{-x/\lambda_{\text{long}}}\right) \tag{2.17}$$

with $A_1 = 0.74$, $A_2 = 0.26$, $\lambda_{\text{short}} = 2.0$ μm, and $\lambda_{\text{long}} = 8.65$ μm. The bound protein can dissociate into either C_{fast} or C_{slow} and the parameter s_1 is the probability of dissociating into C_{fast}. The fast diffusing capping protein can convert to slow with lifetime $\tau_{C_{\text{fast}}}$ and slow can become fast with lifetime $\tau_{C_{\text{slow}}}$. The model in Figure 2.4A, B is another specific case of the general model (Figure 2.1).

The model with membrane binding (Figure 2.4) has more parameters compared to the model with oligomers (Figure 2.3). Similar constraints to Figure 2.3 exist for

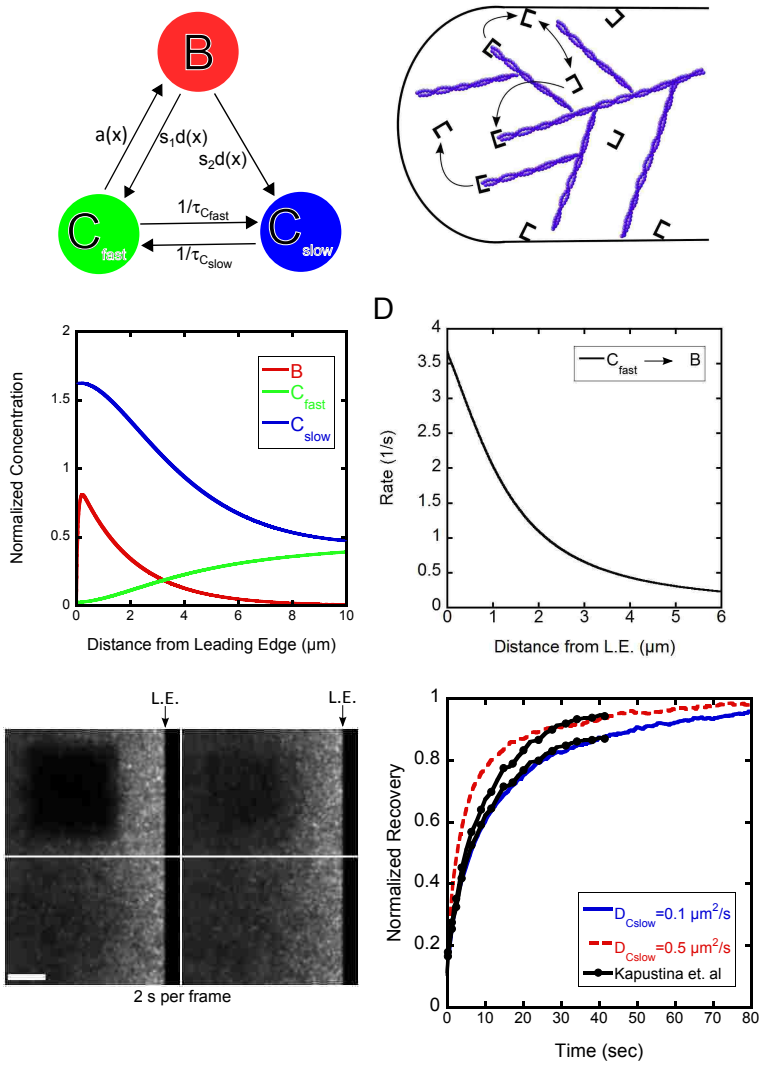

Figure 2.4: Results of model with membrane binding for capping protein. (A, B). Schematic and cartoon of model with membrane binding. (C). Steady state concentration profiles for capping protein (D) Binding rates as function of distance. (E) Snapshot images of simulated FRAP. (F). FRAP curves compared to experimental data from Kapustina et al. [3]. The ending time of the experimental measurement (40 s) is normalized to the value of the simulation at 40 s. The simulated recovery is normalized to one at long times. Simulations in panels C-F use $K = 0.435$ s^{-1}, $D_{C_{\rm fast}} = 2.0$ μm^2/s, $D_{C_{\rm slow}} = 0.5$ μm^2/s, $v_r = 0.03$ μm/s, τ= 2.0 s, $\tau_{C_{\rm fast}} = 5.0$ s, $\tau_{C_{\rm slow}} = 5.0$ s, $s_1 = 0.1$, except for the labeled curve in F that has $D_{C_{\rm slow}} = 0.1$ μm^2/s.

$D_{C_{\text{fast}}}$, $D_{C_{\text{slow}}}$, τ, v_r, and K. The new parameters are the lifetimes $\tau_{C_{\text{fast}}}$, $\tau_{C_{\text{slow}}}$, and the dissociation probability s_1. As mentioned in 3.1.1, the lifetime of the slowly-diffusing capping protein is likely in the range of 5-30 s. We start by assuming that $\tau_{C_{\text{fast}}} = \tau_{C_{\text{slow}}}$ so that C_{fast} and C_{slow} each correspond to 50% of the concentration far from the leading edge [25]. A concentration profile similar to Figure 2.3C can be generated with $K = 0.435$ s^{-1}, $D_{C_{\text{fast}}}$= 2.0 μm^2/s, $D_{C_{\text{slow}}}$= 0.5 μm^2/s, $v_r = 0.03$ μm/s, τ= 2.0 s, $\tau_{C_{\text{fast}}} = 5.0$ s, $\tau_{C_{\text{slow}}} = 5.0$ s, s_1=0.1. These parameters give the reaction rate as a function of distance from the leading edge shown in Figure 2.4D for binding to the network from C_{fast}, which is the only reaction rate to the bound state. We find that we are able to fit the experimental FRAP data using parameters consistent with SiMS data. The simulated recovery for the parameters of Figure 2.4C is shown in a montage in Figure 2.4E and the corresponding recovery curves are shown in Figure 2.4F, along with the experimental data. Both simulated curves with $D_{C_{\text{slow}}} = 0.1$ μm^2/s and $D_{C_{\text{slow}}}$= 0.5 μm^2/s fit the data; however the smaller diffusion coefficient allows for a better fit. Similar to the model with oligomers, $D_{C_{\text{fast}}}$ needs to be on the lower range of the physically plausible values 2-5 μm^2/s (in Figure 2.4C, further lowering of $D_{C_{\text{fast}}}$ also makes the calculated steady state concentration profile of C_{fast} negative). Parameter s_1 needs to be small compared to unity, otherwise the bleached region recovers too quickly and none of the other parameters are able to slow the recovery down enough to capture what occurs in the experiment (see Figure 2.5). Keeping $\tau_{C_{\text{fast}}} = \tau_{C_{\text{slow}}}$, we varied these two parameters together and find that they also need to be in the range of a few seconds (see Figure 2.5). In conclusion, obtaining a good fit drives this model to a similar kinetic scheme as the model with oligomers, with the majority of the bound protein dissociating into slowly diffusing protein. However the lifetime of the slowly-diffusing species can be smaller than in the model with oligomers as slow diffusing capping protein can be generated by both uncapping and conversion from the fast species.

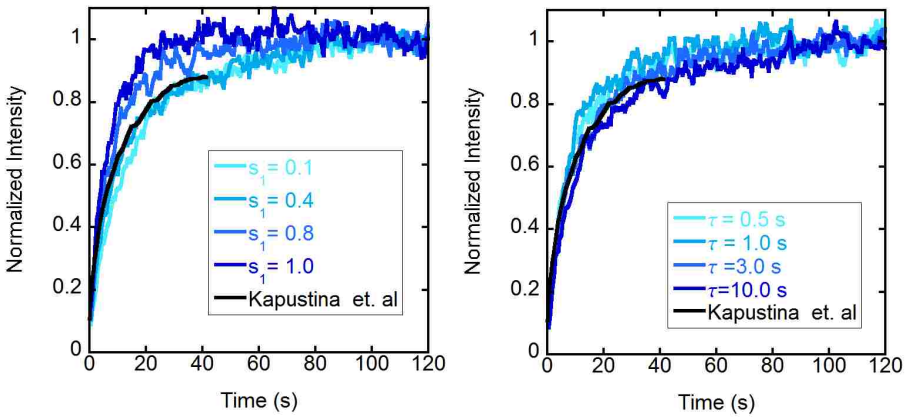

Figure 2.5: Dependence of capping protein simulated FRAP on parameter values in the model with membrane binding. The bleached region is the same as in Figure 2.4 E. Left: Smaller values of the probability s_1 for bound capping protein to dissociate into the fast diffusing cytoplasmic pool give a slower recovery. Right: Larger values of the lifetime $\tau = \tau_{C_{\text{fast}}} = \tau_{C_{\text{slow}}}$ give a slower recovery. Unless otherwise indicated, the parameter values used are $K = 0.435$ s^{-1}, $D_{C_{\text{fast}}} = 2.0$ μm^2/s, $v_r = 0.03$ μm/s, $\tau = 2.0$ s, $s_1 = 0.1$ and $\tau = \tau_{C_{\text{fast}}} = \tau_{C_{\text{slow}}} = 5.0$ s.

Comparison of Two Models for Capping Protein Turnover

Both models of Fig. 3 and 4 work to fit the FRAP results from Kapustina et al. [3] using parameters from the SiMS microscopy data of Miyoshi et al. [8]. The pool of slowly diffusing protein is important to fit FRAP recovery with half-time on the order of 10 s, using a bound lifetime of 2 s. Retrograde flow contributes little to FRAP since the distance traveled by retrograde flow during recovery is small compared to the size of the bleached region. Since both models are driven to similar kinetic transition rates, it is hard to distinguish between them using further FRAP data of either the back or front of the lamellipodium (see Supplementary Figure 2.6). A clearer difference between the two models can be seen in lamellipodium photoactivation simulations with the same parameters as for the FRAP data. There is more rebinding throughout the lamellipodium directly after photoactivation from

the model with oligomers as throughout the lamellipodium compared to the model with membrane binding. This reflects the assumption of oligomer re-association with the actin network at the back of the lamellipodium.

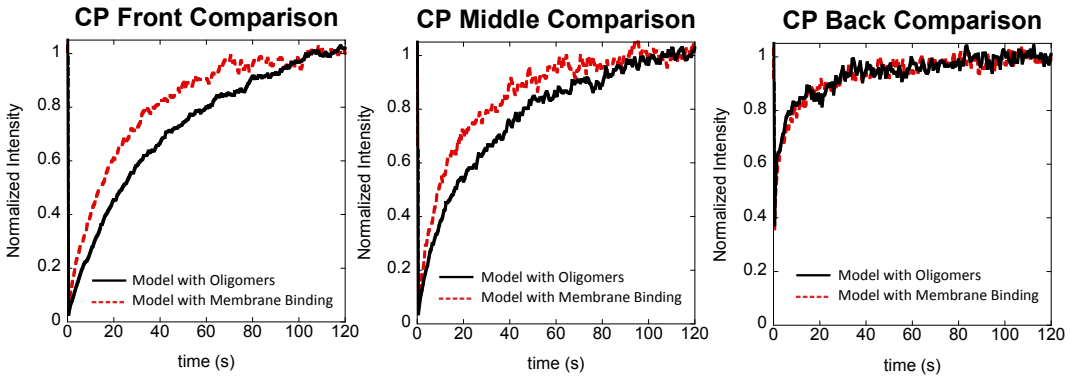

Figure 2.6: Comparison of simulated FRAP for the two capping protein models of Figures 2.3 and 2.4. The bleached region is a square box with one side of length 5 μm along the cell membrane and depth 5 μm into the cell. Left: At 0-1 μm from the leading edge the recovery in the model with membrane binding is somewhat faster. Middle: At 2-3 μm from the leading edge the recovery in the model with membrane binding is faster although the difference is not as large as at the leading edge. Right: At the back of the bleached region 4-5 μm away from the leading edge, the results of the two models are indistinguishable. For all panels, same constants are used as in Figures 2.3 and 2.4.

Interestingly, both models demonstrate significant concentration gradients of the two diffuse species across the lamellipodium (Figures 3C and 4C). The origin of this gradient is mainly the local production of slowly diffusing capping protein close to the leading edge. The inward flux of the slowly-diffusing population plus the retrograde flow of the bound species must be balanced by the diffusive flux of the fast species at steady state. The free energy source to maintain this non-equilibrium gradient must be sought in ATP hydrolysis, the free energy of which drives actin polymerization: in both models the actin network "pumps" fast-diffusing capping protein bound to it into the slowly-diffusing pool.

2.3.2 Application to Arp2/3 Complex Dynamics

Both FRAP and SiMS microscopy experiments have been performed to study the kinetics of Arp2/3 complex in the lamellipodium. Figure 2.7A shows FRAP of the p16 subunit of the Arp2/3 complex by Lai et al. [2]. The bleached region is a 2 μm by 4 μm box positioned at the leading edge of a B16-F1 melanoma cell. Recovery is faster at the leading edge of the cell than it is away from the leading edge. While this has been interpreted to suggest that Arp2/3 complex forms branches within a very narrow region close to the leading edge, SiMS experiments using XTC cells (tagging the p40 and p21 subunits) by Miyoshi et al. [8] show distributed speckle appearances 1 μm away from the leading edge and further (Figure 2.7B) and an exponential distribution of speckle lifetimes with $\tau = 18$ s (Figure 2.7C). Our aim is to (i) use modeling to check if the FRAP recovery observed in Figure 2.7A is consistent with the distributed appearances in Figure 2.7B, and (ii) explore the implications for the concentration profiles of the diffuse species. Smith et al. [1] showed that distributed turnover of EGFP-actin can give faster FRAP at the cell front as compared to the cell back, however this has not been addressed for the Arp2/3 complex.

In the simulations below we used a profile with distributed appearances that is narrower compared to the profile measured in XTC cells, which have wider lamellipodia compared to the B16-F1 melanoma cells. This appearance profile, shown in Figure 2.7B, was calculated to give an Arp2/3 complex concentration profile that matches the concentration profile of the B16-F1 melanoma cells. This was done by measuring the intensity profile in Figure 2.7A in excess of the cytoplasmic background, assuming that this profile is approximately proportional to the bound profile $B(x)$, and using $a(x) = B(x)/\tau + v_r dB(x)/dx$ that can be derived from Equations (2-7). We use the speckle lifetime τ of Miyoshi et al. [8], which is the only available lifetime measurement in live cells. The calculated $a(x)$ profile was fit to a double exponential and the resulting curve is shown in Figure 2.7B. The difference between the calculated appearance profile in Figure 2.7B and the data by Miyoshi et al. is evident further than 1 μm away from the leading edge where the calculated appearance

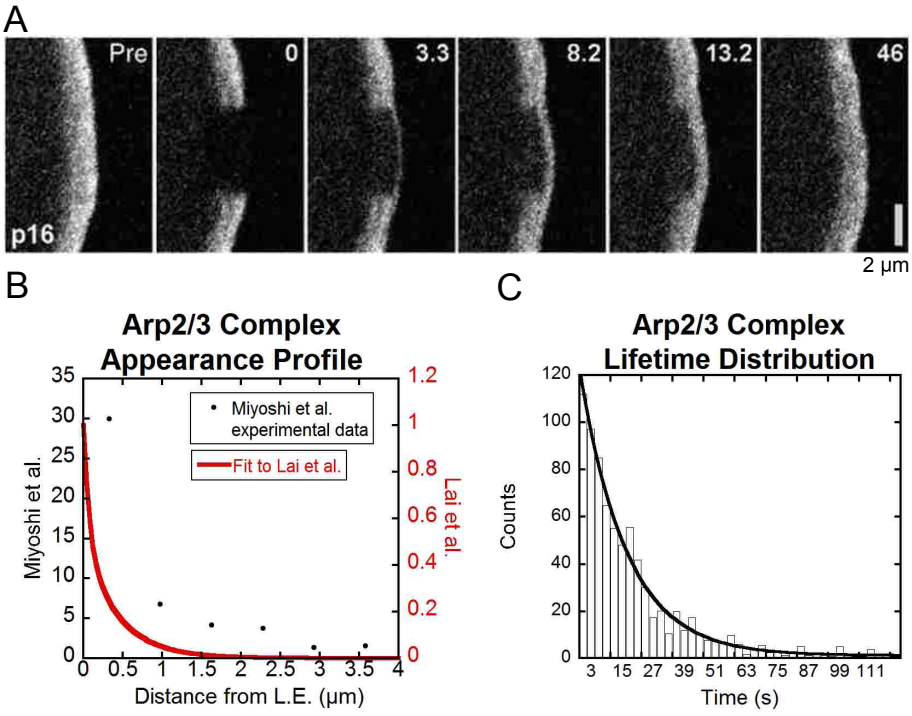

Figure 2.7: Summary of Arp2/3 complex FRAP and SiMS data. (A) FRAP snapshots of leading edge of cell expressing EGFP-ArpC5B (p16 subunit) reproduced from Lai et al. [2]. (B) Speckle appearance rates for Arp2/3 complex from Miyoshi et al. [8] (black dots) and calculated to match the steady state Arp2/3 complex concentration profile in [2] (double exponential with A_1=0.49, A_2=0.51, λ_{short}=0.08 μm, λ_{long}=0.43 μm, see Equation 2.18). (C). Arp2/3 complex speckle lifetime distribution from [8].

distribution approaches zero. In the following two sections we consider two different models to explain for the dynamics of the Arp2/3 complex: a model with a diffuse pool with a single diffusion coefficient and a model with fast and slow diffusing pools.

Model with a Single Arp2/3 Complex Diffuse Cytoplasmic Pool

The simplest model of Arp2/3 turnover involves a single diffusing species, C (Figure 2.8A,B). Diffuse Arp2/3 complex can bind to the actin network to become bound protein B with the appearance rate $a(x)$. The appearance profile for the Arp2/3

complex is given by

$$a(x) = A_1 e^{-x/\lambda_{\text{short}}} + A_2 e^{-x/\lambda_{\text{long}}}. \tag{2.18}$$

with $A_1 = 0.49$, $A_2 = 0.51$, $\lambda_{\text{short}} = 0.08$ μm, and $\lambda_{\text{long}} = 0.43$ μm (Figure 2.7). The bound protein can dissociate into the diffuse species with the detachment rate $d(x)$ corresponding to bound lifetime τ. This lifetime may include Arp2/3 complex attachment without branch formation, as observed in single molecule in vitro experiments where bound Arp2/3 complex has bound lifetimes in the range 2-200 s [39]. The estimated value of retrograde flow in Figure 2.7A is $v_r = 0.04$ μm/s.

Given the above parameters, the only two other parameters for the model are the cytoplasmic diffusion coefficient, D_C, and K, which adjusts the ratio of bound to cytoplasmic protein. Knowing the larger size of the Arp2/3 complex as compared to G-actin or capping protein, we anticipate a diffusion coefficient of 2-6 μm^2/s. In the steady state profile shown in Figure 2.8C, K =5 s^{-1} and $D_C = 4.0$ μm^2/s. This profile matches the experimental profile taken by a line scan in Figure 2.7A, as expected since the appearance profile was calculated using the experimental intensity profile. A small relative depletion is observed in the cytoplasmic profile near the leading edge because the diffusive flow of the cytoplasmic pool towards the leading edge balances the outward retrograde flow of the bound species. The parameters used for Figure 2.8C give the binding rate of cytoplasmic protein to bound protein as function of distance across the lamellipodium shown in Figure 2.8D. We used the model to fit the experimental FRAP data by Lai et al. [2], which shows faster recovery at the lamellipodium front as compared to the back (Figure 2.7A). An example of simulated FRAP is shown in Figure 2.8E (using the same parameters as in Figure 2.8C, D). The recovery is quantified in Figure 2.8F where the front recovery curve is taken 0-1 μm from the leading edge, and the back recovery curve is taken 1-2 μm from the leading edge as in Lai et al. [2]. Having a value for D_C in the higher range described above aids in obtaining a good fit of the recovery at the front (smaller values results in somewhat slower recovery, see Figure 2.9 A - C). The recovery at the back has a small initial increase due to the diffusion of the cytoplasmic component, followed

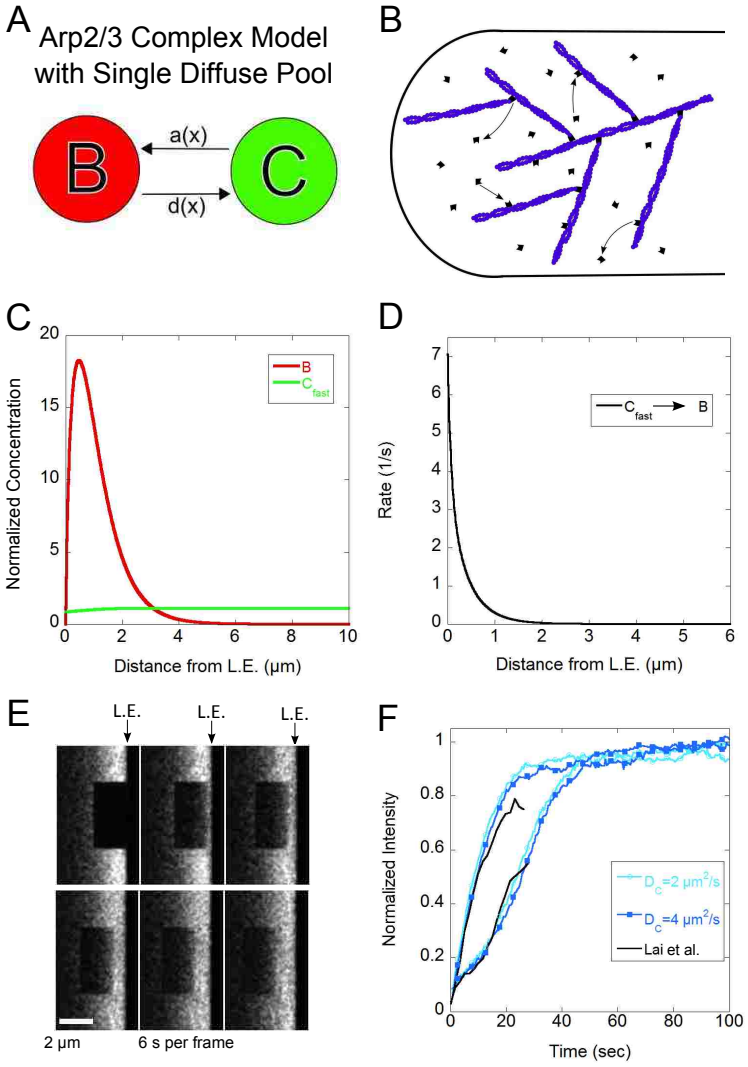

Figure 2.8: Results of model with single diffusive component for Arp2/3 complex. (A, B) Schematic and cartoon of model with single diffusive component. (C) Steady state concentration profile for Arp2/3 complex. (D)Binding rates as function of distance. (E) Snapshot images of simulated FRAP. (F) FRAP curves compared to experimental data from Lai et al. [2]. The simulated recovery is normalized to one at long times. Simulations in panels C−F use K =5 s^{-1}, $D_C = 4$ $\mu m^2/s$ and $v_r = 0.04$ μm/s, except for the curve in F that has $D_C = 2$ $\mu m^2/s$.

by a slower recovery. This slower recovery is driven by binding at the back of the lamellipodium and retrograde flow that brings labelled subunits from the cell front. The fact that the model results capture the shape of the recovery at the back relies on having a cytoplasmic to bound ratio much smaller than unity, which is tuned by parameter K (larger values of this ratio correspond to larger K). Smaller values of K lead to a larger fraction of the fast initial recovery at the back and less agreement with the data (see Figure 2.9 D-G). We note that the values of D_C and K have to be above a threshold that depends on the value of the other such that the solution of the partial differential Equations 2.8-2.10 is non-negative.

Model with Membrane Binding of the Arp2/3 Complex

Using SiMS microscopy, Millius et al. [6] suggested that some Arp2/3 complexes bind to the WAVE complex on the cell membrane of XTC cells and perform a slow diffusion prior to incorporation of the actin network while other Arp2/3 complexes are recruited directly from the cytosol. Millius et al. observed slowly diffusing speckles of Arp2/3 complex components within a few μm from the leading edge. We thus considered a model with membrane binding of the Arp2/3 complex (Figure 2.10 A,B). The two diffuse species in this model represent Arp2/3 complex in the cytoplasm, C_{fast}, and bound to the membrane, C_{slow}. The bound Arp2/3 complex dissociates into C_{fast} only, representing debranching and dissociation of the Arp2/3 complex from the pointed end. This occurs with the detachment rate $d(x)$ corresponding to bound lifetime τ, as in the model with a single diffuse species. We assume that binding to the membrane occurs close to the leading edge with a spatially dependent rate $k(x) = k_m e^{-x/\lambda_m}$ defined by parameters λ_m and k_m. This was achieved in the simulations by using a spatially-dependent $\tau_{C_{\text{fast}}}$ in equations 2.9 and 2.10 and in the Monte Carlo model accordingly. Spontaneous unbinding occurs with lifetime $\tau_{C_{\text{slow}}}$. The appearance profile describing association of membrane-bound Arp2/3 complex to the actin network is the same as in equation 2.18 of the model with a single diffuse species. Using a retrograde flow rate $v_r = 0.04$ μm/s as in the previous model, $D_{C_{\text{slow}}}$

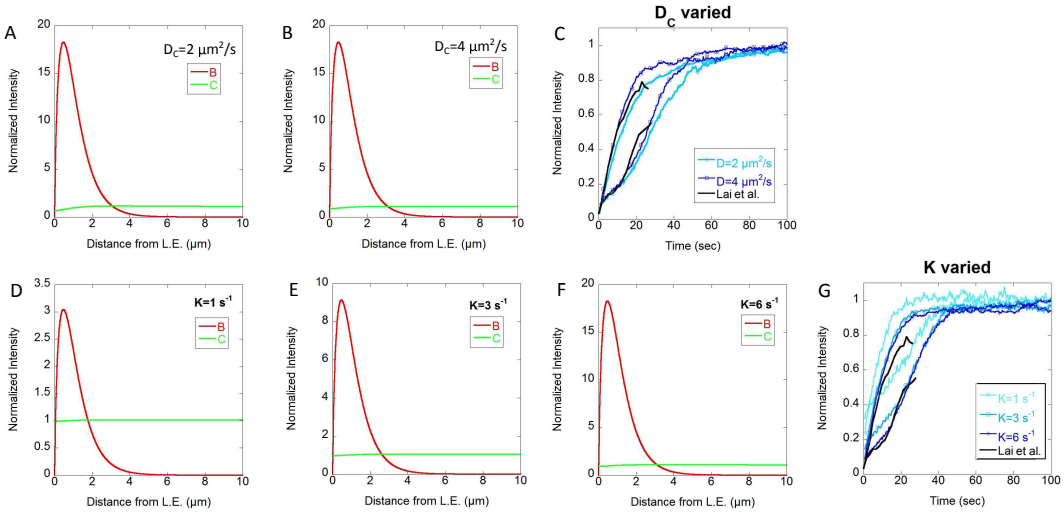

Figure 2.9: Simulations of model with single cytoplasmic species as function of the cytoplasmic diffusion coefficient and K describing the overall magnitude of the transition rate from the cytoplasm towards the bound species. (A, B) Steady state concentration profiles using two different diffusion coefficients. Panel B is same as Figure 2.8C. (C) Effect of value of diffusion coefficient on simulated FRAP. Recovery slows down with decreasing D_C but the effect within the provided range is small because in both cases there is little depletion of diffusing cytoplasmic protein close to the leading edge. (D−F) Steady state concentration profiles for varying K. Larger values of K, which adjusts the ratio of bound to cytoplasmic protein, give a better fit to experimental data. Unless otherwise indicated, the reference values in all panels are $D_C = 4.0$ μm^2/s, K =5 s^{-1} and $v_r = 0.04$ μm/s. The bleached region is the same as in Figure 2.8E.

= 0.6 μm^2/s (the estimate in Millius et al. [6]) and assuming membrane binding occurs close to the leading edge, $\lambda_m = 0.2$ μm, leaves $D_{C_{\text{fast}}}$, K, $\tau_{C_{\text{slow}}}$, and k_m as undetermined parameters. In the steady state profile in Figure 2.10C we use $D_{C_{\text{fast}}}$ = 3.0 μm^2/s, K = 6.0 s^{-1}, $\tau_{C_{\text{slow}}}$ = 20 s, and k_m = 40 s^{-1}. With these parameters, the bound protein is sharply peaked close to the leading edge while the fast diffusing protein is small compared to the bound profile species and slightly depleted at the leading edge. The depletion reflects the diffusive flow towards the leading edge that balances the retrograde flow and diffusive flow of the slow species away from the

lamellipodium. The slowly diffusing protein is also much smaller than the bound concentration at the leading edge; however it is enhanced close to the leading edge. The parameters used in Figure 2.10C lead to the binding rate of the slowly diffusing to bound species as function of distance shown in Figure 2.10D. The simulated FRAP snapshots using the same parameters as in the concentration profile of Figure 2.10C are shown in Figure 2.10E. The recovery curves compare well to experiment (Figure 2.10F). The back recovery curve, which is sampled 1-2 μm away from the leading edge, gives a better fit in this model than in the previous model forwith a single diffuse pool the Arp2/3 complex. This is accounted for by the small amount of slowly diffusing Arp2/3 complex that gives a slower recovery away from the leading edge.

We found that in order to fit the experimental FRAP data by Lai et al. [2] the value of K has to be sufficiently high to keep the bound to cytoplasmic ratio sufficiently smaller than unity; otherwise the back of the lamellipodium recovers faster than in experiments (see Figure 2.11 A-C). Similarly, decreasing the coefficient k_m to a value where the concentration of slowly-diffusing species becomes a small fraction of the bound concentration gives a better fit to the FRAP curve at the back (Figure 2.11 D-G). The recovery is also affected by the diffusion coefficient of the fast diffusing species. Values above $D_{C_{\text{fast}}} = 2.0\ \mu\text{m}^2/\text{s}$ give a good fit to the experimental FRAP data. Compared to the model of section 3.2.1, smaller $D_{C_{\text{fast}}}$ values can now provide comparable fits since the introduction of a membrane diffusing species also aids in the fast recovery.

Comparison of two models for Arp2/3 Complex Turnover

Both models can fit the FRAP data from Lai et al. [2] using SiMS parameters from Miyoshi et al. [8] reasonably well. In these models a free energy source such as ATP hydrolysis on actin or Arp2/3 complex would be needed to establish the rates that maintain a steady state with concentration gradients of the diffuse species. The model including a membrane diffusingon species of the Arp2/3 complex is more

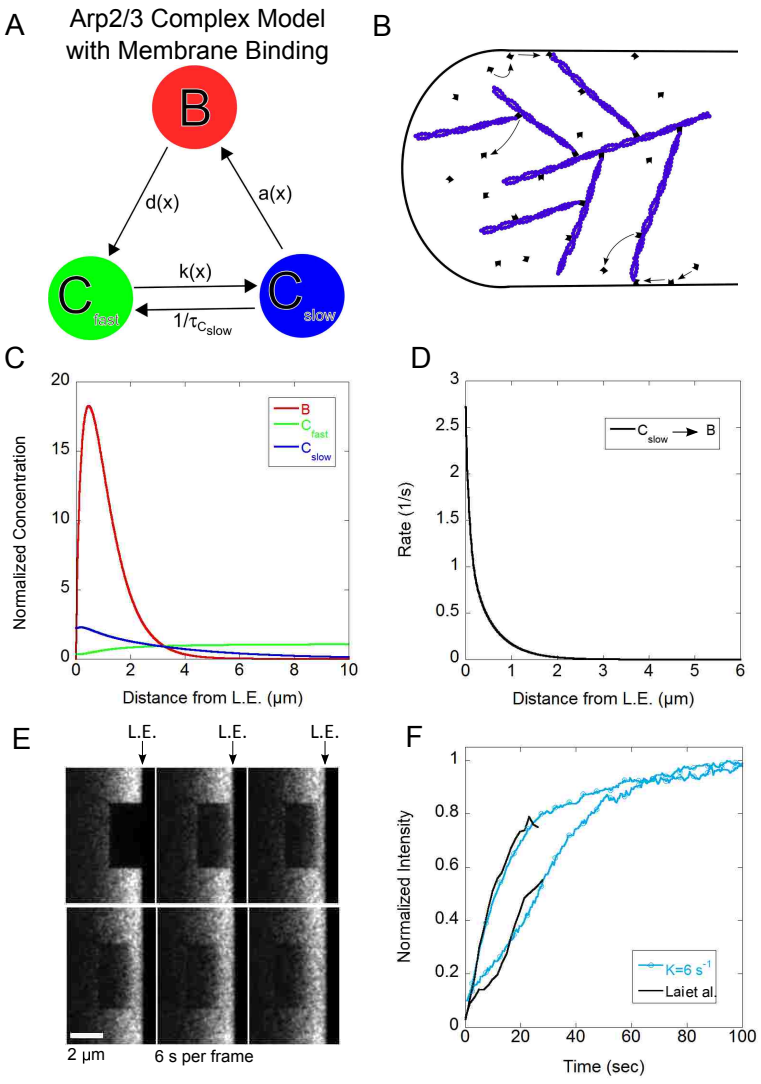

Figure 2.10: Results of model with membrane binding for Arp2/3 complex. (A, B) Schematic and cartoon of model with Arp2/3 complex membrane binding. (C) Steady state concentration profile for Arp2/3 complex. (D) Binding rates as function of distance. (E) Snapshot images of simulated FRAP. (F) FRAP curves compared to experimental data from Lai et al. [2]. The simulated recovery is normalized to one at long times. Simulations in panels C–F use $D_{C_{\text{fast}}} = 3\ \mu\text{m}^2/\text{s}$, $K = 6.0\ \text{s}^{-1}$, $\tau_{C_{\text{fast}}} = 20$ s, $v_r = 0.04\ \mu\text{m/s}$, $\lambda_m = 0.2\ \mu\text{m}$ and $k_m = 40\ \text{s}^{-1}$.

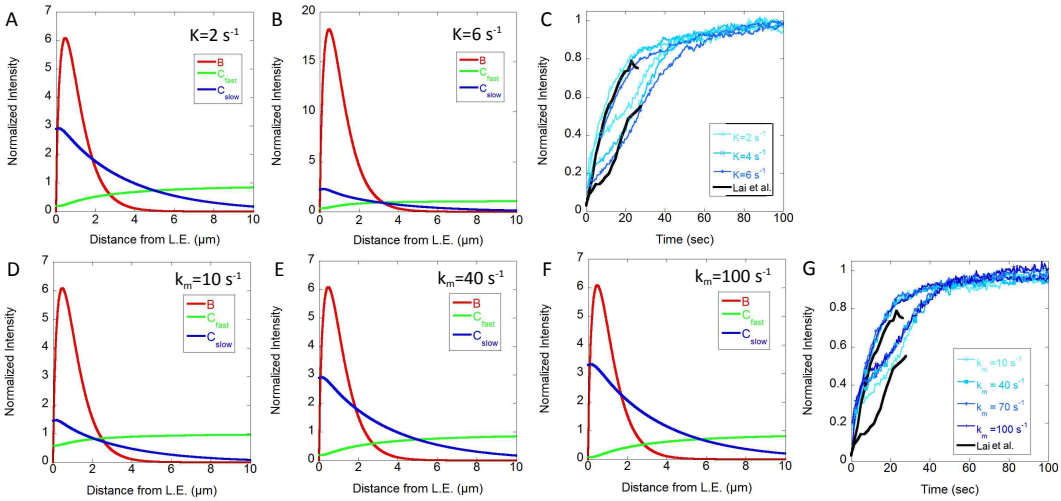

Figure 2.11: Simulations of model with Arp2/3 complex membrane binding as function of parameters K (describing the overall magnitude of the transition rate from the cytoplasm towards the bound species) and k_m (describing the magnitude of membrane binding close to the leading edge). (A−B) Examples of steady state concentration profiles with different K. Panel B is same as Figure 2.10 C. (C) Effect of K on simulated FRAP. A better fit is achieved for the largest among the K values shown. (D−F) Examples of steady state concentration profiles for different k_m. (G) Effect of k_m on simulated FRAP. The larger values of k_m give a smaller lag between the front and the back of the recovery because of the larger contribution of the diffusive species to the recovery at short times. Unless otherwise indicated, the reference values in all panels are $D_{C_{\text{fast}}} = 3.0\ \mu\text{m}^2/\text{s}$, $K = 2.0\ \text{s}^{-1}$, $\tau_{C_{\text{slow}}} = 20$ s, $v_r = 0.04$ μm/s, $\lambda_m = 0.2\ \mu$m, and $k_m = 40\ \text{s}^{-1}$. The bleached region is the same as in Figure 2.10E.

consistent with findings from Millius et al. [6] than the model without a slow diffusing species. However both models with one diffuse species and two diffuse species require that the diffusing population is a small fraction of the bound. The fact that the concentration of Arp2/3 complex increases by about 8-fold after stimulation in XTC cells [40] is consistent with the existence of a small fraction of fast-diffusing Arp2/3 complex (presumably the only species present prior to lamellipodia stimulation). Inspection of the movies in Millius et al. [6] indicates however that the number of

slowly-diffusing speckles is comparable to the bound population. While the slowly-diffusing Arp2/3 complex speckles may also represent Arp2/3 complex bound to debranched actin oligomers (not considered here as a separate species, for simplicity), such a pool would also need to be as small for the model to reproduce the FRAP data. It is possible that the difference may be due to the different cell types: for example, we assumed that the lifetime distribution for the bound Arp2/3 complex is the same in NIH-3T3 cells as in the XTC cells (that have wider lamellipodia but the only cell type in which single molecule lifetime measurements exist). Similar to the case of capping protein, we found that the behavior after photoactivation may be used to compare the two models. When using parameters as in Figures 6 and 7, in the model with membrane binding there is more local rebinding than in the model with a single cytoplasmic diffuse species. The single cytoplasmic diffuse species model also has faster spreading and binding at the leading edge further away from the photoactivated region. Future measurements of this type would be a useful way to further constrain possible Arp2/3 complex dynamics in the lamellipodium.

2.4 Discussion

In this chapter we used modeling to calculate concentration profiles of capping protein (Figures 2.3C and 2.4C) and Arp2/3 complex (Figures 2.8C and 2.10C) based on prior SiMS and FRAP data. In these profiles the cytoplasmic pool is modeled with either one or two types of diffuse populations ("fast" and "slow"). This limit of two pools is a simplifying approximation that is helpful to examine transport limitations across the lamellipodium. Our model can be extended to cover additional diffuse pools to account for protein complexes with a distribution of diffusion coefficients.

The gradients in the diffuse pool will have implications on the behavior of the lamellipodium when perturbed from steady state, for example during the stimulation of a protrusion by increase of free barbed end concentration close to the leading edge [40, 41]. In the model with capping proteins bound to oligomers (Figure 2.3C), such

a sudden increase will not be accompanied by a proportional increase in the capping rate as the system is close to the diffusion rate of "fast" capping protein towards the leading edge. Since the slowly-diffusing capping proteins, assumed to be capped oligomers are produced by the bound species, such a local increase in barbed end concentration would lead to an increase in the concentration of the "slow" diffuse pool. In this model, the slow capping protein will bind to the back of the lamellipodium with an increased overall rate, which could be part of a mechanism of structural remodeling in the lamellipodium during protrusion [8]. In the corresponding case in the model with membrane binding (Figure 2.4C), the response would be similar but in that model the slow membrane-bound pool does not associate with the network and it would just accumulate and dissociate to the cytoplasm. Further, the diffuse pool gradients of both models rely on the continuous production of slow capping protein; tuning of this rate by cells (through severing or uncapping [36]) may remove or enhance the diffusion limitations and thus act as part of a control mechanism. The slow population of the capping protein near the leading edge may also act as a buffer of capping protein close to the leading edge but we note that we did not consider capping protein association to barbed ends through the slowly-diffusing membrane-bound capping protein pool.

Diffusion limitations of the Arp2/3 complex towards the leading edge could become important upon protrusion initiation (see concentration gradients of C_{fast} in Figures 6C and 7C). In addition to enhancing the rate of Arp2/3 complex association to the actin filaments through a 2D diffusive search [6], the slowly-diffusing pool could also act as a buffer of Arp2/3 complex for the faster response of active lamellipodia. The smallness of the diffusion coefficient of Arp2/3 complex (0.6 $\mu\text{m}^2/\text{s}$) is important for keeping it close to the leading edge. Further SiMS and FRAP or photoactivation PA studies of capping protein and Arp2/3 complex under non-steady state conditions should help resolve some of these mechanisms.

Photoactivation experiments can give a clear picture of where binding and unbinding occurs, complimentary to FRAP. Modeling and PA experiments using labeled

actin provided further support for two separate pools of actin [12]: (i) a pool coming from the center of the cell and bound to thymosin $\beta 4$ that targets polymerization at the leading edge of the cell, and (ii) a second pool that is recycling actin at the back of the lamellipodium. The model in [12] included two diffuse actin cytoplasmic pools and one membrane bound in complex with thymosin $\beta 4$ in order to account for the enhanced diffuse actin concentration close to the leading edge of neuroblastoma cells, similar to the models with membrane binding in the current work.

Evidence for incorporation of diffuse actin to the lamellipodia network throughout the lamellipodium has also been provided by the FRAP and PA experiments of labeled actin by Lewalle et al. [15]. These authors also performed FRAP of Arp2/3 complex in lamellipodia and found recovery throughout the lamellipodia pronounced close to the leading edge, consistent with the assumptions in our work. This study describes the distributed turnover of actin, Arp2/3 complex, and capping protein as a system with a unique length-scale [15]. Other studies using fluorescence speckle microscopy however suggest different length scales for each component with capping protein, Arp2/3 complex, and F-actin having increasingly broader concentration profiles [42]. In the results of this our work the capping protein distribution is broader than that of Arp2/3 complex but both are narrower than F-actin. Future work should examine if these differences are cell-type specific. Here we focused on the FRAP experiments by Lai et al. [2] because the width of the Arp2/3 complex distribution in [15] was narrower. We also used SiMS data rather than data for capping protein and Arp2/3 complex from fluorescent speckle microscopy on Drosophila S2 cells [42] where each speckle is a group of molecules rather than single molecules.

Some prior mathematical models have studied aspects that relate to the kinetics of capping protein and Arp2/3 complex across the lamellipodium. The model by Ditlev et al. [22] that includes many known reactions that occur within the lamellipodium was used by Kapustina et al. [3] to model FRAP experiments, as described in section 3.1. However its predictions on Arp2/3 complex turnover have not been explored. Huber et al. [21] and Stuhrmann et al. [23] developed computational and

mathematical models that account for actin monomer diffusion and actin filament severing and annealing throughout the lamellipodium but not accounting for diffusion of filaments after severing. Branch nucleation was assumed to occur only close to the leading edge and the barbed end capping rate was assumed uniform. They assumed that any severed filament that has an Arp2/3 complex bound to it does not anneal to another filament since it is treated as a minus-end capper. Slowly diffusing Arp2/3 complex bound to actin oligomers may represent a third cytoplasmic pool, in addition to the other two pools of Figure 2.10A. We did not include such a third pool in order to focus on the mechanism for slowly diffusing Arp2/3 complex proposed by Millius et al. [6]. Hu and Papoian [43, 44] use a stochastic simulation model that includes physical and chemical interactions for actin, Arp2/3 complex, and capping protein in the lamellipodium to model protrusions. They only allow Arp2/3 complex-mediated activation branching very close to the membrane, similar to Huber et al. and Stuhrmann et al. but in addition account for cytoplasmic diffusion with diffusion coefficient 20 $mu\text{m}^2/\text{s}$ for all species. This reference value is larger than what we used here for the fast and slow diffusing pools. One of the findings in Hu and Papoian is a significant dependence of protrusion dynamics on the concentrations of capping protein and Arp2/3 complex. Since cytoplasmic concentration gradients result for slower values of the diffusion coefficients, this effect would provide an additional influence on protrusion dynamics.

We conclude with a discussion of the diffusive dynamics of some other lamellipodia regulators that have been studied with SiMS, for which our analysis may be applicable in the future. Tsuji et al. [45] studied cofilin and AIP1, which collaborate in actin filament severing [46, 47]. These SiMS studies, as well as FRAP studies of cofilin [2], indicate short bound lifetimes on the order of seconds and a broad appearance profile across the lamellipodium. Cofilin and AIP1 may be bound to the piece of severed filament after detachment for the network, which can be included in the model as a slowly diffusing cytoplasmic pool. Depending on the fraction of bound to diffuse protein, the FRAP curve for both proteins may be similar to that of

capping protein. VASP is another important regulator that typically localizes close to the leading edge of the cell as well as in focal adhesions [8, 48]. SiMS data show very transient associations with the actin network [8] and FRAP of VASP at the leading edge of lamellipodia has a half time of 8.4 s [49]. VASP can form tetramers so future work could explore the role of the anticipated slowing down of cytoplasmic diffusion on these kinetics. The WAVE complex is another interesting protein to study as it is involved in the activation of the Arp2/3 complex. The FRAP recovery of WAVE2 close to the leading edge has a half-time of 8.6 s [2]. SiMS shows a broad distribution of WAVE2 appearance events and lifetimes [6]. Only a small fraction of WAVE complex speckles undergo retrograde flow compared to the Arp2/3 complex (20% compared to 90%) [6]. Extensions of our model can be used to study the implications of slow WAVE2 diffusion with 0.41 μm^2/s [6].

Chapter 3

Model with Two Pools of Actin Supply Leading Edge while Thymosin $\beta 4$ Aids in Fast Diffusion of Actin to the Leading Edge

3.1 Modeling PA-GFP-actin dynamics

In 2013 we met experimentalist Eric Vitriol at an annual American Society for Cell Biology meeting, and we started a collaboration with him while he was a post doctoral researcher at Emory University under Professor James Zheng.

It was observed in [50] that there is an enhancement of G-actin at the leading edge of neuronal CAD (Cath.a differentiated) cells. We wanted to see (1) if it was possible to explain this enhancement of G-actin at the leading edge of motile cells with a model and (2) to study the effect of Thymosin $\beta 4$ knockdown (KD) (Knockdown of a protein is when that protein is suppressed and the cell is not allowed to produce

as much of that protein as it normally would) on actin kinetics and (3) to test if there are two pools of actin that contribute to the kinetics of the lamellipodium. Another important subject that we want to study is whether diffusion is fast enough to deliver actin to the leading edge of the cell. In order to do this we developed a computational model to describe actin turnover in lamellipodia that includes F-actin and three pools of actin in the cytoplasm or bound to the cell membrane [12].

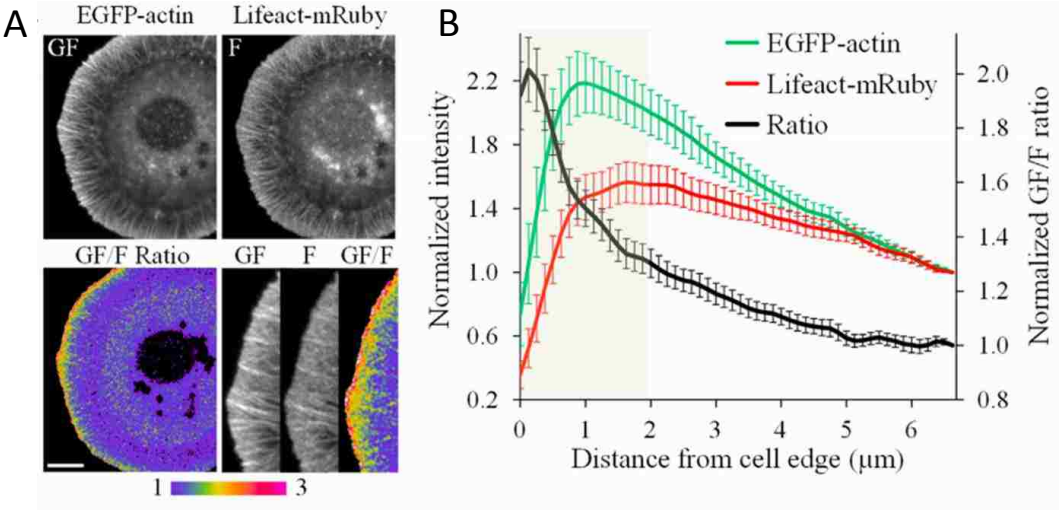

Figure 3.1: Enhancement of G-actin at leading edge of CAD cells from Vitriol et al. A) CAD cells with GFP-actin and Lifeact fluorescing which shows both G and F-actin and F-actin respectively. Scale bar 10 μm. B) Concentrations of actin as a function of distance from the leading edge in CAD cells. [50]

The enhancement at the leading edge of CAD cells is seen in Figure 3.1 A and B. EGFP-actin tags both G-actin and F-actin whereas Lifeact-mRuby tags only the sides of F-actin. So the ratio of these two signals as a function of the distance from the leading edge shows the G-actin enhancement near the leading edge [50]. This can be seen in Figure 3.1 A at the bottom right and in Figure 3.1 B in the black curve.

3.2 Model description

Our model is an extension of Smith et al. [1] which includes 3 pools of diffuse protein instead of 2. The three pools are: R, which is a recycling component that represents all actin which has been recently depolymerized (we do not make assumptions about the nature of the recycled actin, which may include oligomers or actin bound to other protein complexes); G_C, which binds reversibly to Tβ4 in the cytoplasm; and G_M, which binds reversibly to the membrane in complex with other proteins which we do not make assumptions about in this model. G_C and G_M include actin monomers in complex with profilin. This model is shown in Figure 3.2 A. [12]

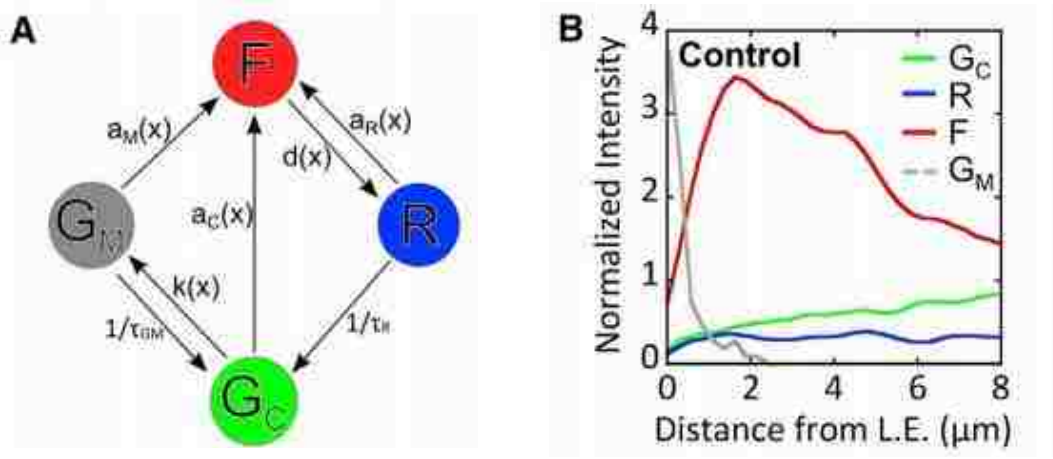

Figure 3.2: A) Diagram for model with Membrane binding protein B) Steady state concentration profiles normalized to G_C far from the leading edge for control case.

The rate of diffuse to bound, $a(x)$, is measured in μM/s and taken from the appearance rate from SiMS data. The appearance rate in this model is split between the three actin pools,

$$a(x) = a_R(x) + a_C(x) + a_M(x). \tag{3.1}$$

The appearance rate from SiMS data is fit with a double exponential with length

scales λ_1 and λ_2, where $\lambda_1 < \lambda_2$. The appearances are defined as follows:

$$a_C(x) = KG_\infty A_C e^{-x/\lambda_1}, a_M(x) = KG_\infty A_M e^{-x/\lambda_1}, a_R(x) = KG_\infty A_R e^{-x/\lambda_2} \quad (3.2)$$

Here G_∞ is the concentration of G_C far from the leading edge, K is a constant that determines the fraction of F to G-actin, and we define $A_C + A_M + A_R = 1$. Lifetimes for F-actin are given by the equation $p(t)$ which gives the probability, given a time t, that the F-actin is still in the F-actin state which is represented by a double exponential as in [1],

$$p(t)/p(0) = C_1 e^{-t/\tau_1} + C_2 e^{-t/\tau_2} \quad (3.3)$$

where C_1=0.741, C_2=0.259, τ_1=16 s, and τ_2=60 s.

The concentration of actin at steady state, $F(x)$, can be calculated from the polymerization rates and lifetime distribution as described in [1]. The equations that describe the steady state concentrations of the diffuse components are as follows:

$$D_R \frac{d^2R(x)}{dx^2} = a_R(x) + \frac{1}{\tau_R} R(x) - d(x), \quad (3.4)$$

$$D_C \frac{d^2G_C(x)}{dx^2} = a_C(x) + k(x)G_C(x) - \frac{1}{\tau_{GM}} G_M(x) - \frac{1}{\tau_R} R(x), \quad (3.5)$$

$$D_M \frac{D^2G_M(x)}{dx^2} = a_M(x) - k(x)G_C(x) + \frac{1}{\tau_{GM}} G_M(x). \quad (3.6)$$

In these equations D_R, D_C, and D_M are the diffusion coefficients for recycled actin, cytoplasmic actin, and membrane bound actin respectively. The lifetimes τ_{GM} and τ_R are the times that G_M and R remain in their respective states until they become G_C. The rate $k(x)$ is a spatially dependent rate that G_C becomes G_M. Equations 3.4-3.6 are solved numerically for the concentration profiles ($G_M(x)$, $R(x)$ and $G_C(x)$) with the Jacobi method. These profiles are shown in Figure 3.2 B and the parameters used to find these profiles are listed in Table 3.1.

The binding rate for the recycled actin, R, to become F-actin is calculated by:

$$r_R(x) = \frac{a_R(x)}{R(x)}. \tag{3.7}$$

Each rate for G_M and G_C is calculated similarly. The simulation is moved forward in time using a 2D off-lattice Monte Carlo particle simulation as in [1]. The simulation box used was a rectangle extending 28.95 μm into the cell and 21.05 μm wide with reflecting boundaries. Each particle is either diffusing freely with a diffusion coefficient chosen by whichever type of species the particle is, or it is a particle in the F-actin state and undergoing retrograde flow. Particles are updated every time step, Δt, which is chosen to be sufficiently small.

The simulation is moved forward in time according to the reactions in Figure 3.2 A. If a particle is F-actin and its lifetime is up, it will dissociate into recycled actin, if not it will undergo retrograde flow a distance $v_r \Delta t$ into the simulated cell in one time step. A recycled actin particle will diffuse with diffusion coefficient D_R unless its lifetime τ_R is reached then it will become cytoplasmic actin. The recycled actin can also become F-actin before its lifetime is up with appearance rate of $a_R(x)$. A cytoplasmic particle can become membrane bound with rate $k(x)$ which is defined in Table 3.1 or it can become F-actin with appearance rate $a_C(x)$ otherwise it will diffuse with diffusion coefficient D_C. A membrane bound particle may become cytoplasmic actin if the lifetime of τ_{GM} is up. If the lifetime has not been reached it can also become F-actin with appearance rate $a_M(x)$ otherwise it will diffuse with diffusion coefficient D_M. Each parameter used can be found in Table 3.1 as well as the source or justification for using that value.

The system is initialized so that the concentrations matched those found after solving equations 3.4-3.6. The lifetimes of the polymerized particles in the initial distribution were picked by applying Bayes' rule [1]. The system was equilibrated for at least 200 s before simulating photoactivation. To simulate experimental images, the particles were treated as diffraction-limited spots that diffuse during camera exposure [1].

Parameter	Value	Reference/Justification
D_R	0.5 $\mu m^2/s$	Smith et al. 2013 [1]
D_C	3.0 $\mu m^2/s$	Measured in [12]
D_M	0.001 $\mu m^2/s$	Small value to represent slow diffusion of membrane-bound component G_M
v_r	70 nm/s	Measured in [12]
K	0.25 s^{-1}	Estimated to give a ratio of F-actin to diffuse components as in Figure 3.2 C.
τ_R	20 s	Smith et al. 2013 [1]
τ_M	0.5 s	Smaller than 1 s
A_R	0.16	Smith et al. 2013 [1]
A_C	0.21	Smith et al. 2013 [1], assuming 25 % of polymerization events from the non-recycling pools at the leading edge are due to G_C
A_M	0.63	Smith et al. 2013 [1], assuming 75% of polymerization events from the non-recycling pools at the leading edge are due to G_M
λ_1	0.5 μm	Smith et al. 2013 [1]
λ_2	4 μm	Smith et al. 2013 [1]
$k(x)$	$20s^{-1}e^{-x/0.5\mu m}$	Selected to occur within a narrow region close to the leading edge and with amplitude giving G_M concentration higher than G_C

Table 3.1: Parameter table for simulated photoactivation of actin

3.3 Comparison to experiment

To perform simulated photoactivation of actin on a region, all particles outside of that region are deleted. Then, all the remaining particles are allowed to move and react in the way described above.

3.3.1 Photoactivation in 5 by 10 μm box at Leading Edge

An example of experimental photoactivation of PA-GFP actin is shown in Figure 3.3 A. This photoactivation is at the leading edge of the cell and is a region of 5 by 10

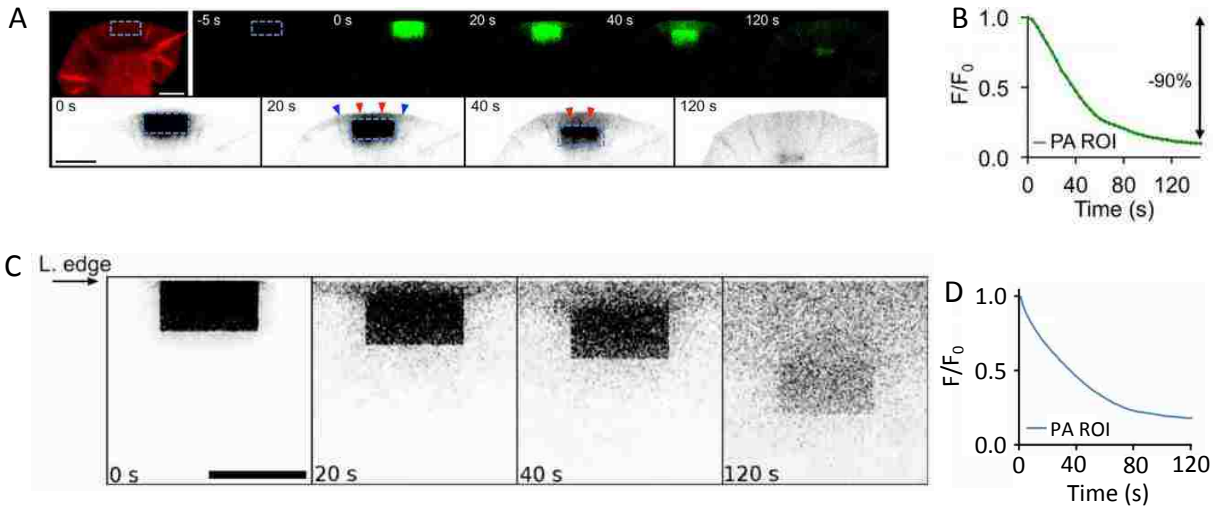

Figure 3.3: Experimental vs. Simulated Photoactivation of 5 by 10 μm box at leading edge in CAD cells. A) Top: Experimental photoactivation of PA-GFP actin of 5 by 10 μm rectangle in [12] Bottom: Inverted image of experimental photoactivation of PA-GFP actin of 5 by 10 μm rectangle in [12] Scale bar 10 μm B) Normalized intensity of fluorescence decay from experimental PA ROI from [12] C) Simulated photoactivation of 5 by 10 μm rectangle. Scale bar 5 μm D) Normalized intensity of fluorescence decay from simulated PA ROI.

μm in size. In Figure 3.3 A (both top and bottom panels) the photoactivated region undergoes retrograde flow with the actin network and most of the fluorescence in the region of interest (ROI), which is the same as the region of photoactivation, leaves the ROI as shown in the graph in Figure 3.3 B. In the bottom panels of Figure 3.3 A, which is an inverted grayscale image, it is easier to see that there is incorporation of photoactivated actin at the leading edge indicating that some recycling occurs locally. We also ran a simulation of actin photoactivation of the same size and position as that in the experiment. In the simulation we see similar behavior shown in Figure 3.3 C, D with some local recycling with rebinding near the photoactivated region as well as similar decay in fluorescence for the ROI.

3.3.2 Photoactivation in Cell Center

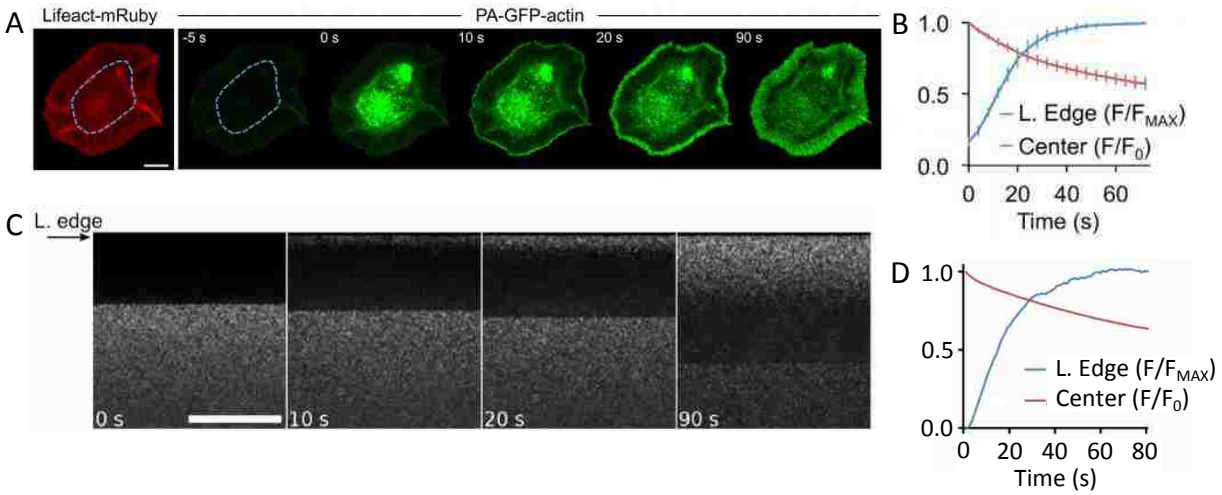

Figure 3.4: Photoactivation of cell center of CAD cells. A) Experimental photoactivation of PA-GFP actin of the cell center from [12] Scale bar 10 μm B) Intensity of fluorescence after experimental photoactivation of PA-GFP actin within 1 μm of the leading edge and entire cell center over time C) Simulated photoactivation of actin of the cell center. Scale bar 5 μm D) Intensity of fluorescence after simulated photoactivation within 1 μm of the leading edge and entire cell center over time

Figure 3.4 A shows the experimental images of photoactivation of the cell center. The PA-GFP actin within the cell center was activated to watch how the actin from the cell center moves out of the cell center and into the lamellipodium. The graph in Figure 3.4 B shows the normalized fluorescence in two separate places, the leading edge, which is all the fluorescence within 1 μm of the leading edge of the cell and normalized to its maximum intensity, and the center, which is the total fluorescence within the cell center and normalized to its beginning intensity. In Figure 3.4 A it can be seen that there is fast recovery at the leading edge of the cell. This brings up the question of whether diffusion is fast enough to allow travel from the cell center to the leading edge in this amount of time. With our model, we run a simulation of the same type of photoactivation where everything but the lamellipodium is activated

and then the recovery is monitored. The results of this simulation can be seen in Figure 3.4 C, D. The recovery and graphs both look similar to the experimental photoactivation when the graphs are normalized in the same way as the experimental data. Since our model is a reaction diffusion model with no active transport and the recovery at the leading edge happens on the same time scale as in the experiment, we can conclude that diffusion is likely sufficient for delivery of actin from the cell center to the leading edge of the cell.

3.3.3 Whole Lamellipodium Photoactivation

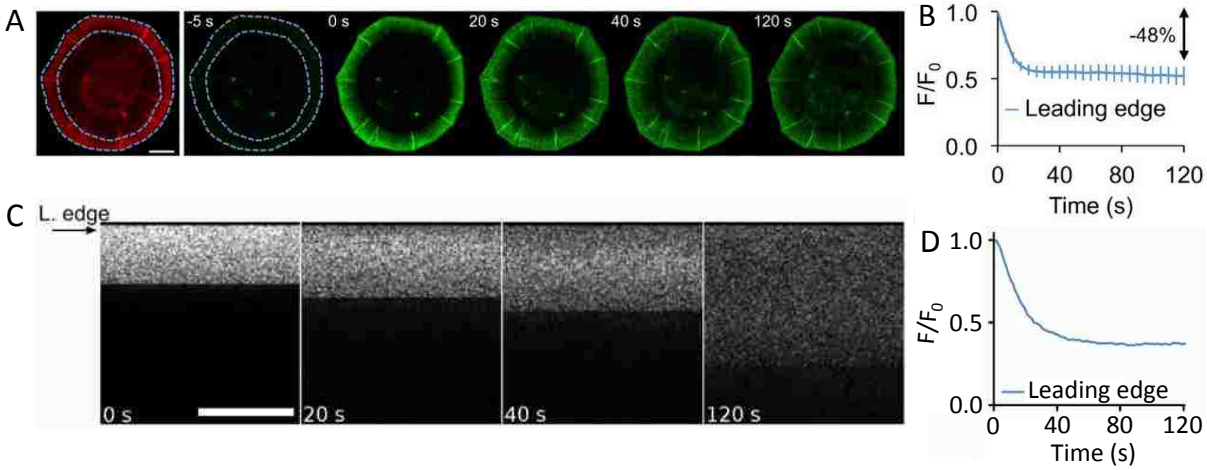

Figure 3.5: Experimental vs. Simulated Photoactivation of lamellipodium for CAD cells. A) Experimental photoactivation of PA-GFP actin of the lamellipodium from [12] Scale bar 10 μm B) Intensity of fluorescence after experimental photoactivation of PA-GFP actin within 1 μm of the leading edge over time C) Simulated photoactivation of actin of the lamellipodium. Scale bar 5 μm D) Intensity of fluorescence after simulated photoactivation within 1 μm of the leading edge

The next photoactivation experiment performed by Eric Vitriol was activating the PA-GFP actin in the lamellipodium and observing how the fluorescence changes within the cell. The experimental images of the photoactivation are shown in Figure

3.5 A. The fluorescence at the leading edge of the cell (within 1 μm of the leading edge) is monitored throughout time and normalized to the initial value in Figure 3.5 B. The fluorescence decays to about 50% of its original value where it plateaus. The authors of [12] suggest that this points to a pool of actin that is recycled within the lamellipodium which will be discussed more in Chapter 4. We also run a photoactivation simulation activating the lamellipodium in the same way as the experiment in Figure 3.5 C. The leading edge simulated intensity is monitored over time and normalized in the same way as the experiment and shown in Figure 3.5 D. For the simulated image, the plateau of the fluorescence occurs at the level of total amount of actin that was photoactivated. This may not be the case for the experimental PA-GFP photoactivation in CAD cells since the underlying mechanism may be more complicated than the mechanisms included in our model. This is discussed later in Chapter 4.

3.4 Thymosin β4 KD's effect on actin kinetics in the lamellipodium

Thymosin β4 (Tβ4) is a protein that is known to bind to actin monomers and sequester them, not allowing polymerization which is demonstrated in Figure 3.6. About 70% of G-actin is typically sequestered by thymosin β4 [52]. It was previously unclear how Tβ4 affected the kinetics of the lamellipodium. So the authors in [12] performed photoactivation experiments of PA-GFP actin to learn about these kinetics by knocking down Tβ4, using shRNA to knock down, and comparing these experiments to the control case. In Figure 3.7 A the cell center has been photoactivated and the leading edge is monitored to watch the recovery. The Tβ4 KD experiment within the first 60 s has a lag in recovery at the leading edge compared to the control case (Figure 3.7 A.) There is also a small difference in the F-actin profile between the control and knockdown case shown in Figure 3.7 B with the control slightly enhanced compared to the knockdown. We wanted to compare our model

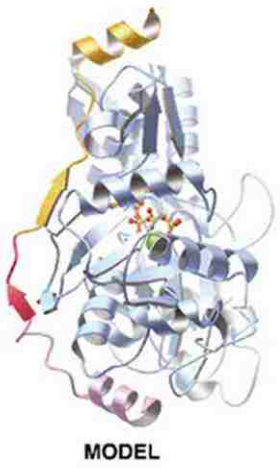

Figure 3.6: Thymosin $\beta 4$ sequesters actin monomers from Irobi et al.. An actin monomer is shown in gray while a Thymosin $\beta 4$ protein is seen in yellow and red and is bent around the actin monomer. Figure from [51]

to the experimental photoactivation to explain this lag in recovery. After varying all parameters that would affect this recovery, we found that in order to get a lag in recovery with our model we had to increase the binding rate of G_C at the back of the lamellipodium shown in Figure 3.8 A. We also require the diffusion coefficient to be reduced by 50% in order to match the lag in recovery at the leading edge. This produces a steady state profile for the T$\beta 4$ KD shown in Figure 3.8 B. These combined effects give a lag in recovery at the leading edge in our simulations which is shown in Figure 3.8 C. From this we predicted a less sharp sigmoidal recovery at the back of the lamellipodium (2-3 μm away from the leading edge) for the T$\beta 4$ KD cells compared to the control case [12] which is also shown in Figure 3.8 C. This prediction about the experiments is correct and can be seen in Figure 3.9.

We also monitored the recovery within the cell center in the experimental case where the cell center is photoactivated (Figure 3.10 A) and found that there was good agreement with our simulated cell center activation (Figure 3.10 B). Lamellipodium photoactivation was also simulated for T$\beta 4$ KD and compared to the control case

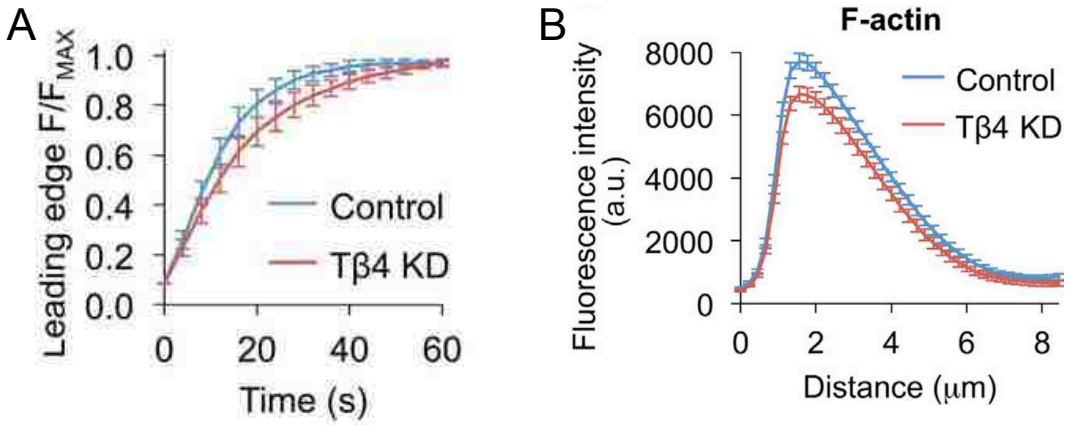

Figure 3.7: Experimental control and Tβ4 KD photoactivation and F-actin profiles. A) PA-GFP photoactivation of cell center with intensity recorded within 1 μm of the leading edge over time for both control and Tβ4 KD over time [12] B) F-actin profile in the lamellipodium for both control and Tβ4 KD cases

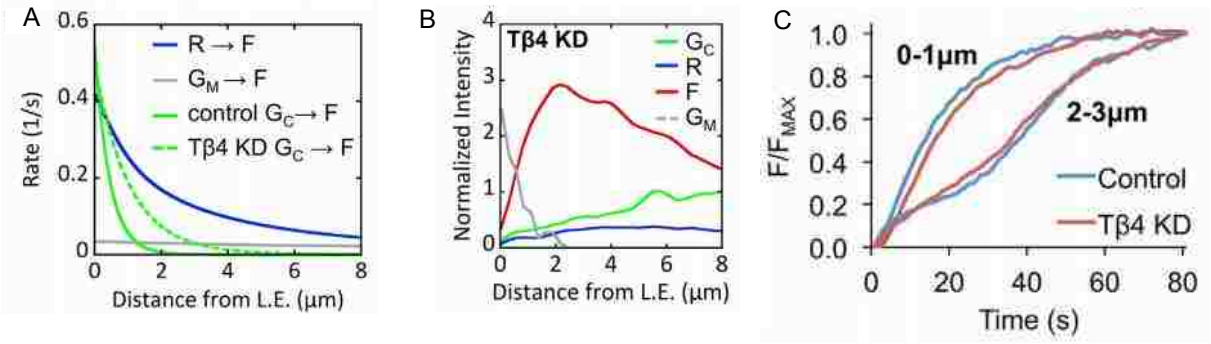

Figure 3.8: Simulated photoactivation with knockdown of Tβ4. A) Rates of binding for each diffusive species in units of 1/s for both control and Tβ4 KD cases. B) Steady state concentration profiles normalized to G_C far from the leading edge for Tβ4 KD case. C) Simulated photoactivation of actin of the cell center for both control and Tβ4 KD cases with intensity recorded at 0-1 μm from the leading edge as well as 2-3 μm from the leading edge.

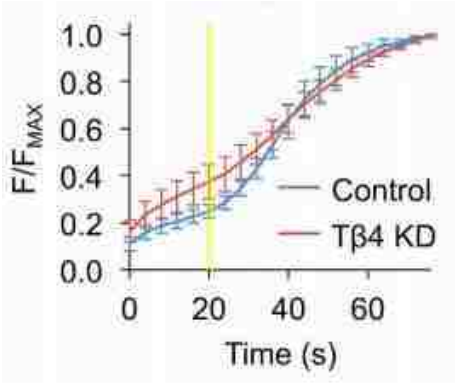

Figure 3.9: PA-GFP photoactivation of cell center with intensity recorded 2-3 μm from the leading edge over time for both control and Tβ4 KD over time [12]

and by monitoring fluorescence at the leading edge we found that there was little difference between the two cases (Figure 3.10 C). We tested if the rate allowing G_C to become G_M was set to zero if this would give a similar effect to the Tβ4 KD experiments. So we performed a simulation with this in place and compared it to the control case as shown in Figure 3.10 D. There is also little difference between the case with the rate set to zero and the control case. Which means setting that rate to zero is not equivalent to the KD case.

3.5 Conclusions

This collaboration with Eric Vitriol resulted in the following conclusions. We have shown that actin within the lamellipodium exists within two pools, one which is bound to Thymosin β4 and allows for fast diffusion through the lamellipodium and another pool which diffuses slowly and is not bound to Thymosin β4 [12]. Actin bound to Thymosin β4 is prevented from binding to actin towards the back of the lamellipodium and tends to diffuse to the leading edge of the cell where it may associate in a complex with profilin and allow the actin to incorporate into the actin network through the aid of formins. Although we suspect that Thymosin β4

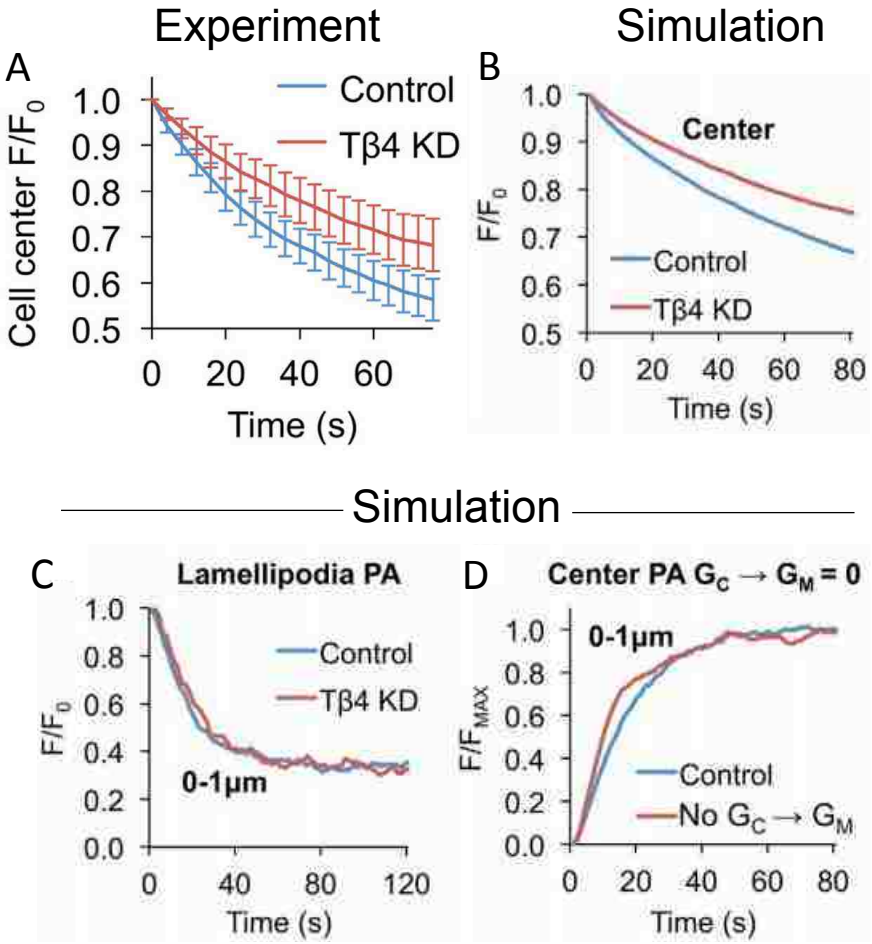

Figure 3.10: Comparison of experimental photoactivation with simulated photoactivation for control and Tβ4 KD casess. A) Experimental cell center photoactivation B) Simulated cell center photoactivation with normalized intensity recorded Left: both within 1 μm of the leading edge and 2-3 μm from the leading edge right: intensity decay for both control and Tβ4 KD simulations within the cell center C) Simulated lamellipodium photoactivation for actin with recorded intensity within 1 μm of the leading edge D) Center photoactivation of the cell center for actin with the rate from $G_C \longrightarrow G_M$ set to zero compared to the control case.

may make a complex with profilin and actin near the leading edge of the cell, more experiments are needed to verify this hypothesis [12]. The model suggests that the actin that is not bound to Thymosin $\beta 4$ is incorporated into the actin network away from the leading edge. We also find that diffusion is sufficient for delivery of actin to the leading edge and no active transport is needed in order to have actin delivered to the leading edge in a timely manner, although we find that our system is close to being limited by diffusion. Thymosin $\beta 4$ aids in this diffusion by sequestering the actin monomers and not allowing them to bind promiscuously to other actin binding proteins throughout the lamellipodial network [12].

Chapter 4

Turnover of Actin in 3D Whole Cell Model

In previous modeling studies in this thesis, the modeling performed was in 2D and the 3D geometry of the cell was not taken into account. It is useful to investigate modeling done in 3D and include the complete geometry of the cell. In making a model of the cell that includes the whole cell instead of just the lamellipodium we can study if diffusion is sufficient for delivery of G-actin to the leading edge. Within the cell center there are some forms of F-actin that we have not included in previous models presented in this thesis. One is cortical actin which is located in the cortex of the cell. The cortex is located near the membrane of the cell. Other types of F-actin include stress fibers and non-stress fibers. These are F-actin populations that are near the basal surface of the cell. Stress fibers are relatively long-lived with lifetimes in the range of minutes [35] while non-stress fibers and cortical actin are generally more short lived with lifetimes on the order of tens of seconds [35, 53].

Another consideration for our whole cell model is answering the question of how much actin is distributed within the lamellipodium compared to the rest of the cell. It is estimated in Vitriol et al. [12] that about 10-20% of the total actin in the cell is in the lamellipodium. We are interested in checking if this is consistent with

Figure 3.5 and the estimation of the amount of actin in the lamellipodium given the information that we have with the photoactivation experiments.

Some previous studies have suggested that diffusion is not fast enough to deliver monomeric actin to the leading edge of the cell. Zicha et al. [24] argue that the rapid delivery of actin to the leading edge after FLAP (fluorescence loss after photoactivation, described in chapter 1 implies that it is impossible that diffusion is fast enough to allow this to happen. The authors argue this because 4 s after photoactivation occurs, photoactivated actin is seen at the leading edge of the cell which is pointed out by the arrows in Figure 4.1. They develop a model in which they allow for only G-actin diffusion with a diffusion coefficient of $5.65\mu m^2/s$ and find that with this diffusion coefficient and protrusion, they cannot account for the FLAP ratio that is seen in their experiments [24]. In order to account for this FLAP ratio enhancement at the leading edge they need to include a constant drift velocity for G-actin towards the leading edge of 6 $\mu m/s$ [24]. By contrast another work based on s-FDAP suggests a high diffusion coefficient of $D = 13.7\ \mu m^2/s$ would be fast enough for delivery of G-actin to the leading edge of motile cells [13].

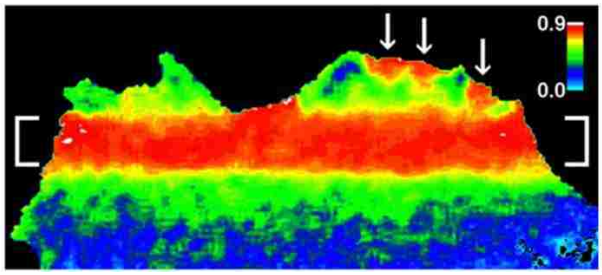

Figure 4.1: FLAP showing fast delivery of diffuse actin to the leading edge of cell Zicha et al. Ratio of FLAP which shows newly photoactivated actin in hot colors and arrows point to spots where photoactivated actin arrived at the leading edge 4 s after photoactivation occurred. Figure from [24]

Fan et al. [26] argue that Myo1, which is a motor protein, is needed in order to transport G-actin to the leading edge of a motile cell. The support for their hypothesis can be seen in Figure 4.2 where in the top row they knocked down Myo1

(which means that Myo1 has a lower expression rate than normal), by siRNA and shRNA, and they found that very little G-actin is at the leading edge of the cell. Open arrows indicate areas of reduced G- or F-actin [26]. The direction of motion of the cell is shown by the long solid arrow. In the bottom row, however, Myo1 levels are normal and there is more G-actin at the leading edge of the cell [26], and the filled arrows indicate areas of enhanced G- or F-actin. The authors suggest that Myo1 is transporting G-actin to the leading edge of motile cells so that it can polymerize into F-actin [26].

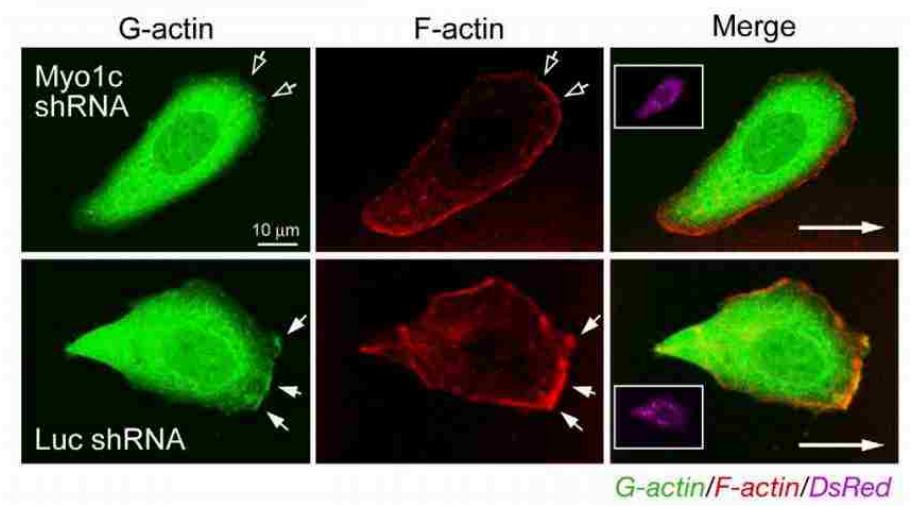

Figure 4.2: Fluorescent microscopy supporting the important role of Myo1 in the transport of G-actin to the leading edge of motile cells from Fan et al. Green tagged protein is G-actin and red tagged protein is F-actin. Top row: Myo1 has been suppressed and the effect on actin kinetics is that not as much G-actin is seen at the leading edge of the motile cell. Bottom row: With Myo1 at normal levels G-actin can been seen localizing at the leading edge of motile cells. Figure from [26]

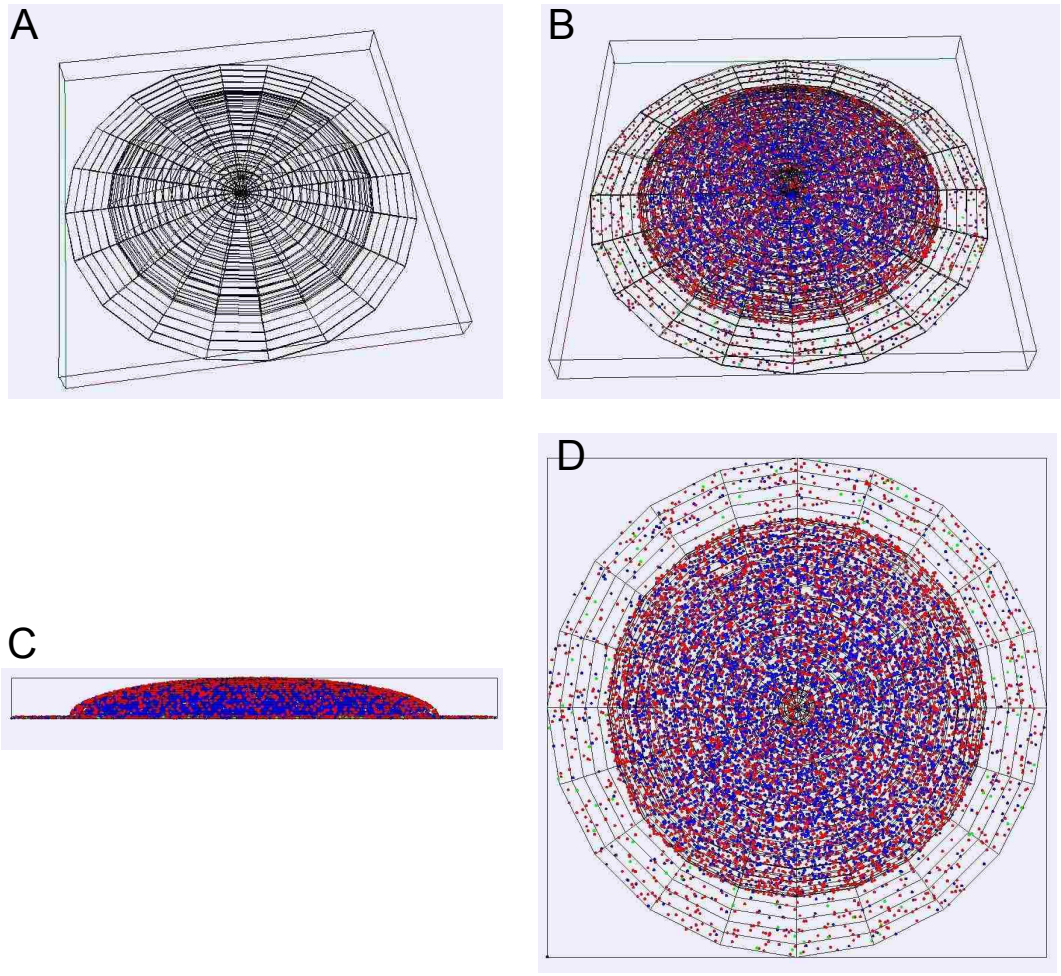

Figure 4.3: Example of shape of 3D whole cell model. A) top view of simulated cell with no particles inside to show shape. B) top view of 3D simulated cell with particles distributed within the cell. C) side view of 3D simulated cell to display distribution of particles within the cell. D) Top view of simulated cell to display distribution of particles within the cell. For all imaged the diameter of the cell is 50 μm.

4.1 Model Description

The geometry of this simulated cell which is similar to CAD cells and non-polarized is modeled as follows: the lamellipodium consists of a disk with a height h_{lamell} above

the slide and has a chosen width of w. The cell center is a half ellipsoid with x and y axes equal and the diameter of this center ellipsoid determined by taking the cell diameter and subtracting double the lamellipodium width. Some examples of the geometry are shown in Figure 4.3 A-D. Figure 4.3 A is the shape of the cell with no particles distributed inside the cell. The lamellipodium is the outer part of a thin disk while the cell center is a half ellipsoid that sits on top of the thin disk. Figure 4.3 B is an example of a cell that has particles distributed within it. Red particles are bound, blue particles are fast diffusing, and green particles are slower diffusing than the fast diffusing particles. Figure 4.3 C is a side view of the cell while D is a top view of the cell.

4.1.1 Lamellipodium

Within the lamellipodium we use a previous model by Smith et al. [1] which is described in chapter 1 and is a model with both oligomers and monomers contributing to appearance events shown in Figure 4.5. The model as stated in [1] is a 2D model written in Cartesian coordinates. In order for this model to be used in a circular geometry the 2D equations are written in polar coordinates. In this model the lamellipodium is only the thin annulus that does not touch the half-ellipsoid. The rates of binding are the same for each height within the lamellipodium but now are based on radial distance from the leading edge instead of distance from the leading edge which was used in [1]. Flow of the actin network rearward occurs in the radial direction (remaining at the same height) and moves a distance of $v_r dt$ each time step towards the center of the cell, where v_r is the retrograde flow velocity. Diffusion within the lamellipodium occurs and the boundaries of both the top and bottom of the lamellipodium as well as the edges exert a soft boundary force ($F = -kd$, where d is the distance that the particle steps outside the boundary) on diffuse particles that attempt to step outside the cell boundary to push the particle back within the cell. The distribution of F-, G-, and O- actin within the lamellipodium is shown in Figure 4.4.

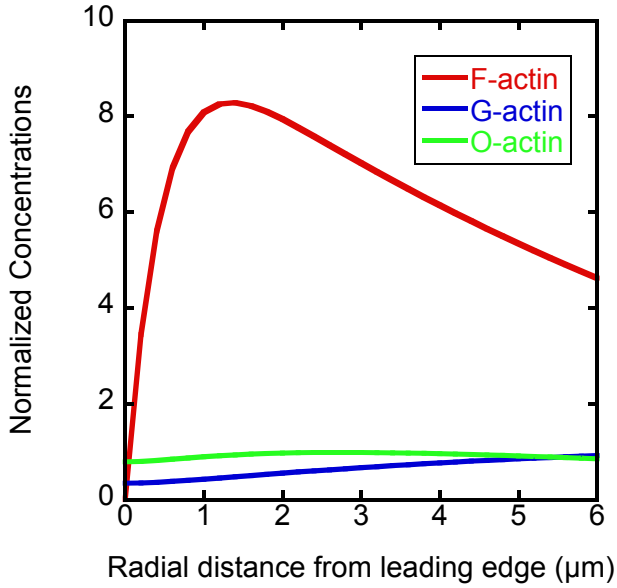

Figure 4.4: Steady state concentrations for actin within the lamellipodium in 3D model.

4.1.2 Cell Center

In the cell center there are both particles that are in the G- and F-actin pools. The density of G-actin within the cell center is calculated to be the same as the density of G-actin where the lamellipodium touches the cell center. F-actin within the cell center can be one of three different types: stress fibers, non-stress fibers, or cortical actin. Stress fibers and non-stress fibers are localized in this model to the bottom of the cell center within a thickness that is equal to the thickness of 0.15 μm [54]. The lifetimes of stress fibers and non-stress fibers can be found in Table 4.1, where the lifetimes for stress fibers and non-stress fibers are measured from SiMS [35]. Cortical actin is localized in this model to the top dome of the ellipsoid within a thickness of 0.1 μm [54]. The lifetimes of cortical actin can also be found in Table 4.1 and are measured from FRAP. The fast component of non-stress fibers is on the order of the slower lifetime of cortical actin. F-actin can only be found near the cortex within the cell center and so the rates of binding from G-actin to F-actin take into account the

volume within the F-actin pool can exist. G-actin within the cell center is diffusing with the same rate as the G-actin within the lamellipodium.

4.1.3 Excluded volume

Another feature within the cell is the organelles. For eukaryotic cells, the organelles that take up the most volume within the cell are the nucleus and mitochondria [55]. On average the nucleus occupies approximately 10% of the cell volume [56], while the mitochondria occupy about 20-25% of the cell volume [55]. This means that the sum for all major organelles is about 30-35% of the total volume is excluded for movement of protein. In order to account for this I have added one large excluded volume that occupies approximately 32% of the cell that is ellipsoidal in shape and is placed within the cell center. This excluded volume represents both the nucleus and mitochondria combined because the other organelles take up much smaller amounts of volume within the cell. An example of this within the cell can be seen in Figure 4.6. Figure 4.6 A shows a side view where the nucleus can be seen in black in the center of the cell while B shows a top view where the nucleus is more shaded than the rest of the cell.

4.1.4 Initialization

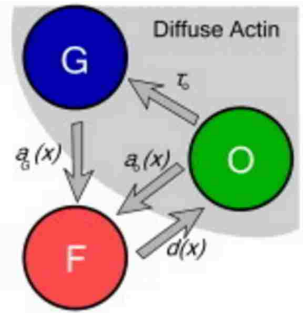

Figure 4.5: 3D Model with monomer and oligomers contributing to appearance events from [1].

In order to initialize this simulation, we start by assuming that F-actin in the lamellipodium is distributed radially with the same $F(x)$ described in 1.4. We solve for G and O actin in polar coorinates. We can then solve these equations 1.8-1.10 numerically for $G(r)$ and $O(r)$, where r is the radial distance from the leading edge of the cell. To then distribute the particles properly within the lamellipodium, which is a thin disk, the disk is broken up into small slices of dr so that within each slice particles can be placed correctly for each species.

In order to place each particle one can find the total number of particles for each species that should be in each dr slice. For any one slice, dr, for the model with only monomers as the diffuse species the fraction G-actin in that slice is given by:

$$\frac{\int_{r_i}^{r_{i+1}} G(r)2\pi r dr}{\int_0^L G(r)2\pi r dr + \int_0^L F(r)2\pi r dr}, \tag{4.1}$$

where L is the length of the lamellipodium. This is then done similarly for F-actin. If we use the model that includes oligomers and monomers contributing to appearance events, the denominator will also include the integral of O-actin for the entire lamellipodium. Particles within the lamellipodium are given lifetimes from the distribution measured from SiMS data.

To distribute G-actin particles within the cell center, the density of particles is calculated based on the density of G-actin far from the leading edge in the lamellipodium. Then, using this density and the volume that is not excluded within the cell center the number of G-actin particles is calculated and that number of particles is placed randomly throughout the cell center.

Particles in the F-actin pool are placed only within the cortex in the cell center. The number of F-actin particles placed depends on the ratio of G-:F-actin within the cell center that is chosen. If a 1:1 ratio is chosen then the same number of F-actin is placed as G-actin in the cell center. All the F-actin within the apical cortex is cortical actin and the fraction placed there (of the total F-actin in the cell center) is based on volume: $V_{\text{top shell}}/(V_{\text{top shell}} + V_{\text{bottom disk}})$ where $V_{\text{top shell}}$ is the volume of

the top shell and $V_{\text{bottom disk}}$ is the volume of the bottom disk in the cell center. The actin in the apical cortex is given lifetimes of cortical actin given in Table 4.1, and the actin in the basal cortex is split between stress fibers and non-stress fibers and is given lifetimes from Table 4.1.

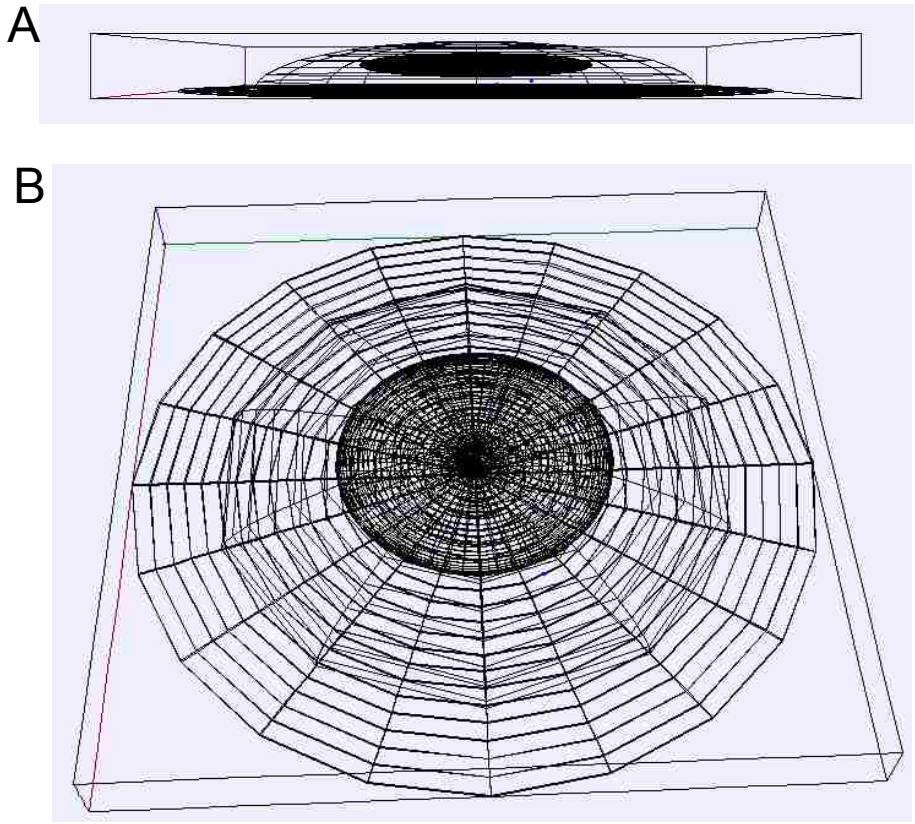

Figure 4.6: Example of cell with nucleus in simulation. A) Side view mage of cell shape showing nucleus within the cell center. B) Top view of cell shape showing nucleus within the cell center.

Parameter	Value	Reference/Justification
dt	1.0×10^{-5} s	Must be small to keep step size of diffusing particles small enough to not step outside of thin lamellipodium
D_{fast}	4.0 μm^2/s	Smith et al. 2013 [1]
K	0.5 s^{-1}	Smith et al. 2013 [1]
D_{fslow}	0.5 μm^2	Smith et al. 2013 [1]
Center cell height	4.0 μm	Kapustina et al. [3]
Cell diameter	50 μm	Measured from [12]
Lamellipodium height	0.15 μm	Laurent et al. [57]
Lamellipodium width	6.0 μm	Measured from [12]
Retrograde flow (v_r)	0.07 μm/s	Measured in [12]
Stress Fiber τ_{short}	26.7 s	Yamashiro et al. [35]
Stress Fiber τ_{long}	448.8 s	Yamashiro et al. [35]
Fraction of short-lived Stress Fibers	0.15	Yamashiro et al. [35]
Fraction of long-lived Stress Fibers	0.85	Yamashiro et al. [35]
Non-Stress Fiber τ_{short}	46.6 s	Yamashiro et al. [35]
Non-Stress Fiber τ_{long}	336.8 s	Yamashiro et al. [35]
Fraction of short-lived Non-Stress Fibers	0.73	Yamashiro et al. [35]
Fraction of long-lived Non-Stress Fibers	0.27	Yamashiro et al. [35]
Cortical actin $\tau_{\text{cort short}}$	0.73 s	Fritzsche et al. [53]
Cortical actin $\tau_{\text{cort long}}$	25 s	Fritzsche et al. [53]
Fraction of short-lived cortical actin $C_{\text{cort short}}$	0.69	Fritzsche et al. [53]
Fraction of long-lived cortical actin $C_{\text{cort long}}$	0.31	Fritzsche et al. [53]
Excluded volume radius	13 μm	Chosen to get proper excluded volume
Excluded volume height	3 μm	Chosen to get proper excluded volume

Table 4.1: Parameter table for whole cell model

4.1.5 Stepping in Time

The diffuse particles throughout the cell are moved by choosing their displacement stochastically from a Gaussian distribution. Diffuse particles within the lamellipodium are allowed to become F-actin with a rate given by

$$r_G(x) = \frac{a_G(x)}{G(x)}, \tag{4.2}$$

where $a_G(x)$ is the double exponential fit to the appearance rate from SiMS,

$$a_G(x) = A_1 e^{-x/\lambda_{short}} + A_2 e^{-x/\lambda_{long}}. \tag{4.3}$$

Particles in the O-actin pool can become particles in the F-actin pool with rate:

$$r_O(x) = \frac{a_O(x)}{O(x)}. \tag{4.4}$$

Particles that are in the F-actin pool can become particles in the O-actin pool whenever the lifetime, which is chosen from an exponential distribution, of the F-actin pool is reached. Particles in the O-actin pool can also become particles in the G-actin pool when its lifetime, which is chosen from an exponential distribution, has expired. If a particle is in the F-actin pool and it has not reached its lifetime, it will undergo retrograde flow in the radial direction away from the leading edge. If particles in the F-actin pool reach the back of the lamellipodium it is automatically depolymerized and turned into the fast diffusing G-actin pool.

Within the cell center, if a particle is in the G-actin pool, unless it is near the membranes where particles in the F-actin pool are localized, it diffuses freely. However, if particles in the G-actin pool are within the top shell where cortical actin exists the rate to bind is:

$$r_{\text{cort}} = \frac{V_{\text{total}}}{V_{\text{top}}} \left(C_{\text{cort,short}} \frac{1}{\tau_{\text{cort,short}}} + C_{\text{cort,long}} \frac{1}{\tau_{\text{cort,long}}} \right) f_{\text{cort}}, \tag{4.5}$$

where V_{total} is the total available volume of the cell center, V_{top} is the volume of the top shell where cortical actin exists, and f_{cort} is the fraction of cortical actin

compared to the total F-actin in the cell center. F-actin in the cell center can become G-actin when their lifetimes expire. The F-actin lifetimes are chosen from exponential distributions depending on if the F-actin is designated as cortical actin, stress fibers, or non-stress fibers. Particles in the F-actin state do not move.

Particles which try to step outside of the cell center, the top of the ellipsoid and the bottom of the disk, are moved towards the available space with step $dx = \text{const}dt$ which corresponds to a constant forces inwards when crossing the boundary. The ellipsoid, which represents the volume taken up by the nucleus and mitochondria as well as other organelles, exerts the same soft boundary force normal to the surface as above to not allow diffusing particles to enter it so as to exclude that volume.

4.2 Results

4.2.1 Whole Lamellipodium Photoactivation

In order to investigate recycling of actin within the lamellipodium, we photoactivated only the lamellipodium of our simulated cell and compared it to the experimental data from [12]. In doing this simulation we could see how various chosen parameters affected the plateau level of fluorescence decay. In Figure 4.7 A experimental photoactivation of PA-GFP actin of the lamellipodium is shown at various time points. Figure 4.7 B is a graph of the fluorescence intensity over time within 1 μm of the leading edge which is normalized to the intensity at the first time point. The fluorescence decays to a plateau within 40 s, and the level of this decay could mean two things: 1) 50% of the PA-GFP actin is initally activated and then spread throughout the cell, or 2) a smaller fraction of PA-GFP actin than 50% is initally activated but a big fraction remains trapped in the lamellipodium for long times. We suggest an experiment to resolve the difference between these two explanations by allowing the experiment to be recorded for longer times.

Next we ran a simulation of photoactivation of the lamellipodium to observe if the simulated intensity decay at the leading edge of our model is similar to the

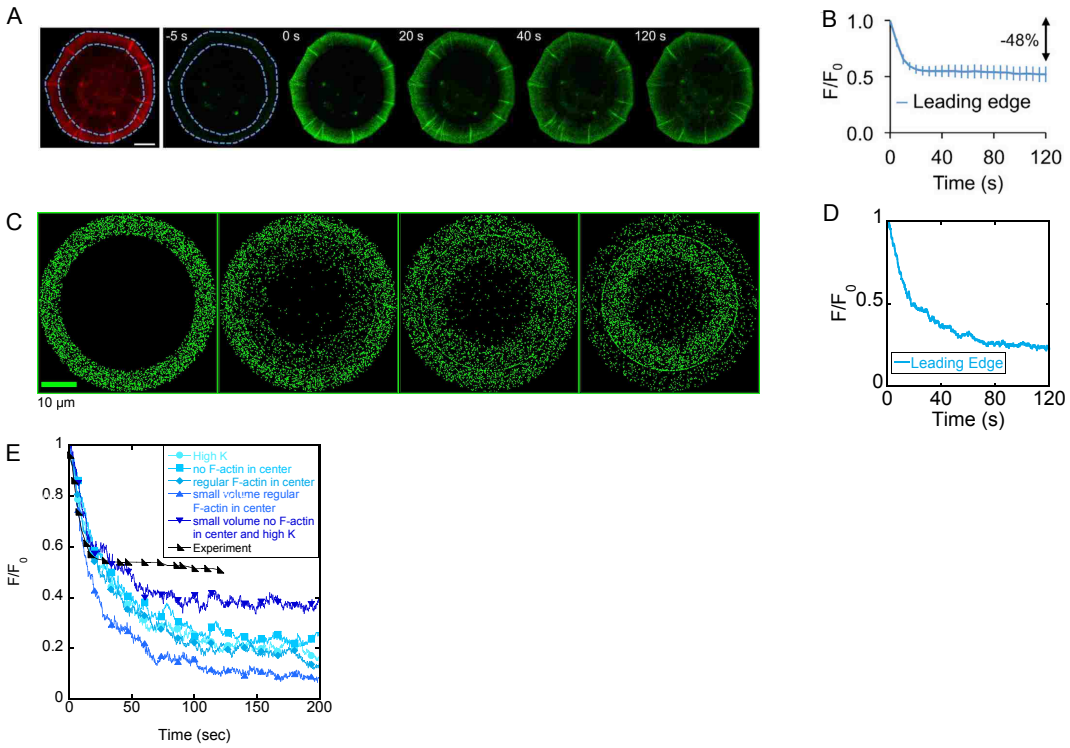

Figure 4.7: Experimental lamellipodium photoactivation compared to simulated photoactivation. A) Experimental photoactivation of CAD cells from [12] B) Graph of fluorescence decay within 1 μm of the leading edge of the cell from [12] Scale bar 10 μm. C) Images of activated lamellipodium in simulated cell at same time points as in experimental image for parameters seen in Table 4.1 D) Graph of decay of particle number within 1 μm of leading edge of the simulated cell E) Graph of decay of particle number within 1 μm of leading edge of simulated cell with parameters seen in Table 4.1 unless listed below: High K has K=2.0 s^{-1}, no F-actin in the cell center has no F-actin in the cell center, regular F-actin in the cell center has all the parameters seen in Table 4.1, small volume with regular F-actin in the cell center has half the cell center height as that seen in Table 4.1, small cell center volume no F-actin in the cell center and high K has half the cell center height as that listed in Table 4.1, no F-actin in the cell center and K=2.0 s^{-1}.

experimental decay. Figure 4.7 C shows an example of a simulation run with F-actin in the cell center as well as a value of K that is 1.5 s^{-1} and a nucleus that occupies 32% of the total cell volume which is within the range of total volume occupied by eukaryotic cell organelles. The of the leading edge graph of the particle number within 1 μm is shown in Figure 4.7 D. This graph is normalized to the first time point in the same manner as Figure 4.7 B. The plateau of simulated intensity decay in this simulation is lower than the plateau of fluorescence decay in the experiment.

In order to investigate various influences on decay, we varied some parameters in our simulation to see how they affect the decay of particles near the leading edge after lamellipodium photoactivation. In Figure 4.7 E the black curve shows the experimental data while the blue curves are various simulation runs. The first case to observe is the one with regular F-actin in the center. These simulations have a 1:1 ratio of G- to F-actin within the cell center. We suggest that one way to affect the height of the plateau of the decay is to decrease the amount of actin in the cell center. So we maintained the same amount of G-actin within the cell center and removed all the F-actin within the cell center. (This is also analogous to making all the F-actin in the cell center very long lived.) This moved the plateau of the decay upward slightly, comparing the no F-actin in center curve to the regular F-actin in center curve in Figure 4.7 E. Another option would be to increase the amount of actin in the lamellipodium compared to the cell center. The most effective way to do this is with the parameter K which adjusts the ratio of F-actin to G-actin. By making the parameter K larger we also make more actin in the lamellipodium. Another way to accomplish this same trend is simply to reduce the available volume within the cell center which is seen in the curve labeled small volume in cell center regular F-actin in Figure 4.7 E. Our closest fit to experimental data with our simulation is obtained by combining all three of these methods: no F-actin in the cell center, a higher K value, and a smaller volume in the cell center seen in Figure 4.7 E.

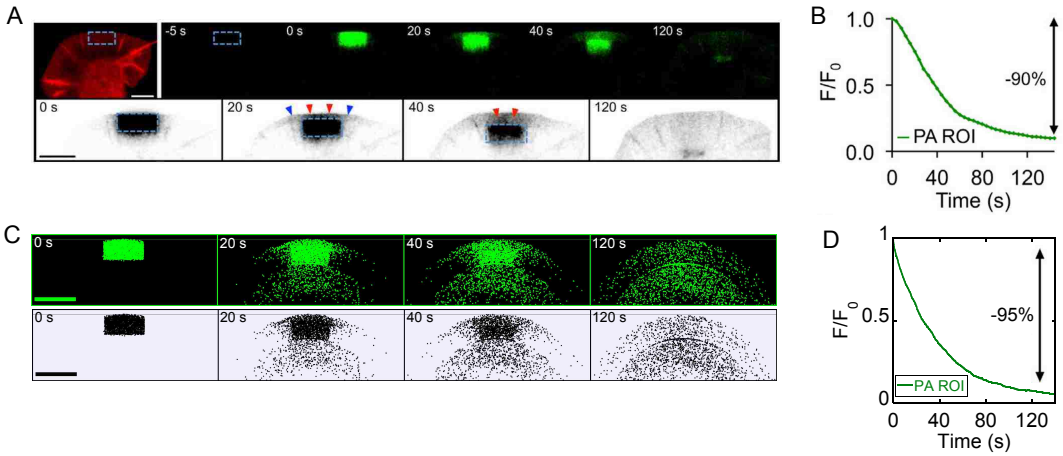

Figure 4.8: Experimental photoactivation compared to simulated photoactivation of 5 by 10 μm box at leading edge of cell. A) PA-GFP actin photoactivation of 5 by 10 μm box at leading edge of CAD cell from [12]. Scale bar 10 μm. B) Graph of fluorescence decay within the original photoactivated region from [12]. C) Images of photoactivated 5 by 10 μm box at leading edge in simulated cell shown at same time points as in experimental images. Parameter used are seen in Table 4.1 D) Graph of decay of particle number within the original photoactivated region of the simulated cell.

4.2.2 Photoactivation in 5 by 10 μm box at Leading Edge

To study local recycling of actin within the lamellipodium [12] photoactivated PA-GFP actin in a 5 by 10 μm box at the leading edge of a CAD cell, and we photoactivated the same box size in our simulation to compare to experiment. Figure 4.8 A shows experimental photoactivation at the leading edge of the cell. The bottom row of images is the inversion of the top row of images which is done to be able to more clearly see the reincorporation of PA-GFP actin at the leading edge and nearby the original photoactivated site. These images show that there is some recycling of actin within the lamellipodium locally around the photoactivated region. A graph of the fluorescence decay within the photoactivated region is shown in Figure 4.8 B which is normalized to the intensity at time 0 s. There is a 90% decay of fluorescence within the bleached region in 140 s. Simulated images show a very similar trend with

local recycling in Figure 4.8 C where the bottom row of images is the inversion of the top row. One can see in Figure 4.8 C at the 20 s and 40 s time points that there is similar local recycling of actin nearby the photoactivated region throughout the lamellipodium as well as close to the leading edge of the cell. Figure 4.8 D is a graph of the particle number decay within the photoactivated region of the simulated cell that is normalized to the particle number at 0 s. It decays by 95% in 140 s which is a very similar level to that seen in the experiment.

4.2.3 Photoactivation in Cell Center

Cell center photoactivation in CAD cells of PA-GFP actin was performed in [12] to study movement of actin from within the cell center to the leading edge of the cell. Experimental photoactivation is shown in Figure 4.9 A along with an image of the cell before photoactivation expressing Lifeact. At 10 s after photoactivation of the center there is some fluorescence seen at the leading edge of the cell. We want to know if diffusion is fast enough to account for this effect. The graph in Figure 4.9 B monitors the fluorescence in two separate places in the cell, one is the photoactivated region which is the cell center and the other is the leading edge of the cell which is within 1 μm of the leading edge. The curve corresponding to the cell center is normalized to the intensity at time 0 s and the curve for the leading edge is normalized to the maximum intensity in the 90 s that the fluorescence is monitored.

Next we simulate photoactivation of the cell center. In Figure 4.9 C there are particles near the leading edge at 10 s similar to the experimental images. The band of particles broadens similarly throughout time to the experiments as well. The graph in Figure 4.9 D is normalized in the same way as in B except the maximum for the leading edge graph is near 200 s instead of within 80 s. The leading edge simulated intensity recovery in Figure 4.9 D is similar to the recovery in the experimental graph in B but more noisy because of a small particle number. There are a few notable differences, however, between the graphs in Figure 4.9 B and D. The cell center particle number in Figure 4.9 D does not decay as much as in the experimental

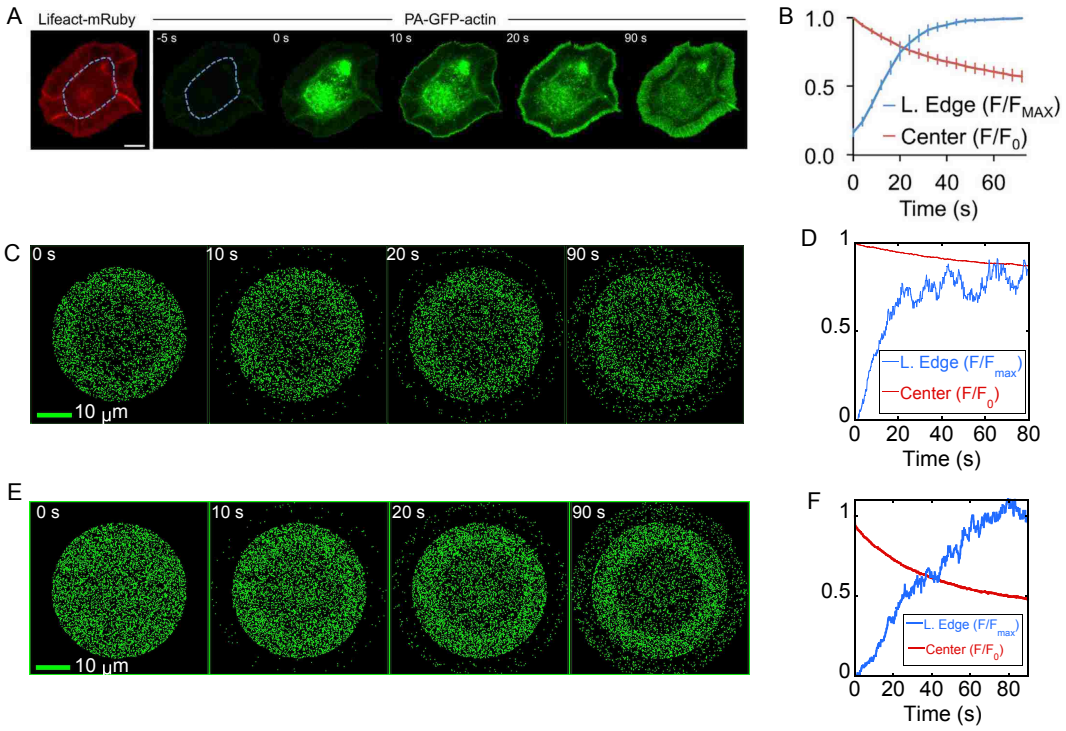

Figure 4.9: Experimental photoactivation of cell center compared to simulated photoactivation. A) PA-GFP actin photoactivation of only center of CAD cell from [12]. Scale bar 10 μm. B) Graph of fluorescence change within both the cell center and at the leading edge of the cell from [12]. C) Images of photoactivated cell center of simulated cell at same time points as in experimental images. Parameters for this simulation are listed in Table 4.1 D) Graph of number of particles within region over time both for the cell center and for the leading edge. E) Images of photoactivation of a 0.3 μm thick width at the bottom of the cell center. F) Graph of number of particles within the photoactivation region over time as well as within 1 μm of the leading edge.

case. This could be due to a few things: one possibility is that there is more actin in the lamellipodium than is estimated in [12] which is discussed in 4.2.1; another possibility is that the photoactivation of the cell center is only occurring near the bottom surface of the cell for the experimental case. Then the fluorescence decay would be greater if it is only monitored within the focal plane that is near the bottom of the cell and the decay would be greater because the photoactivated actin would

be able to move not only to the lamellipodium but also towards the top of the cell center. This doesn't happen in Figure 4.9 C-D because we activate everything within the cell center and monitor everything within the cell center, making the decay less pronounced in Figure 4.9 D.

In order to investigate how only activating a thin plane of particles near the bottom of the cell center would affect the decay within the photoactivated region I activated a 0.3 μm thickness bordering the bottom of the cell center excluding the lamellipodium shown in Figure 4.9 E. Then the particle number within the photoactivated region is recorded over time and normalized and plotted in the same way as in Figures 4.9 B and D. Decay of the particle number within the photoactivated region in the graph in Figure 4.9 F is now very similar to that seen in the experiment in Figure 4.9 B which means that this could be an explanation as to why activating the entire center gives us a different decay within 80 s.

4.2.4 Half Cell Photoactivation

Half of a CAD cell expressing PA-GFP actin was activated in Figure 4.10 A in [12] and monitored over time in order to observe how quickly actin equilibrates in the cell. The fluorescence in the half of the cell that was photoactivated was normalized to the intensity at time 0 s is shown in a graph in Figure 4.10 B. At 88 s the fluorescence has decayed to a level of about 70% of the original level. Half of our simulated cell is also photoactivated and the particle number is monitored throughout time shown in Figure 4.10 C at the same time points as in the experiment. The graph of particle number decay within the original photoactivated half of the simulated cell is seen in Figure 4.10 D and is normalized in the same way as the graph for the experimental fluorescence decay. The particle number decays to about 80% of its initial value but if allowed to run for longer times decays to 50% of its original value since that is how much actin is orignally activated within the cell. It is clear from looking at the graphs in Figure 4.10 B and D that the PA-GFP actin within the cell has not yet reached equilibrium and an experiment would need to be performed longer in order

to reach a steady state. Also, as in the previous section, it would be possible to simulate photoactivating only a thin slice of particles near the bottom of half the cell; however, it would make little difference for this simulation since this activation would include particles within the lamellipodium and cell center unlike in Figure 4.9 where the activation was only occurring the cell center.

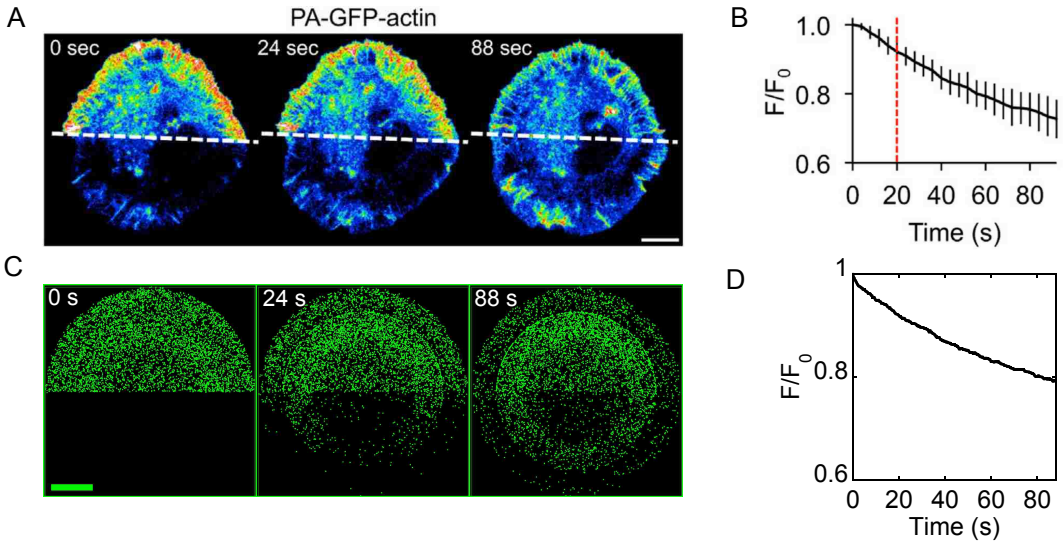

Figure 4.10: Experimental photoactivation of half of cell compared to simulated photoactivation. A) PA-GFP actin photoactivation of half of cell from [12]. Scale bar 10 μm. B) Decay of fluorescence within the photoactivated half of the cell over time from [12]. C) Images of photoactivated half cell of simulated cell at same time points as in experimental images. Parameters used are listen in Table 4.1 D) Graph of number of particles within the original photoactivated region over time.

4.3 Conclusions

In this study we learn that we cannot rule out the possibility that there is some fraction of actin within the lamellipodium that is recycled within the lamellipodium continuously and does not get into the cell center. We also do not rule out the

possibility that there is a larger fraction of actin contained within the lamellipodium than predicted in [12]. More testing would need to be done in order to determine which possibility is correct. We also suggest that photoactivation of the cell center may be occurring for only photoactivatable proteins within the focal plane which is thin compared to the entire thickness of the entire cell. While monitoring the loss of fluorescence within the cell center within the focal plane, the photoactivated particles might not be going only to the lamellipodium which is within the focal plane, but could also be diffusing outside of the focal plane towards to apical side of the cell.

Our model supports the hypothesis that diffusion is fast enough to deliver G-actin to the leading edge for incorporation into the F-actin network for CAD cells in steady state and that active transport is not necessary for these cells. The model of Zicha et al [24] only considers a specific diffusion coefficient that is obtained through a best fit method in order to analyze whether diffusion is fast enough to allow delivery of G-actin to the leading edge and uses their model to describe motile cells. However, it would be more realistic if the diffusion coefficient were chosen from a distribution instead.

Chapter 5

Conclusion

In this thesis I studied turnover of actin protein and its regulators within motile cells. First I studied capping protein and the Arp2/3 complex within the lamellipodium. About 50% of capping protein is estimated to be slowly diffusing [1], in XTC cells and I suggested two models that include slowly diffusing capping protein and then use these models to simulate FRAP of capping protein and to compare with experimental FRAP from Kapustina et al. [3]. One mechanism for slow diffusing capping protein was that capping protein is pulled off the ends of actin filaments by the membrane of the cell and then stays associated with the membrane and continues to diffuse on the membrane until it dissociates from the membrane and diffuses freely. Another mechanism for slowly diffusing capping protein is that capping protein may be bound to the end of a slowly diffusing actin oligomer. This work motivates experiments for photoactivation of capping protein experiments to distinguish between these two mechanisms and monitor where the fluorescence would first move to directly after photoactivation. Slowly diffusing Arp2/3 complex has also been observed in Milius et al. [6]. We propose two models for the Arp2/3 complex kinetics and use them to simulate FRAP and then compare to experimental FRAP of the Arp2/3 complex from [2]. One model we test has no slowly diffusing Arp2/3 complex, and the other model includes slowly diffusing Arp2/3 complex that diffuses slowly while bound

to the membrane. The model that includes slowly diffusing Arp2/3 complex was developed based on the observations from Milius et al. [6] and fits the experimental FRAP data from Lai et al. [2] better than the model with a single diffuse species of the Arp2/3 complex.

Next, we developed a model for actin turnover in the lamellipodium that included 3 diffuse pools of actin which were then used to simulate photoactivation to compare to experimental photoactivation of PA-GFP actin. One pool was fast diffusing actin that was in dynamic equilibrium with thymosin $\beta 4$. The second pool recycled actin which was slowly diffusing. The third pool was actin bound to the membrane. Together with experiments by Vitriol [12], we find that thymosin $\beta 4$ aids in the fast diffusion of actin to the leading edge of the cell to incorporate into the F-actin network. We suspect that thymosin $\beta 4$ may make a complex with profilin at the leading edge of the cell, and this aids in polymerization of actin at the leading edge. Using our model, we find that diffusion is sufficient for delivery of actin to the leading edge of the cell although this diffusion is close to being limiting for delivery of actin to the leading edge because of gradients of diffuse actin concentration near the leading edge.

Finally, we utilize a previous model of actin in the lamellipodium from [1] and similar to the model used above in a 3D whole cell model of actin turnover to simulate photoactivation of actin and compare to experimental photoactivation of PA-GFP actin. In doing this, we learn that we cannot rule out the possibly that some fraction of actin within the lamellipodium is continuously recycled; however, it is also possible that the level of the decay plateau represents the fraction of actin contained within the photoactivated region compared to the entire cell. Our model suggests that diffusion of actin is fast enough to deliver G-actin to the leading edge of the stationary cell without active transport.

Future work would include modeling other actin regulating proteins within the lamellipodium for which SiMS data is available such as: Cofilin, AIP1, VASP, and WAVE complex. Other work could be done in extending the model within the

lamellipodium to a 3D whole cell model in order to study the protein's role within the entire cell instead of just the lamellipodium and to study how protein in the bulk of the cell might affect the kinetics of that protein within the lamellipodium. Utilizing the 3D whole cell model, s-FDAP [13] could be simulated and compared with experimental s-FDAP to draw conclusions on various proteins at different parts of the cell, including the lamellipodium and cell center.

Bibliography

[1] Matthew B. Smith, Tai Kiuchi, Naoki Watanabe, and Dimitrios Vavylonis. Distributed actin turnover in the lamellipodium and frap kinetics. *Biophys J*, 104(1):247–257, Jan 2013.

[2] Frank P. L. Lai, Malgorzata Szczodrak, Jennifer Block, Jan Faix, Dennis Breitsprecher, Hans G. Mannherz, Theresia E. B. Stradal, Graham A. Dunn, J. Victor Small, and Klemens Rottner. Arp2/3 complex interactions and actin network turnover in lamellipodia. *EMBO J*, 27(7):982–992, Apr 2008.

[3] Maryna Kapustina, Eric Vitriol, Timothy C. Elston, Leslie M. Loew, and Ken Jacobson. Modeling capping protein frap and cali experiments reveals in vivo regulation of actin dynamics. *Cytoskeleton (Hoboken)*, 67(8):519–534, Aug 2010.

[4] Thomas D. Pollard and Gary G. Borisy. Cellular motility driven by assembly and disassembly of actin filaments. *Cell*, 112(4):453–465, Feb 2003.

[5] T. D. Pollard, L. Blanchoin, and R. D. Mullins. Molecular mechanisms controlling actin filament dynamics in nonmuscle cells. *Annu Rev Biophys Biomol Struct*, 29:545–576, 2000.

[6] Arthur Millius, Naoki Watanabe, and Orion D. Weiner. Diffusion, capture and recycling of scar/wave and arp2/3 complexes observed in cells by single-molecule imaging. *J Cell Sci*, 125(Pt 5):1165–1176, Mar 2012.

[7] D. A. Schafer, P. B. Jennings, and J. A. Cooper. Dynamics of capping protein and actin assembly in vitro: uncapping barbed ends by polyphosphoinositides. *J Cell Biol*, 135(1):169–179, Oct 1996.

[8] Takushi Miyoshi, Takahiro Tsuji, Chiharu Higashida, Maud Hertzog, Akiko Fujita, Shuh Narumiya, Giorgio Scita, and Naoki Watanabe. Actin turnover-dependent fast dissociation of capping protein in the dendritic nucleation actin network: evidence of frequent filament severing. *J Cell Biol*, 175(6):947–955, Dec 2006.

[9] T. K. Meyvis, S. C. De Smedt, P. Van Oostveldt, and J. Demeester. Fluorescence recovery after photobleaching: a versatile tool for mobility and interaction measurements in pharmaceutical research. *Pharm Res*, 16(8):1153–1162, Aug 1999.

[10] Naoki Watanabe and Timothy J. Mitchison. Single-molecule speckle analysis of actin filament turnover in lamellipodia. *Science*, 295(5557):1083–1086, Feb 2002.

[11] Jennifer Lippincott-Schwartz, Nihal Altan-Bonnet, and George H. Patterson. Photobleaching and photoactivation: following protein dynamics in living cells. *Nat Cell Biol*, Suppl:S7–14, Sep 2003.

[12] Eric A. Vitriol, Laura M. McMillen, Maryna Kapustina, Shawn M. Gomez, Dimitrios Vavylonis, and James Q. Zheng. Two functionally distinct sources of actin monomers supply the leading edge of lamellipodia. *Cell Rep*, 11(3):433–445, Apr 2015.

[13] Tai Kiuchi, Tomoaki Nagai, Kazumasa Ohashi, and Kensaku Mizuno. Measurements of spatiotemporal changes in g-actin concentration reveal its effect on stimulus-induced actin assembly and lamellipodium extension. *J Cell Biol*, 193(2):365–380, Apr 2011.

[14] G. A. Dunn, I. M. Dobbie, J. Monypenny, M. R. Holt, and D. Zicha. Fluorescence localization after photobleaching (FLAP): a new method for studying protein dynamics in living cells. *J Microsc*, 205(Pt 1):109–112, Jan 2002.

[15] Alexandre Lewalle, Marco Fritzsche, Kerry Wilson, Richard Thorogate, Tom Duke, and Guillaume Charras. A phenomenological density-scaling approach to lamellipodial actin dynamics. *Interface Focus*, 4(6):20140006, Dec 2014.

[16] Alex Mogilner and Leah Edelstein-Keshet. Regulation of actin dynamics in rapidly moving cells: a quantitative analysis. *Biophys J*, 83(3):1237–1258, Sep 2002.

[17] Igor R. Kuznetsov, Marc Herant, and Micah Dembo. Analysis of actin flap dynamics in the leading lamella. *PLoS One*, 5(4):e10082, 2010.

[18] P. J. Michalski and A. E. Carlsson. The effects of filament aging and annealing on a model lamellipodium undergoing disassembly by severing. *Phys Biol*, 7(2):026004, 2010.

[19] Christian H. Schreiber, Murray Stewart, and Thomas Duke. Simulation of cell motility that reproduces the force-velocity relationship. *Proc Natl Acad Sci U S A*, 107(20):9141–9146, May 2010.

[20] Igor L. Novak, Boris M. Slepchenko, and Alex Mogilner. Quantitative analysis of g-actin transport in motile cells. *Biophys J*, 95(4):1627–1638, Aug 2008.

[21] Florian Huber, Josef Käs, and Björn Stuhrmann. Growing actin networks form lamellipodium and lamellum by self-assembly. *Biophys J*, 95(12):5508–5523, Dec 2008.

[22] Jonathon A. Ditlev, Nathaniel M. Vacanti, Igor L. Novak, and Leslie M. Loew. An open model of actin dendritic nucleation. *Biophys J*, 96(9):3529–3542, May 2009.

[23] Björn Stuhrmann, Florian Huber, and Josef Käs. Robust organizational principles of protrusive biopolymer networks in migrating living cells. *PLoS One*, 6(1):e14471, 2011.

[24] Daniel Zicha, Ian M. Dobbie, Mark R. Holt, James Monypenny, Daniel Y H. Soong, Colin Gray, and Graham A. Dunn. Rapid actin transport during cell protrusion. *Science*, 300(5616):142–145, Apr 2003.

[25] Matthew B. Smith, Erdem Karatekin, Andrea Gohlke, Hiroaki Mizuno, Naoki Watanabe, and Dimitrios Vavylonis. Interactive, computer-assisted tracking of speckle trajectories in fluorescence microscopy: application to actin polymerization and membrane fusion. *Biophys J*, 101(7):1794–1804, Oct 2011.

[26] Yi Fan, Sandeepa M. Eswarappa, Masahiro Hitomi, and Paul L. Fox. Myo1c facilitates g-actin transport to the leading edge of migrating endothelial cells. *J Cell Biol*, 198(1):47–55, Jul 2012.

[27] Thomas D. Pollard and John A. Cooper. Actin, a central player in cell shape and movement. *Science*, 326(5957):1208–1212, Nov 2009.

[28] Alex Mogilner and Kinneret Keren. The shape of motile cells. *Curr Biol*, 19(17):R762–R771, Sep 2009.

[29] Naoki Watanabe. Inside view of cell locomotion through single-molecule: fast f-/g-actin cycle and g-actin regulation of polymer restoration. *Proc Jpn Acad Ser B Phys Biol Sci*, 86(1):62–83, 2010.

[30] Gaudenz Danuser, Jun Allard, and Alex Mogilner. Mathematical modeling of eukaryotic cell migration: insights beyond experiments. *Annu Rev Cell Dev Biol*, 29:501–528, 2013.

[31] Laurent Blanchoin, Rajaa Boujemaa-Paterski, Ccile Sykes, and Julie Plastino. Actin dynamics, architecture, and mechanics in cell motility. *Physiol Rev*, 94(1):235–263, Jan 2014.

[32] J. L. McGrath, Y. Tardy, CF Dewey, Jr, J. J. Meister, and J. H. Hartwig. Simultaneous measurements of actin filament turnover, filament fraction, and monomer diffusion in endothelial cells. *Biophys J*, 75(4):2070–2078, Oct 1998.

[33] Agnieszka Kawska, Kévin Carvalho, John Manzi, Rajaa Boujemaa-Paterski, Laurent Blanchoin, Jean-Louis Martiel, and Cécile Sykes. How actin network dynamics control the onset of actin-based motility. *Proc Natl Acad Sci U S A*, 109(36):14440–14445, Sep 2012.

[34] Eric A. Vitriol, Andrea C. Uetrecht, Feimo Shen, Ken Jacobson, and James E. Bear. Enhanced egfp-chromophore-assisted laser inactivation using deficient cells rescued with functional egfp-fusion proteins. *Proc Natl Acad Sci U S A*, 104(16):6702–6707, Apr 2007.

[35] Sawako Yamashiro, Hiroaki Mizuno, Matthew B. Smith, Gillian L. Ryan, Tai Kiuchi, Dimitrios Vavylonis, and Naoki Watanabe. New single-molecule speckle microscopy reveals modification of the retrograde actin flow by focal adhesions at nanometer scales. *Mol Biol Cell*, 25(7):1010–1024, Apr 2014.

[36] Ikuko Fujiwara, Kirsten Remmert, Grzegorz Piszczek, and John A. Hammer. Capping protein regulatory cycle driven by carmil and v-1 may promote actin network assembly at protruding edges. *Proc Natl Acad Sci U S A*, 111(19):E1970–E1979, May 2014.

[37] Ikuko Fujiwara, Kirsten Remmert, and John A Hammer, 3rd. Direct observation of the uncapping of capping protein-capped actin filaments by carmil homology domain 3. *J Biol Chem*, 285(4):2707–2720, Jan 2010.

[38] Marc Edwards, Yun Liang, Taekyung Kim, and John A. Cooper. Physiological role of the interaction between carmil1 and capping protein. *Mol Biol Cell*, 24(19):3047–3055, Oct 2013.

[39] Benjamin A. Smith, Karen Daugherty-Clarke, Bruce L. Goode, and Jeff Gelles. Pathway of actin lament branch formation by arp2/3 complex revealed by single-molecule imaging. *PNAS*, 110:1285–1290, 2013.

[40] Gillian L. Ryan, Heather M. Petroccia, Naoki Watanabe, and Dimitrios Vavylonis. Excitable actin dynamics in lamellipodial protrusion and retraction. *Biophys J*, 102(7):1493–1502, Apr 2012.

[41] Stefan A. Koestler, Anika Steffen, Maria Nemethova, Moritz Winterhoff, Ningning Luo, J Margit Holleboom, Jessica Krupp, Sonja Jacob, Marlene Vinzenz, Florian Schur, Kai Schlter, Peter W. Gunning, Christoph Winkler, Christian Schmeiser, Jan Faix, Theresia E B. Stradal, J Victor Small, and Klemens Rottner. Arp2/3 complex is essential for actin network treadmilling as well as for targeting of capping protein and cofilin. *Mol Biol Cell*, 24(18):2861–2875, Sep 2013.

[42] Janet H. Iwasa and R Dyche Mullins. Spatial and temporal relationships between actin-filament nucleation, capping, and disassembly. *Curr Biol*, 17(5):395–406, Mar 2007.

[43] Longhua Hu and Garegin A. Papoian. Mechano-chemical feedbacks regulate actin mesh growth in lamellipodial protrusions. *Biophys J*, 98(8):1375–1384, Apr 2010.

[44] Longhua Hu and Garegin A. Papoian. How does the antagonism between capping and anti-capping proteins affect actin network dynamics? *J Phys Condens Matter*, 23(37):374101, Sep 2011.

[45] Takahiro Tsuji, Takushi Miyoshi, Chiharu Higashida, Shuh Narumiya, and Naoki Watanabe. An order of magnitude faster aip1-associated actin disruption than nucleation by the arp2/3 complex in lamellipodia. *PLoS One*, 4(3):e4921, 2009.

[46] Meng-Chi Lin, Brian J. Galletta, David Sept, and John A. Cooper. Overlapping and distinct functions for cofilin, coronin and aip1 in actin dynamics in vivo. *J Cell Sci*, 123(Pt 8):1329–1342, Apr 2010.

[47] Silvia Jansen, Agnieszka Collins, Samantha M. Chin, Casey A. Ydenberg, Jeff Gelles, and Bruce L. Goode. Single-molecule imaging of a three-component ordered actin disassembly mechanism. *Nat Commun*, 6:7202, 2015.

[48] K. Rottner, B. Behrendt, J. V. Small, and J. Wehland. Vasp dynamics during lamellipodia protrusion. *Nat Cell Biol*, 1(5):321–322, Sep 1999.

[49] Derek A. Applewhite, Melanie Barzik, Shin-Ichiro Kojima, Tatyana M. Svitkina, Frank B. Gertler, and Gary G. Borisy. Ena/vasp proteins have an anti-capping independent function in filopodia formation. *Mol Biol Cell*, 18(7):2579–2591, Jul 2007.

[50] Chi Wai Lee, Eric A. Vitriol, Sangwoo Shim, Ariel L. Wise, Radhi P. Velayutham, and James Q. Zheng. Dynamic localization of g-actin during membrane protrusion in neuronal motility. *Curr Biol*, 23(12):1046–1056, Jun 2013.

[51] Edward Irobi, Adeleke H. Aguda, Mrten Larsson, Christophe Guerin, Helen L. Yin, Leslie D. Burtnick, Laurent Blanchoin, and Robert C. Robinson. Structural basis of actin sequestration by thymosin-beta4: implications for wh2 proteins. *EMBO J*, 23(18):3599–3608, Sep 2004.

[52] Vivianne T. Nachmias Lynne Cassimeris, Daniel Safer and S. H. Zigmond. Thymosin $\beta 4$ sequesters the majority of g-actin in resting human polymorphonudear leukocytes. *Journal of Chemical Biology*, 119:1261–1270, 1992.

[53] Marco Fritzsche, Alexandre Lewalle, Tom Duke, Karsten Kruse, and Guillaume Charras. Analysis of turnover dynamics of the submembranous actin cortex. *Mol Biol Cell*, 24(6):757–767, Mar 2013.

[54] Andrew G. Clark, Kai Dierkes, and Ewa K. Paluch. Monitoring actin cortex thickness in live cells. *Biophys J*, 105(3):570–580, Aug 2013.

[55] Lodish H, Berk A, and Zipursky SL. *Molecular Cell Biology*. W.H. Freeman, 2000.

[56] Micah Webster, Keren L. Witkin, and Orna Cohen-Fix. Sizing up the nucleus: nuclear shape, size and nuclear-envelope assembly. *J Cell Sci*, 122(Pt 10):1477–1486, May 2009.

[57] Valrie M. Laurent, Sandor Kasas, Alexandre Yersin, Tilman E. Schffer, Stefan Catsicas, Giovanni Dietler, Alexander B. Verkhovsky, and Jean-Jacques Meister. Gradient of rigidity in the lamellipodia of migrating cells revealed by atomic force microscopy. *Biophys J*, 89(1):667–675, Jul 2005.

Laura M. McMillen

16 Memorial Walk East, Bethlehem, PA, 18015,
(717) 348-5997

EDUCATION

Lehigh University, Bethlehem, PA — Expected February 2016
PhD, Physics
Dissertation title: Kinetics of Turnover of Actin and Regulators in Motile Cells
G.P.A. 3.55/4.0

Lehigh University, Bethelehem, PA — January 2013
Master of Science, Physics
G.P.A. 3.55/4.0

Lebanon Valley College, Annville, PA — May 2011
Bachelor of Science, Physics
Minor in Music
Overall G.P.A. 3.65/4.0
Major G.P.A. 3.918/4.0

EXPERIENCE

Research Assistant — August 2011-Present

Lehigh University, Bethlehem, PA

- Developed novel models for explaining protein dynamics within the lamellipodium
- Built new 3D Monte Carlo particle simulation for explaining protein dynamics within the cell

• Analyzed both experimental and simulated data

• Advised two undergraduate students in independent research projects

Teaching Assistant August 2011-Present

Lehigh University, Bethlehem, PA

• Taught recitations for both semesters of the introductory physics course as well as a lab section for the first semester

• Independently organized extra problem solving sessions for the entire lecture to aid in student understanding of concepts

Student Researcher June 2009-August 2010

Lebanon Valley College, Annville, PA

• Created new computational tools for determining stabilizers for quantum states

• Worked closely with other student researchers and professors to classify symmetric states by their stabilizers

PUBLICATIONS

•Diffusive Dynamics of Capping Protein and Arp2/3 Complex
in the Lamellipodium
Under Review
Laura M. McMillen and Dimitrios Vavylonis

•Two Functionally Distinct Sources of Actin Monomers
Supply the Leading Edge of Lamellipodia
11:433-445 Cell Reports, March 2, 2015
E.A. Vitriol, L. McMillen, S. Gomez, M. Kapustina,
D. Vavylonis, J.Q. Zheng.

•Symmetric states: local unitary equivalence via stabilizers
Quantum Information and Computation,10:1029-1041, November 2010
Curt D. Cenci, David W. Lyons, Laura M. Snyder,
and Scott N. Walck

TALKS

• Model of Capping Protein and Arp2/3 Complex Turnover
in the Lamellipodium
Based on Single Molecule Statistics
-APS March Meeting, Baltimore, MD, 3/18/13-3/22/13

• Mathematical Modeling of Protein Turnover in the Lamellipodium
of Motile Cells (Invited)
-Biomathematics and Ecology: Education and Research Conference,
Claremont, CA,
10/10/14-10/12/14

POSTERS

• Classifying two-qubit states by their subsystems
-AAPT meeting, LaSalle University, 3/12/10

• Stabilizer Formalism and Symmetric States
-Joint Mathematics Meeting, New Orleans, LA, 1/6/11-1/9/11

• Model of Capping Protein and Arp2/3 Complex Turnover
in the Lamellipodium
Based on Single Molecule Statistics
-ASCB Annual Meeting, San Francisco, CA, 12/15/12-12/19/12
-BPS Annual Meeting, Philadelphia, PA, 2/15/13-2/19/13

• Modeling Protein Turnover in the Lamellipodium Based on
Single Molecule
Speckle Microscopy Data
-BPS Pennsylvania Network Meeting, PSU, University Park, PA, 10/4/13
-ASCB Annual Meeting, New Orleans, LA, 12/14/13-12/18/13

SKILLS

• Programming languages: Python, Java, SAGE, GAP

• ImageJ, Powerpoint, Excel, Word, Inkscape

HONORS AND AWARDS

• 2nd place Lehigh PGSA poster session January 2015

• GAANN (Graduate Assistance in Areas of National Need) fellowship 2011-2012

• Vickroy Scholarship at Lebanon Valley College (half tuition scholarship for 4 years)

• Deans List (Spring 2009, Fall 2009, Spring 2010, Fall 2010)

• Lebanon Valley Physics Club Secretary (2010-2011)

• 2009 and 2010 National Fastpitch Coaches Association Scholar Athlete

• 2010 Lebanon Valley College Scholar Athlete (awarded to student athletes of junior or senior standing with a cumulative GPA of 3.5 or above)

• 2010 Middle Atlantic Conference Academic Honor Roll (awarded to student athletes with a GPA of 3.2 or above with at least sophomore standing)

EXTRACURRICULAR ACTIVITIES

• Volunteering at a local nursing home

• Co-coach for interdepartmental summer softball league Physics team